Synaptic and peptidergic connectome in the marine annelid *Platynereis dumerilii*

Dissertation

Der Mathematisch-Naturwissenschaftlichen Fakultät
der Eberhard Karls Universität Tübingen
zur Erlangung des Grades eines
Doktors der Naturwissenschaften
(Dr. rer. nat.)

vorgelegt von
Csaba Verasztó
aus Budapest, Ungarn

Tübingen
2017

Gedruckt mit Genehmigung der Mathematisch-Naturwissenschaftlichen Fakultät der Eberhard Karls Universität Tübingen.

Tag der mündlichen Qualifikation:

Dekan:	Prof. Dr. Wolfgang Rosenstiel
1. Berichterstatter:	Dr. Gáspár Jékely
2. Berichterstatter:	Prof. Dr. Nico Michiels

Acknowledgements

“Many things happened before I was called a Doctor...”

I would like to acknowledge the support that I received during the course of my PhD. Foremost, I am grateful for my supervisor Gáspár Jékely, who provided me the opportunity to follow my own ideas, and turned out to be the guide and scientific support I needed throughout the years to complete this project.

I would also like to thank all of the current and former members and short-term visitors of the Jékely lab. May your contributions be enormous or small, they were all valuable beyond measure. I learned a lot.

Finally I would like to acknowledge my family, my friends, and Harshul for the support and love. Colleagues and people who see me on a daily basis think I smile because I am a proud person, but the truth is, I smile because I reflect the help, freedom, and love I received in my life. I thank all of you!

Table of Content

Abbreviations and Symbols

ANS: apical nervous system

ATPase: adenylpyrophosphatase

ChAT: Choline Acetyltransferase

DIC: differential interference contrast

EM: electron microscopy

GCaMP6s: GFP-calmodulin-protein version 6 slow

GPCR: G protein-coupled receptor

MRI: magnetic resonance imaging

NOS: nitric-oxide synthase

sGCbeta1: soluble guanylyl cyclase-beta

siGOLD: serial immunogold labeling

ssTEM: serial-section transmission electron microscopy

TrpH: tryptophan hydroxylase

VAChT: Vesicular acetylcholine transporter

WMISH: whole-mount *in situ* hybridization

Zusammenfassung

Platynereis dumerilii ist ein meeresbewohnender Annelid mit einer kosmopolitischen geographischen Verbreitung. Wegen seiner Ursprünglichkeit und phyletischen Position ist *Platynereis* ein bemerkenswerter Modellorganismus für die Biologie der Invertebraten.

Ich habe in meiner Doktorarbeit das einfache Nervensystem dieses Wurms untersucht. Ich habe einen elektronmikroskopischen Datensatz benutzt um die apikale Gehirnstruktur (das größte neurosekretorische Zentrum der Larve) und die Motorneuronen für die ziliäre Fortbewegung zu rekonstruieren. Durch die Erforschung dieser Gehirnstrukturen hatte ich die Möglichkeit, zwei wichtige Arten der Signalübertragung – synaptische und peptiderge – im Larvengehirn zu studieren.

Ich habe eine Calcium-Imaging-Methode in *Platynereis* entwickelt, um die Funktion der rekonstruierten neuronalen Schaltkreise zu analysieren, und um das larvale Verhalten zu verstehen. Außerdem habe ich transgene Marker, Antikörperfärbung, und Einzelzelltranskriptom-Daten benutzt, um einzelne Neurone des Netzwerks zu identifizieren. Das Calcium-Imaging ergab, dass ein autonomes Netzwerk von Motorneuronen die Zilienaktivität reguliert, wobei Neurone mit unterschiedlichen Neurotransmitterprofilen auch unterschiedliche Aufgaben erfüllen (z. B. das Schwimmen beginnen oder enden zu lassen).

Das apikale Nervensystem von *Platynereis* besteht aus 70 sensorischen Neuronen und 8 Interneuronen. Es gelang mir, mehrere Neurone eindeutig zu identifizieren und ihre peptiderge Identität zu bestätigen. Ich habe die elektronmikroskopische Rekonstruktion als Referenz benutzt und ein Netzwerk von Peptiden und Rezeptoren ergänzt. Meine Kollegen und ich haben ein locker verbundenes peptiderges Netzwerk entdeckt, das sowohl synaptisch als auch chemisch mit dem Rest des Nervensystems verbunden ist. Ich konnte durch Calcium-Imaging den neuromodulatorischen Effekt eines der Neuropeptide analysieren und zeigen, wie die sensorische Information aus dem apikalen Nervensystem die ziliäre Fortbewegung reguliert.

Insgesamt trägt die vorliegende Arbeit dazu bei, larvales Verhalten und das zugrundeliegende larvale Nervensystem besser zu verstehen. Ich habe Konnektomik

mit funktionellen Analysen kombiniert, um die „primäre Sprache des Nervensystems“ zu entziffern.

Summary

Platynereis dumerilii is a marine annelid with a cosmopolitan geographic distribution. The ancestrality and phylogenetic position of *Platynereis* make it a noteworthy model organism in invertebrate biology.

In this thesis, I studied the simple nervous system of the early larval stages of this worm. I used an electron microscopy dataset to reconstruct the apical nervous system (the largest neurosecretory center in the larva) and the motor neuron circuit for ciliary locomotion. Through studying these different brain regions, I could investigate two major forms of nervous system signaling - synaptic and peptidergic signaling - in the larval brain.

I developed calcium imaging in *Platynereis* to functionally analyze the reconstructed circuits and relate them to larval behavior. Further, I used transgenic labeling, immunohistochemistry and single-cell transcriptome data to classify individual neurons in the circuits. Calcium imaging revealed an autonomic motor neuron circuit regulating ciliary beating, where neurons with different neurotransmitter profiles are assigned different tasks (e.g. to stop the animal or to initiate swimming).

The apical nervous system of *Platynereis* consists of 70 sensory neurons and 8 interneurons. I was able to classify many neurons at single-cell resolution and confirm their peptidergic identity. I used the electron microscopy reconstruction as a reference template, and overlaid a peptide - receptor network on this map. My coworkers and I have discovered a sparsely connected peptidergic network, which is connected both synaptically and chemically to the rest of the nervous system. I used calcium imaging to functionally analyze one peptide’s neuromodulatory effect and show how the sensory information from the apical nervous system can regulate ciliary locomotion.

Taken together, the present work further refines our understanding of larval behavior and the underlying simple brain. I combined connectomics with experimental analyses to decipher the complexity of the “primary language of the nervous system”.

Publications incorporated into the thesis

Csaba Verasztó, Nobuo Ueda, Luis A Bezares-Calderón, Aurora Panzera, Elizabeth A Williams, Réza Shahidi, Gáspár Jékely Ciliomotor circuitry underlying whole-body coordination of ciliary activity in the Platynereis larva eLife 2017;6:e26000 DOI:10.7554/eLife.26000

Elizabeth A Williams, Csaba Verasztó, Sanja Jasek, Markus Conzelmann, Réza Shahidi, Philipp Bauknecht, Gáspár Jékely Synaptic and peptidergic connectome of a neurosecretory center in the annelid brain DOI:10.1101/115204

Own contribution to the publications

Csaba Verasztó, Nobuo Ueda, Luis A Bezares-Calderón, Aurora Panzera, Elizabeth A Williams, Réza Shahidi, Gáspár Jékely Ciliomotor circuitry underlying whole-body coordination of ciliary activity in the *Platynereis* larva eLife 2017;6:e26000 DOI:10.7554/eLife.26000

I established the calcium-imaging technique in *Platynereis* and did the imaging and microscopy myself. Python and ImageJ scripts were written by me and Gáspár Jékely. Aurora Panzera helped with microinjections and the preparation of animal samples. I performed the confocal laser ablations and the pharmacological assays, and the photoactivation experiments. I did the immunostainings with Luis A Bezares-Calderón, and Nobuo Ueda. I designed and created expression vectors with Luis A Bezares-Calderón, Nobuo Ueda, and Elizabeth A Williams. Gáspár Jékely and I did the data analysis and movies. I did neuron reconstruction and revision with contributions from the entire Jékely lab. The figures and movies were prepared together with Gáspár Jékely. Drafting and revision were done by me and Gáspár Jékely.

Elizabeth A Williams, Csaba Verasztó, Sanja Jasek, Markus Conzelmann, Réza Shahidi, Philipp Bauknecht, Gáspár Jékely Synaptic and peptidergic connectome of a neurosecretory center in the annelid brain DOI:10.1101/115204

I performed neuron reconstruction and revision for the neurosecretory plexus. Gáspár Jékely and I designed and wrote the Python and ImageJ scripts for the analysis. Elizabeth A Williams and I did the calcium-imaging experiments.

Introduction

My thesis lies at the intersection of several scientific fields. The underlying theme of my research is the investigation of neuronal functions with ancient evolutionary origin. The overarching techniques that I employ for this investigation are the electron microscopy reconstruction of neurons and circuits, together with the visualization of brain activity through calcium imaging. This combination of approaches (introduced below) was necessary to understand tiny portions of the brain of a microscopic creature. I used connectomics in an electron microscopy dataset to create a framework, to which I could relate neuronal activity imaging, transcriptome data, immunohistochemistry and transgenic labeling to answer fundamental questions about nervous system signaling, such as what is the underlying neuronal regulation of multiple ciliary bands, or what is the best map of a neurosecretory center one can create?

Cilia, Ciliary movement and coordination in Ciliates

Eukaryotic cilia and flagella are multifunctional organelles made of a microtubule scaffold powered by dynein ATPase motors. Cilia and flagella are slender membrane structures extending into the environment. There is overwhelming evidence (Lang et al., 2002, Jekely et al., 2008, Stechmann and Cavalier-Smith, 2003, Nikolaev et al., 2004) that these biological machines are ancient inventions of evolution, conserved between humans and algae (Pazour et al., 2005, Salathe, 2007, Satir, 1999). Cilia evolved prior to the radiation of all extant eukaryotes (Avidor-Reiss et al., 2004); every branch of the eukaryotes have organisms with motile cilia or flagella. Flagella and cilia (there is no consistent functional or structural difference between organelles with these two designations in eukaryotes (Mitchell, 2007)) are composed of the axoneme and the basal body (Figure 1A). The axoneme stems from the root of the cilium, which is called the basal body. The axoneme consists of a characteristic cytoskeletal structure of nine duplets of microtubules that form a ring around a central pair of single microtubules. In the basal body, nine microtubule triplets are anchored to the cell surface and stabilized

in the cytoplasm. Ciliary movement occurs when each pair of microtubules takes a turn to (consecutively) “move up a little bit” to create the undulating sinusoidal movement of the structure with the help of rows of dynein ATPase’s, which power the bending. There are two different types of cilia, (1) motile cilia, and (2) non-motile or primary cilia (Figure 1B). Primary cilia typically serve as sensory organelles. One of the most well studied examples of cilia is found in the embryonic mouse node, where the two types of cilia coexist. Motile cilia drive the embryonic fluid to flow leftward, while non-motile cilia detect the direction of the flow and play a role in the embryo’s development, determining left-right symmetry (Drummond, 2013). Primary cilia, contrary to their definition, can be both sensory and motile. Motile sensory cilia can detect fluid flow, osmotic and shear forces, but they can also play a role in chemoreception (e.g. detection of sex hormones or bitter taste) (Jain et al., 2012). While sensory cilia act as antennae for signal transduction, the basic motile machinery appears to be highly conserved, thus the ancient function of cilia is likely locomotion (Mitchell, 2007).

Cells with hundreds of motile cilia on their surface have important roles in our brain, reproductive system and airways (Shoemark and Hogg, 2013, Lyons et al., 2006, Worthington and Cathcart, 1963). By beating coordinately, cilia cause fluid to flow in a particular direction. Cilia keep the cerebrospinal fluid in motion, they clean the airways of particles, and they are an important factor in normal egg transport in the fallopian tubes. Ciliary locomotion, as opposed to muscle-based locomotion, is considered to be a more ancient form of locomotion, as it is created by the membrane extension of a (single) cell. Nearly every natural body of water on Earth contains a wide variety of ciliary swimmers, including but not limited to the larvae of sponges, cnidarians, and bilaterians, but also protozoans and algae, which use cilia or flagella as their main locomotory organ (Figure 1C). These organisms can propel themselves forward at a velocity of up to 1 mm/sec (Lodish, 2003), or use cilia to effectively collect food particles (Gilpin et al., 2017), i.e. ciliary activity causes the displacement of the particles around the cell, not the cell itself.

In many cases, ciliary beat synchronization can be achieved if polarized cilia are arranged regularly along the planar axis of the ciliated surface (Mitchell et al., 2007). Thus, if cilia are oriented properly, beat synchronization can emerge from the hydrodynamic coupling of adjacent cilia (Gueron and Levit-Gurevich, 1999, Osterman and Vilfan, 2011, Elgeti and Gompper, 2013). This biophysical mechanism alone,

however, can only explain coordinated beating patterns of ciliated structures completely covered by cilia. Circadian or any temporal regulation of ciliary beating (Faubel et al., 2016, Zantke et al., 2014, Zantke et al., 2013), or fast coordination of multiple or complex ciliated surfaces in animals (Figure 1C), require neuronal control.

Albeit our knowledge of the mechanistic details is scarce, neuronal ciliary coordination is widespread in the animal kingdom. From ctenophores (Tamm, 2014) through to annelids (Conzelmann et al., 2011) and to vertebrates (Maruyama et al., 1984, Konig et al., 2009, Walentek et al., 2014), ciliary beating is regulated by neurons. How animals regulate and control multiciliated surfaces is still unknown. The neuronal circuitry coordinating ciliary activity has not yet been described in any animal.

Elaborate ciliary coordination is best observed and studied in invertebrate ciliary swimmers (Arkett et al., 1987, Tamm, 2014), where ciliated cells often form into circumferential bands which are under neuronal control. Aiming to elucidate neuronal ciliary coordination, I used the larvae of the marine annelid, *Platynereis dumerilii* (Audouin & Milne-Edwards, 1834), as a model (Fischer et al., 2010) for my PhD studies. This marine polychaete has a biphasic life cycle, which includes a pelagic (free-swimming) larval phase that uses cilia for swimming (Figure 1D), and a benthic tube-dwelling adult phase. Ciliary beating emerges in the *Platynereis* larvae 20 hours post fertilization, with swimming becoming more coordinated in the next few hours. Due to their negative buoyancy, the vertical distribution of the larvae is determined by the sum of periods of active swimming (cilia are beating) and passive sinking (cilia are closed) (Chia et al., 1984). In this early trochophore larval stage the eyespots (which directly innervate the ciliated cells) control swimming and act as a sensory-motor unit (Jekely et al., 2008). By the second day of development, the larvae have two ciliary bands and can navigate in seawater by responding to environmental stimuli (Arendt et al., 2004). After only three days, multiple ciliary bands propel the animal forward, and it can utilize muscle-based turning to navigate more efficiently (Randel et al., 2014). The underlying neuronal circuit of larval swimming is unknown.

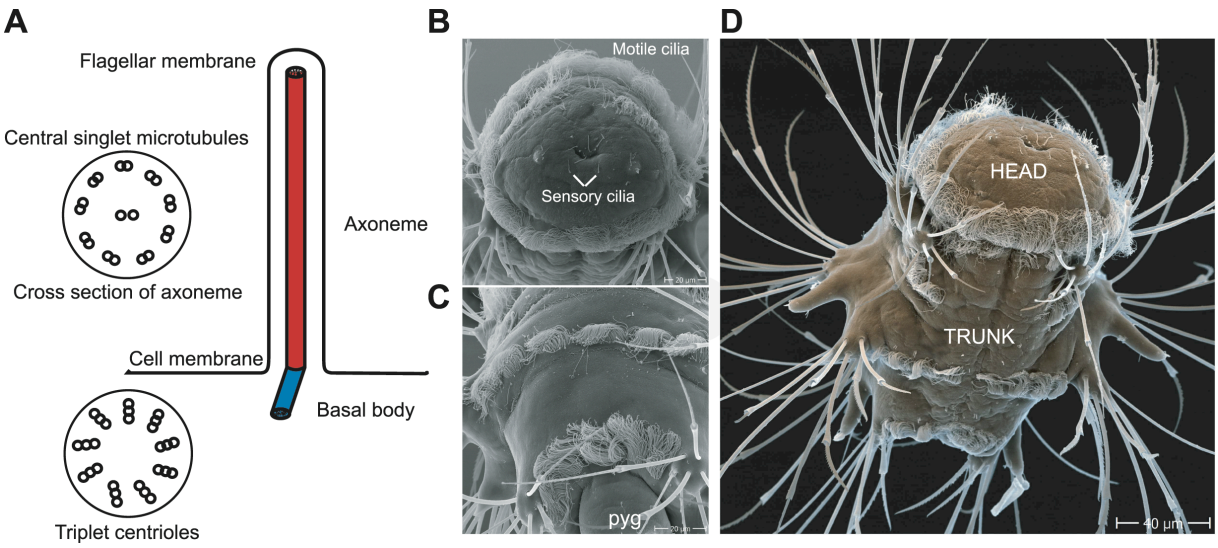

Figure 1. The structure of cilia and scanning electron micrographs of *Platynereis* larvae
(A) Schematic diagram of motile cilium structures. Cross sectional and longitudinal views of the relationship between the axoneme and the basal body. **(B)** Apical view of the three-day-old nectochaete larva. Sensory cilia cover the apical organ area and the tip of the growing antennae, while the prototroch and the akrotoch contain motile cilia. **(C)** Dorsal view of the three-day-old nectochaete larva. The trunk and the pygidium (pyg) are surrounded with multiciliated cells forming the ciliary bands along the body. **(D)** Ventral view of the three-day-old *Platynereis* larva. SEM image credits: Jürgen Berger (MPI for Developmental Biology).

In summary, *Platynereis* larvae (Fischer et al., 2010) use multiple segmentally arranged ciliary bands to swim and the ciliary bands are under neuronal control (Tosches et al., 2014) and can be influenced by neuropeptides and hormones (Conzelmann et al., 2011, Tosches et al., 2014). In the last decade *Platynereis* has also emerged as a powerful model for studying neural cell types and development (Tomer et al., 2010, Williams et al., 2017, Tessmar-Raible et al., 2007).

Full body connectomics and neuronal imaging

Creating a map of the brain, also known as a connectome (Hagmann, 2005), creates a complete structural database that allows us to look simultaneously at all neuronal connectivity patterns and thus all possible synaptic signaling pathways within the nervous system (Beyer et al., 2013, Kuceyeski et al., 2015). There are two main tools

for such studies, (1) diffusion magnetic resonance imaging (MRI) at the macroscale level, and (2) electron microscopy (EM) at the microscale level. The sufficient level of detail required to understand how brains work is unclear even today, thus many scientists argue that mapping synaptic connectivity or neuronal activity patterns in the brain might not hold all the answers to the questions of nervous system signaling, but it will certainly help to shed light on many mysteries of the brain and will bring us closer to our goal(s) (Leergaard et al., 2012). Unsurprisingly, the fields of connectomics and neuroscience are rapidly developing fields (Editorial, 2017a, Editorial, 2017b). A large amount of data has been contributed to these fields in recent years through technical advancements in electron microscopy and data storage and processing (Cardona, 2013). Apart from humans, many other organisms have been developed as models in the connectomics field, including the mouse (Bock et al., 2011), the fruit fly (Chklovskii et al., 2010), and the barn owl (Pena and DeBello, 2010). However, since even a mouse brain is approximately 100,000 times larger than the volume of tissue that is currently possible to image, the field of connectomics started small. The first connectivity diagram of an entire nervous system came from the nematode *Caenorhabditis elegans* (White et al., 1986, Emmons, 2015). Thirty years after the *C. elegans* brain, the tadpole larva of the sea squirt (*Ciona intestinalis*) (Ryan et al., 2016) became the second reconstructed nervous system, and showed fundamental new information can be found in small invertebrate nervous systems. The less than 200 nerve cells primarily form highly connected circuits linked together by a smaller number of long-range connections. This aspect can be found in the *C. elegans* connectome and other artificial networks, such as power grids and social networks. Both connectome works provided a connectional reference dataset for future comparative studies in the field for neuronal circuits.

Other partial connectome studies (Takemura et al., 2013, Ohyama et al., 2015, Takemura et al., 2017) come from insects, due to their relative small size and neuron number. These studies are driven by interest in parallels between invertebrates and vertebrates (Katz et al., 2013, Borst and Helmstaedter, 2015, Strausfeld and Hildebrand, 1999), and new technologies and databases (Chiang et al., 2011, Jenett et al., 2012, Costa et al., 2016).

Without a connectivity map, the brain is a black box for behavioral studies (Berkman and Lieberman, 2011). To tackle this problem, I turned to micro-connectomics to study the

nervous system. I focused on a small invertebrate larval nervous system for the aforementioned technical reasons and the following consideration.

To respond to the strongest criticism on micro-connectomics, that “circuit structure is different from circuit function” (Morgan and Lichtman, 2013), where the argument is that behaviors derive from the functional properties of the brain, I wanted to study neural circuits where I could overlay an activity map on the anatomical map, and I could identify neurons *in vivo* and record their activity during specific behaviors. While there is a plethora of approaches available to assign molecular identities to neurons (Brodfuehrer and Thorogood, 2001, Borst and Haag, 2002, Leonard, 2000, Shahidi et al., 2015, Achim et al., 2015, Van Dijck et al., 2013, Gotz et al., 1995, Molyneaux et al., 2007, Ekstrand et al., 2014, Sugino et al., 2006, Knight et al., 2012, Jiang et al., 2015, Chiu et al., 2014), and these are essential tools for neuron identification, the gap between the neurons and their function can only be bridged by monitoring the activity patterns of the same neurons and their partners (Tian et al., 2012). In order to record neuron activity in *Platynereis dumerilii*, I developed neuronal activity imaging in the larvae of this polychaete worm. Microinjection of single cell embryos had already been established in *Platynereis* (Zantke et al., 2014, Ackermann, 2003). Using this technique to inject a genetically encoded calcium indicator GCaMP6s (Chen et al., 2013), I was able to observe the neuronal activity with sufficient signal-to-noise ratio. To my knowledge, *Platynereis* is at present the only marine invertebrate where one can reliably record calcium transients from several larval stages using genetically encoded fluorophores.

For the *Platynereis* EM reconstruction, Reza Shahidi sectioned an entire three-day-old larva into 5056 serial sections to create a whole-body EM data set. Sections were 40 nm in thickness. All sections were imaged using a transmission electron microscope. The resolution of scanned images was 5.71 nm/pixel. Once the serial imaging was completed, images were montaged and aligned into a digital stack using TrakEM2 software (Cardona et al., 2012). Neurons, cellular structures and organelles of interest were traced, segmented, and 3D reconstructed using TrakEM2 and Catmaid software (Cardona et al., 2012, Saalfeld et al., 2009).

Introduction to peptidergic connectomes

We look at the nervous system as the organ that controls the activities of the body. These activities are carried out through interactions of the neurons connected to each other (Ramón y Cajal, 1889a). Signaling between neurons mainly occurs at specific sites, called synapses, which link neurons to each other, forming elaborate signaling networks (Sudhof and Malenka, 2008).

A second way neuronal cells can communicate with each other, which may be equally as important as synaptic signaling, is via releasing diffusible chemicals that reach other cells that can detect the signal by expressing specific receptors for the particular chemical molecule (Fuxe et al., 2013, Role and Berg, 1996, Hille, 1994). This is one method of non-synaptic signaling, as the information does not travel through synapses, it diffuses through the space between neurons. Some parts of the brain, such as the hypothalamus (Lechan and Toni, 2000), are regarded as neurosecretory centers because they primarily signal non-synaptically. Neurosecretory centers play an important role in behavior, metabolic processes, and other activities as these diffusible chemicals can also modify the activities of neurons through their synaptic connections, this is known as neuromodulation (Nadim and Bucher, 2014).

We know little about how neurosecretory centers work. Anatomical staining and connectome studies reveal the synaptic network but tell us little about non-synaptic transmission of peptides, monoamines, or hormones. The most common and diverse group of diffusible signaling molecules is the neuropeptides (Liu et al., 2008), which can act both as neurotransmitters and hormones. Neuropeptides are conserved between cnidarians and bilaterians (Jekely, 2013a, Bauknecht and Jekely, 2015). Bioactive peptides are stored within the cell in organelles known as dense-core vesicles, from which they are secreted upon a signal. Neuropeptides commonly act as ligands of G-protein coupled receptors (GPCRs) on a target cell's surface (Bradford et al., 2013). GPCRs are usually made up of seven transmembrane helices connected by short loops. The bioactive peptide ligand changes the conformation of the helices in the cell membrane. This conformational change activates G-proteins (guanine nucleotide-binding protein) inside the target cell. G-proteins upon activation dissociate and elicit further downstream signaling.

Recent functional studies show that the understanding of neuropeptide signaling is important (Bargmann, 2012, Marder, 2012) and necessary if we want to understand the contribution of this wireless network to nervous system signaling (Bentley et al., 2016, Schlegel et al., 2016, Stein et al., 2007, Thirumalai and Marder, 2002). While vertebrate neurosecretory centers make up a small fraction of the neurons of the entire nervous system, at present they are still several times larger than it is feasible to study. There has not been any attempt to map such a brain center as a whole in detail.

One of the earliest and more prominent neurosecretory centers of the early larval stages in *Platynereis* is the apical sensory organ (Nielsen, 2005, Nielsen, 2004). Annelid larvae and the larval stages of other marine invertebrates have an anterior sensory center, known as the apical organ, with a conserved molecular fingerprint and sensory-neuroendocrine structure (Hadfield et al., 2000, Byrne et al., 2007). Stainings revealed that this region is neurosecretory and peptidergic (Figure 2A-B) in nature (Marlow et al., 2014, Conzelmann et al., 2013b). The apical organ of *Platynereis* shows molecular similarities to the vertebrate counterpart, the hypothalamus, suggesting a common ancestry (Tessmar-Raible et al., 2007). Three days after fertilization, this region is populated by sensory neurons, which form a bulbous neuropil (Figure 2D-F), and a non-sensory ciliated cell with a crescent shape. At this stage, the larvae are ~250 µm long with ~1500 neurons in the head, potentially expressing 98 proneuropeptides. These proneuropeptides can be grouped from an evolutionary perspective into ancient eumetazoan-, bilaterian-, protostome-, lophotrochozoan- and annelid-specific families, and proneuropeptides found only in *Platynereis* (Bauknecht and Jekely, 2017, Conzelmann et al., 2013a). The relatively small size of the larva allows for its full ssTEM reconstruction, and for connectomics and behavioral studies.

Using electron microscopy and functional studies, I present the very first comprehensive analysis of a neurosecretory center, the anterior neurosecretory center of the larval *Platynereis dumerilii* (Figure 2C). Since the hypothalamus' role is to link the nervous system to the endocrine system in humans, I aim to show how the anterior nervous system in *Platynereis* interacts with the rest of the larval nervous system.

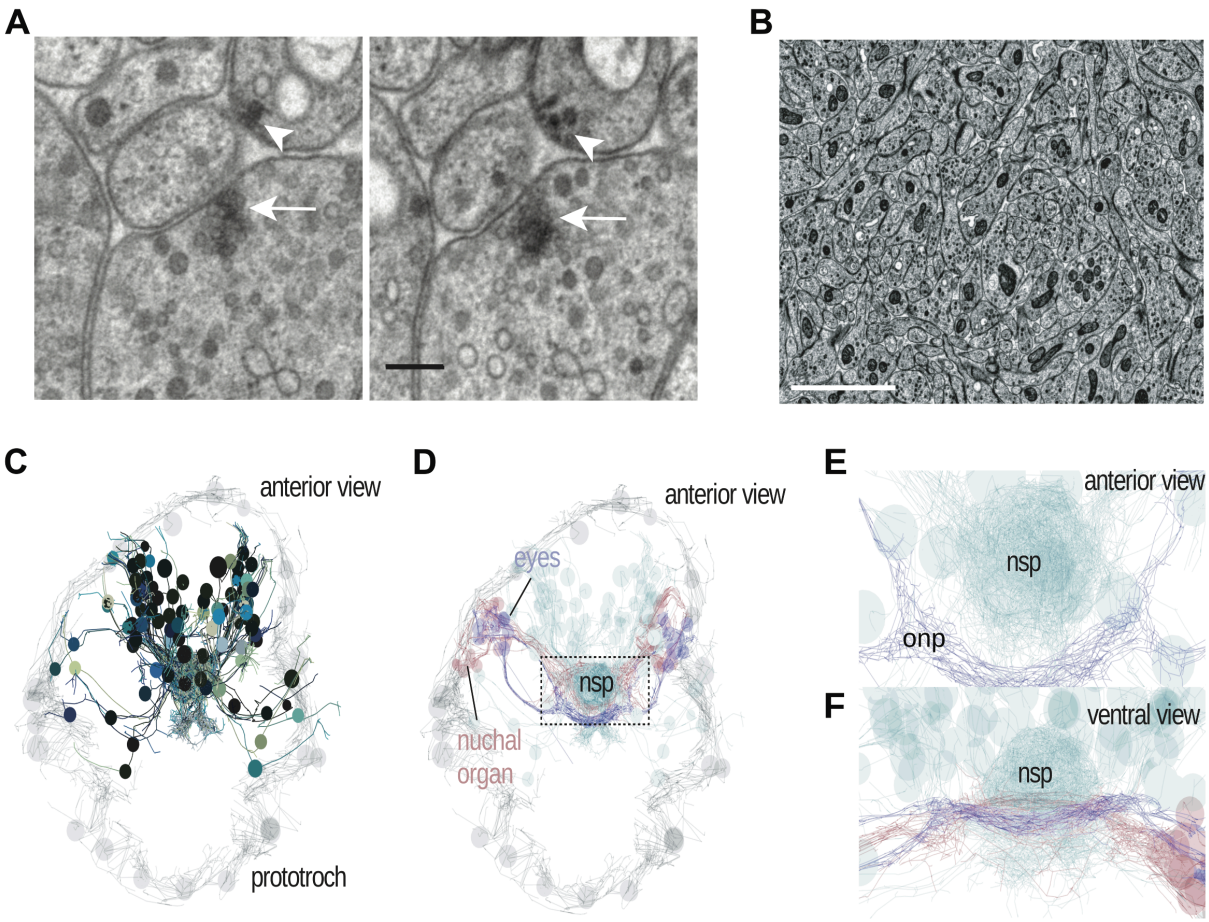

Figure 2. Transmission electron microscopy reconstruction of the anterior nervous system of *Platynereis* larvae

(A) Comparison of a cholinergic synapse (with transparent vesicles) of a ciliary photoreceptor (white arrow) to a peptidergic synapse (with dense-core vesicles) of a peptidergic sensory neuron (white arrowhead) in the apical nervous system (ANS). Two consecutive sections are shown. **(B)** Close-up view of the neurosecretory plexus. Axonal cross sections are full with dense-core vesicles. **(C)** Reconstructed ANS neurons (shades of blue) in the transmission electron microscopy dataset of a three-day-old larva, shown against a framework of reconstructed ciliated cells (light grey). **(D)** ANS neurons project to an apical neurosecretory plexus in the center of the head, which forms a small sphere dorsal and apical to the optic neuropil and nuchal organ neuropil. **(E-F)** Close-up views show the neurosecretory plexus in the neuropil. Abbreviations: nsp, apical neurosecretory plexus; onp, optic neuropil. Scale bars: **(A)** 200 nm, **(B)** 2 µm.

Aims of the thesis

What level of detail is sufficient to study nervous systems in order to understand how they work? The overall aim of my thesis is to shed light on the complexity of this question. In order to do this, I will use two examples: a functional characterization of the synaptic circuitry for ciliary locomotion, and the reconstruction of a primarily non-synaptic neurosecretory organ of a tiny marine larva.

Planktonic organisms migrate up and down the water column following the rhythm of the sun. While planktonic migration has substantial effects on the dynamics of saltwater and freshwater environments, we know remarkably little about how and why plankton migrate. Functional characterization of the underlying neuronal circuitry of aquatic locomotion in a planktonic ciliary swimmer will help us understand these processes in the ocean.

Non-synaptic signaling provides a new challenge in the study of nervous systems. We have to take into account that synaptic connectomes will not provide all the answers to understanding nervous system signaling. What happens when peptidergic signaling is involved in the neuronal signaling process?

To address these questions I studied the marine annelid *Platynereis dumerilii,* an emerging laboratory model organism. I used an ssTEM dataset of the three-day-old larva to reconstruct the functional circuitry for swimming and the main neurosecretory center of its brain. I established calcium imaging in the early larval stages and created a workflow to explore brain circuits and neuronal activity in single neuron detail.

The goals of my doctoral thesis are therefore to reconstruct the complete locomotory connectome for ciliary locomotion and to shed light on peptidergic signaling in the simple nervous system of the *Platynereis* larva.

Results

Summary of Publication 1

Csaba Verasztó, Nobuo Ueda, Luis A Bezares-Calderón, Aurora Panzera, Elizabeth A Williams, Réza Shahidi, Gáspár Jékely

Ciliomotor circuitry underlying whole-body coordination of ciliary activity in the *Platynereis* larva eLife 2017;6:e26000 DOI:10.7554/eLife.26000

The neuronal circuits for ciliary swimming have not yet been described in any animal. Here, I reconstructed and functionally analyzed the complete motor circuitry for ciliary locomotion in the planktonic larva of the marine annelid *Platynereis dumerilii*. I found that an extensive motor neuron network innervates ciliated cells in three-day-old larvae. Using transgenic labeling, immunohistochemistry, and immunogold labeling, I could group neurons by their neurotransmitter profiles. Using calcium imaging, the role of two neurotransmitters could be identified within the circuit.

Platynereis nectochaete larvae have segmentally arranged ciliary bands. Additionally, multiciliated cells cover chemosensory areas on the head. I used a whole-body ssTEM dataset of a three-day-old larva to identify and reconstruct all ciliary band cells and the motor neurons innervating them. Altogether, 80 ciliated cells were reconstructed, with 2055 synapses, implicating a large neuronal circuit in the coordination of ciliary beating.

When imaging ciliary activity in immobilized animals using differential interference contrast (DIC) imaging, I found that ciliary closures were synchronized across all the ciliary bands. The only ciliated cell that did not arrest its cilia with the other cells was the apical crescent cell. In fact, this cell was beating in an anti-synchronous manner compared to the other ciliated cells. The crescent cell has fewer cilia, but the flow that it generates is likely strong enough to sample the water for sensory functions during the time when the animal arrests its locomotory cilia and is not swimming.

To investigate beat coordination and the cellular mechanism behind ciliary arrests, I used calcium imaging to look at calcium signals in each cell of the ciliary bands. I ubiquitously expressed GCaMP6s, a genetically encoded fluorescent calcium indicator, using RNA microinjections in *Platynereis* eggs one hour post fertilization. I detected a

synchronous periodic increase of fluorescence in every ciliary band cell accompanying the arrest of cilia. I found that ciliary activity correlates with the time derivative of fluorescence. As long as calcium levels increase, cilia stay closed. As soon as fluorescence intensity starts to decrease, cilia resumed beating. In the case of the crescent cell, the ciliary arrests co-occurred with the decrease of fluorescence. In accordance with this, ciliary activity did not correlate with the absolute levels of [Ca^{2+}].

Next, I identified and reconstructed all neurons that were presynaptic to any of the multiciliated cells in the larva. By definition I call these neurons ciliomotor neurons, or ciliomotors. Combining transgenic labeling, immunohistochemistry, and serial immunogold labeling (siGOLD) (Shahidi et al., 2015), I could assign a neurotransmitter and/or a neuropeptide to most of the ciliomotor neurons. Based on these marker molecules I could group the reconstructed motor neurons into cholinergic, serotonergic, and mixed catecholaminergic and/or peptidergic neuron groups.

To ascertain which neurons express acetylcholine, first I used the registration of gene expression pattern based on WMISH for the cholinergic marker gene *ChAT*. Furthermore, Nobuo Ueda developed a transgenic reporter construct of the *sGCbeta1* gene that is co-expressed with *ChAT*. Additionally, I could confirm the cholinergic identity of specific neurons with pharmacological experiments (see below).

I identified 11 cholinergic ciliomotors in the larva. For a comprehensive list of cholinergic ciliomotors, I included the previously described ventral motor neurons (Randel et al., 2014). I improved the previous reconstruction of these neurons. I also included the two rhabdomeric photoreceptor cells of the larval eyespots, which also directly innervate some of the prototroch cells. Three biaxonal neurons, a single unpaired cilomotor neuron in the head - the MC neuron - and a pair of trunk ciliomotor neurons - the Loop neurons - were also identified as cholinergic in nature. I define neurons as biaxonal when a neuron has two main axons (usually to innervate left and right or posterior and anterior sides of the animal). These neurons have larger axons than the average axon length and span across the entire larva.

The MC neuron's soma is slightly to the left of the exact center of the *Platynereis* larval brain. The axons of the MC neuron project to the prototroch where they divide into dorsal and ventral branches and run around the inner sides of the prototroch rings, innervating every prototroch cell. With 343 synapses, the MC neuron is the most

synapse-rich neuron in the entire animal (unpublished data); 336 of these synapses target each of the 23 prototroch cells (3-26 synapses per prototroch cell).

The cell bodies of the Loop neurons are located along the left and right side of the ventral nerve cord in the first trunk segment. This segment becomes part of the head during cephalic metamorphosis (Fischer et al., 2010). The Loop neurons each project one axon into the nerve cord, which runs down on the lateral edge of each side of the nerve cord, and sends branches to each paratroch region, innervating every multiciliated cell along the ipsilateral side of the larva. The second axon of each of the Loop neurons enters the nerve cord in the anterior direction, joins the prototroch nerve ring and runs down the dorsal side of the animal, meeting with the first axon and thus forming a loop. The second axon also sends branches to the ciliary bands on the ipsilateral dorsal side, and to the other ciliated structures (nuchal cilia, crescent cell). The Loop neurons are the only cholinergic neurons that innervate the crescent cell and the ciliated cells of the nuchal organ. This innervation occurs via the anterior axons of the Loop neurons. The only ciliary bands that are not innervated by the Loop neurons are the metatroch bands (eight cells). It is also important to note that not all prototroch cells receive innervation from the Loop neurons. While the ventral motor neurons and the rhabdomeric photoreceptors have been previously described (Jekely et al., 2008, Randel et al., 2014, Randel et al., 2015) as playing a role in positive phototaxis, the EM reconstruction of these cells was not fully completed in the previous publications. By completing a more detailed reconstruction of these cells, I could confirm their synaptic role in the nervous system and complete the cholinergic motor neuron set for the three-day-old larva. Having a more complete reconstruction helped us to determine the total number of sensory-ciliomotor neurons in the *Platynereis* larva, which were previously predicted to be a main motoric input for cilia (Conzelmann et al., 2011). I confirmed that only three sensory-ciliomotor neurons exist in the entire three-day-old larval body, two of which are the cholinergic photoreceptor cells in the larval eyes.

I was unable to confirm the molecular identity of two cells in the ciliomotor connectome. This motor neuron pair is likely cholinergic in nature based on their position in the circuit and the *VAChT in situ* expression pattern, but I could not resolve the average gene expression pattern of *VAChT* to single cell resolution, despite using the transgenic promoter expression of *sGCbeta1*. This motor neuron pair contralaterally innervates the

metatrochs (which were not synaptically contacted by the Loop neurons) and some of the prototroch and anterior paratroch cells. The function of this motor neuron pair will be elucidated in future experiments (e.g. calcium imaging in older, actively feeding larvae).
In summary, the cholinergic circuitry is the largest of the three groups of ciliomotor cells both in neuron number (11), and synapse count (1347).
The second largest group of ciliomotor cells was the serotonergic group. I found five serotonergic ciliomotors with 437 synapses on ciliated cells. I used staining with an antibody raised against serotonin to identify the spatial distribution and identities of the neurons. I also used mosaic transgenic labeling to unambiguously identify the neurons and confirm their morphologies by comparing the fluorescent promoter expression pattern with the EM reconstruction. To fluorescently label the neurons, I used a 5 kb upstream fragment of the *TrpH* gene, a serotonergic marker driving the fluorescent reporter tdTomato.
The first pair of serotonergic ciliomotors that appears during larval development is located in the head. The somas are located close to the ciliary photoreceptor cells, while their axons cross the midline and enter the prototroch nerve ring, innervating the prototroch cells on the contralateral side. These two neurons innervate every prototroch cell, therefore I consider them to be the serotonergic counterpart of the MC neuron. Although these serotonergic ciliomotors send an extra axonal branch down the nerve cord, they did not innervate any of the other ciliated cells.
Similar to the anatomy of the cholinergic circuitry, I identified a pair of serotonergic neurons in the trunk, hence the name “Ser-tr” cells, with similar axonal morphology to the Loop neurons. The somas of the Ser-tr cells are located in the same body segment as the Loop neuron somas, just above the first commissure of the ventral nerve cord. These cells are also biaxonal and bilaterally symmetrical. One axon crosses the midline and innervates ciliated cells on the upper contralateral side of the larva, then runs down dorsally to innervate the dorsal contralateral paratroch cells. The other axon runs down the nerve cord on the ipsilateral side and consecutively innervates the ventral paratroch bands. The two axons thus form a loop with each other across the sagittal plane.
The fifth serotonergic ciliomotor is also a sensory-motor neuron. The soma of this ciliomotor is in the pygidium and sends a sensory dendrite with two penetrating sensory cilia towards the posterior end of the animal. This serotonergic sensory-motor neuron is

also biaxonal with two axons running up the two sides of the nerve cord. Upon reaching the prototroch ring nerve, they split into three axonal branches; two branches run along the prototroch nerve ring in both directions, and the third branch runs towards the neuropil.

The third group of ciliomotors consists of three asymmetric biaxonal ring neurons that were initially grouped based on their anatomy. Their somas are all located at the level of the main ciliary band, two underneath and one above; their axons traverse the prototroch nerve ring. The ventral-lateral ciliomotors express the dopaminergic marker *tyrosine-hydroxylase*, one of them also expresses the noradrenergic marker *dopamine-beta-hydroxylase*. As all three ciliomotors are also full of dense-core vesicles, suggestive of a peptidergic mode of signaling in the connectome. The third member of this ciliomotor group is purely peptidergic. This ciliomotor group is directly connected to the main ciliary band and reciprocally connected to both the cholinergic and serotonergic ciliomotors that innervate the prototroch.

In addition to grouping the ciliomotors by their molecular identities, modularity analysis of the entire ciliomotor connectome revealed three strongly connected groups which could be distinguished based on the types of ciliated cells they innervate. The first module contains cells that predominantly innervate the prototroch cells, while the second and third modules include cells innervating ciliated cells on the left and right body side, respectively. Each group contains serotonergic and cholinergic neurons, while the first group incorporates all the catecholaminergic and peptidergic neurons.

To understand whether the ciliomotor neurons drive ciliary locomotion, I used calcium imaging to record their activity. For imaging, I used 1-2.5 days old animals because at this stage of development the ciliomotor neurons are fully developed, while the muscles are not yet fully present or properly innervated, which allowed me to image the larvae without substantial motion artifacts caused by muscle contractions.

I found that cholinergic neuron activity is periodic and strongly correlates with ciliary closures. I measured the median cycle length of the MC neuron's activity period: 41 of 96 larvae had a cycle length of 50-100 sec. To test whether the MC neuron is responsible for the rhythmic closures, I ablated this neuron, the main motor input to the prototroch, and looked at subsequent changes in ciliary closures. MC neuron ablations eliminated rhythmic activity in the prototroch cells, but did not completely abolish

closures. To test the effect of acetylcholine on the prototroch, I incubated larvae in alpha-bungarotoxin, a specific blocker for nicotinic acetylcholine receptors. In this experiment, the MC neuron retained its rhythmic activity, while ciliary arrests disappeared. From this experiment I could conclude that cholinergic signaling is not required for the generation of the rhythm of the cilomotor circuit, but is essential for ciliary closures.

I used calcium imaging to ascertain the function of the serotonergic neurons. Both the head serotonergic neurons and the two serotonergic neurons in the ventral nerve cord showed rhythmic activity; this activity was inversely correlated with cholinergic neuron activity and ciliary closures. Next I treated larvae with serotonin to study the effect of this neurotransmitter on larval behavior. After the treatment, larvae showed fewer ciliary closures and increased ciliary beat frequency compared to control larvae. This suggests that serotonin have an acetylcholine-antagonistic effect both in the ciliary band cells and in the ciliomotor circuit.

Lastly, calcium imaging revealed that the catecholaminergic and/or peptidergic group of ciliomotor neurons also displays a spontaneous rhythmic activity pattern. Two of these neurons were activated in synchrony with the ciliary band, while the third neuron's activity was inversely correlated with the ciliary band. I could detect this activity in larvae as early as 24 hours post fertilization. While I could not unambiguously identify the source of the rhythmic pattern, at this developmental stage only the three catecholaminergic neurons, the MC neuron, and the serotonergic neuron in the pygidium (although I could never see rhythmic activity in this neuron) are present from the three-day-old ciliomotor circuitry. To elucidate what the source of the pattern generation is on a cellular level, more experiments are needed.

In summary, the coordination of cilia in *Platynereis* larvae is achieved through a dedicated ciliomotor nervous system with different motor neuron types and neurotransmitters assigned to different tasks. The circuitry is one functional motoric unit with its own spontaneous activity, which is modulated by the rest of the brain (Conzelmann et al., 2011, Randel et al., 2014, Jekely, 2013b, Williams et al., 2017).

Summary of Publication 2

Elizabeth A Williams, Csaba Verasztó, Sanja Jasek, Markus Conzelmann, Réza Shahidi, Philipp Bauknecht, Gáspár Jékely

Synaptic and peptidergic connectome of a neurosecretory center in the annelid brain

DOI:10.1101/115204

Animal brains contain high numbers of neurosecretory cells whose peptidergic signaling molecules travel farther than the molecules acting at synapses to fulfill their regulatory role in development, physiology, and behavior. While we know a lot about these seemingly ancient peptidergic signaling molecules (Watanabe et al., 2009, Grimmelikhuijzen et al., 1991, Mackie and Stell, 1984, Mitgutsch et al., 1999, Anderson et al., 2004, Fujisawa, 2008), few studies have detailed the signaling networks occurring within neuroendocrine centers. In this work, I took on the challenge of reconstructing and interpreting the function of a neurosecretory brain center. Using the same EM dataset with which I reconstructed the ciliomotor circuitry and will ultimately reconstruct the entire nervous system of the three-day-old marine annelid *Platynereis dumerilii*, I could identify an anatomically distinct area in the neuropil, the anterior neurosecretory plexus (ANS).

The ANS neuropil (Figure 2B) is a bulbous region formed by neurites apical to the rest of the brain, and does not intermingle with the nuchal organ or optic neuropils (Figure 2D-F) (Randel et al., 2014, Randel et al., 2015, Shahidi et al., 2015). The ANS is also easily separable from the other neuropils by the high density of dense-core vesicles transported throughout ANS nerve projections. By tracing all neurites that project to the neurosecretory plexus and their corresponding somas, I reconstructed every neuron whose axons make up the ANS (Figure 2C). I could identify 70 sensory neurons and eight projection interneurons (i.e. they project their axons out of the ANS). The sensory neurons have extensive axonal arborizations restricted to the ANS region. The axons of the interneurons also branch extensively in the ANS, and then extend into other brain regions. Based on morphological criteria (e.g. number of sensory cilia, bilateral symmetry, and extended sensory membrane structures) I could group the sensory neurons into >20 different cell types which likely have different sensory modalities. The

eight projection interneurons are all postsynaptic to four ciliary photoreceptor cells, and a set of four of these interneurons express *nitric-oxide synthase* (NOS). These NOS-expressing interneurons are presynaptic to the other four interneurons, which express the neuropeptide RGWamide. Identified neuron pairs displayed bilaterally symmetric arborization morphologies, revealing a fine-scale order in the overall structure. The most prominent feature of the ANS is the low number of synapses in this region. 33% of the neurons have 0-2 synapses. Moreover the axons of these neurons are filled with dense-core vesicles, and their dense branching provides them with a large surface area for volume-transmission. With the exception of the projection interneurons and the ciliary photoreceptors, the majority of the ANS neurons form peptidergic synapses rather than neurotransmitter-containing synapses. Peptidergic synapses are smaller than neurotransmitter-containing synapses and have electron-dense rather than transparent vesicles (Figure 2A). The overwhelming majority of synapses are formed between the four cholinergic ciliary photoreceptors and the projection interneurons, which means a non-random and sparse graph for the overall neuronal connectivity in the ANS.

To better understand the peptidergic nature of the ANS, Elizabeth Willams and I looked at the neuropeptides expressed in this area. Elizabeth Williams and I looked at the expression patterns of 51 of 98 proneuropeptides (Conzelmann et al., 2013a) in the gene expression atlas of the three-day-old *Platynereis* (Asadulina et al., 2012). Elizabeth Williams and I found that the ANS was the region in the larva that was expressing the highest number of proneuropeptides. Using *in situ* hybridization expression patterns and a single-cell transcriptome database (Achim et al., 2015), Sanja Jasek, Elizabeth Williams and I calculated a list of neuropeptides expressed in the ANS: 51 neuropeptides in two-day-old larvae, and 54 neuropeptides in three-day-old larvae. Finally, by comparing unique ciliary morphologies between WMISH and the EM dataset, Elizabeth Williams and I could map neuropeptide expression to 25 reconstructed ANS neurons.

To analyze the peptidergic signaling network in the *Platynereis* larva, Elizabeth Williams and I used the *Platynereis* deorphanized GPCR database (Bauknecht and Jekely, 2015) and the aforementioned single-cell transcriptome database to map the expression of neuropeptides and their specific GPCRs on a two-dimensional virtual map of the *Platynereis* brain. The expression patterns of 80 proneuropeptides and 23 deorphanized

GPCRs were mapped on the 107-cell spatial map of the brain. It is important to note that this map can only visualize potential peptidergic signaling networks, as it contains information about transcript rather than protein levels. It was possible to correlate 15 cell nodes to the reconstructed ANS neurons by comparing the WMISH expression patterns of different neuropeptides. Interestingly, similar to the synaptic connectome, the peptidergic connectome is sparsely connected, with specific wiring and non-overlapping nodes for each peptide-receptor pair. Elizabeth Williams and I found that a pair of these cells were expressing up to 24 neuropeptides. Conversely, by expressing more than one GPCR receptor, nodes in the map can be targeted by heterogeneous populations of cells via the peptidergic network, creating a small-world network (Watts and Strogatz, 1998) supplementary to the synaptic network.

The main relay connecting the ANS to the synaptic brain is two pairs of RGWamide-expressing projection interneurons, which also express many GPCRs and have many post-synaptic partners outside the ANS. One of the main targets of these RGWamide interneurons is the pair of serotonergic ciliomotor neurons in the head involved in ciliary beating (see previous chapter for more details). I combined calcium imaging with pharmacological treatment to test whether these interneurons can relay peptidergic signals from the ANS to their partners outside of the ANS. The two pairs of RGWamide-expressing interneurons also express seven deorphanized GPCRs, including a receptor for achatin. I used achatin to test whether this neuropeptide can act as a neuromodulator and influence the downstream network of the projection interneurons. The correlation analysis of the downstream neuronal activity showed that only the active form of achatin (D-achatin, compared to the inactive L-achatin control) changed the activity of the network. D-achatin coupled the activity of the relay interneurons to the active phase of head serotonergic ciliomotors and strengthened the serotonergic rhythmic activity, which affects the locomotor output of the cilia. This experiment indicates how and through which modes of signaling sensory input can affect the autonomic activity of *Platynereis* ciliary locomotion.

In summary, I reconstructed the ANS of the three-day-old *Platynereis* larva, discovering a complex non-synaptic network, and I could show how this peptidergic center modulates the synaptic circuitry. This is only one example of how a peptidergic center interacts with the rest of the nervous system. More works are needed to have a

comparative overview and clear understanding of neurosecretory center development, evolution and function.

Discussion

A STOP and GO circuit for the coordination of multiciliated surfaces

In this work I described the way larvae of the marine annelid *Platynereis dumerilii* control swimming and regulate their position in the water. Ciliary swimmers often spend days to weeks/months swimming in open water *(Young et al., 2003)*. Their vertical distribution is influenced by light, temperature, food availability, developmental stage, and other environmental factors. It has been observed that many planktonic organisms alternate between active upward swimming and passive sinking to maintain optimal depth (Chia et al., 1984, Maldonado, 2006, Nielsen, 2004, Nielsen, 2005). Previous work from the Jékely lab implicated that peptidergic sensory neurons directly translate sensory cues to locomotor output by altering ciliary beating frequency and phases of swimming and sinking (Conzelmann et al., 2011). Here, I show that *Platynereis* larvae have a sophisticated yet simple autonomic motor neuron network capable of synchronizing cilia and creating the behavioral repertoire of planktonic vertical migration. Previous studies showed that swimming of *Platynereis* larvae is regulated by neuromodulators such as neuropeptides and melatonin (Conzelmann et al., 2011, Conzelmann et al., 2013a, Tosches et al., 2014). These neuromodulators are often expressed by sensory neurons and inhibit or elicit ciliary closures. I showed here that *Platynereis* larvae have specific motor neuron groups with separate tasks. Therefore the neuromodulators can specifically regulate one or multiple groups of ciliomotors to create a rich behavioral repertoire. In accordance with this, I have found several regions with microtubule-free twigs (Schneider-Mizell et al., 2016) on these motor neurons, which are the principal site for synaptic input and candidate areas for fast synaptic regulation. For example, apical mechanosensory neurons synapsing on twigs of the MC neuron axons to elicit immediate ciliary arrest when bumping into physical barriers, or interneurons innervating the serotonergic ciliomotors in a heavily branched area particularly rich in synapses to activate escape responses to harmful stimuli. Either through slower peptidergic input or through fast synaptic transmission, the modular organization of the ciliomotor circuitry

allows precise regulation of swimming.

The modularity of the ciliomotor circuit suggests that there is a rhythmic pattern of activation with two alternating circuits behind the alternating phases of swimming and sinking. In one phase, a dopaminergic, a peptidergic and several cholinergic neurons are activated together with the ciliary band cells, causing ciliary arrest. In the other phase, a noradrenergic motor neuron and several serotonergic neurons are active and the cilia beat.

The pharmacology experiment with serotonin showed that larvae respond to serotonin with increased ciliary beating frequency and fewer ciliary closures. This indicates that serotonin can act directly on the cholinergic neurons and on the ciliated cells, an action that is mirrored by the hierarchy of synaptic connectivity, where serotonergic ciliomotors are directly presynaptic to both ciliated cells and cholinergic ciliomotors. It is also possible however that serotonin can inhibit the pacemaker activity through the catecholaminergic and peptidergic neurons, which will then increase the elapsed time between the ciliary closures. The increase in beat frequency suggests that serotonin is released at the ciliated cells, however whether serotonin is released at synapses or through volume transmission and diffusion remains an open question. Previous light-microscopic and electron microscopic immunocytochemical studies demonstrated intravesicular serotonin immunoreactivity, thus it is possible to answer this question.

In *Platynereis* larvae, phases of both swimming and sinking are controlled at the motor neuron level. The connectome and imaging data suggest that the interaction of the catecholaminergic and peptidergic motor neurons is involved in the generation of the ciliary beating and closing rhythm. This theory is supported by several observations. The catecholaminergic and peptidergic neurons have distinct transmitter profiles that suggest antagonistic reciprocal signaling. The catecholaminergic and peptidergic neurons are presynaptic or reciprocally connected to the other ciliomotor neurons. Their rhythmic activity is already present at a developmental stage where the entire brain consists of less than 20 differentiated neurons. The MC and the Loop neurons are not directly synaptically connected to each other, yet they activate synchronously.

I cannot exclude however the possibility that other neurons are also involved in the generation of the ciliary rhythm. I found interneurons that may play a role in relaying the rhythm to the cholinergic ventral motor neurons that also show positive correlation with

ciliary closures (unpublished data). The precise identification of the pacemaker neurons would require further experiments. Ideally one should look at each candidate neuron isolated from any presynaptic input by severing its axons. Preliminary studies deemed this experiment to be complicated, as it is very hard to ablate axons without damaging other axons (axons of these neurons are part of a large nerve bundle, the ventral nerve ring, and they are likely to be serving as axon guidance cues during early development). Further, previous attempts of cutting one axon of the MC neuron rendered the neuron not viable.

My results suggest that the MC neuron and the two Loop neurons in combination are capable of closing all the cilia except the metatroch cilia, which are only innervated by a pair of motor neurons (also assumed to be cholinergic in nature) and serotonergic neurons. The metatroch is a postoral ciliary band and is primarily used in feeding in other invertebrate larvae. It beats in the opposite direction as the preoral prototroch cilia (Nielsen, 2005, Pernet and Strathmann, 2011). I was unable to image any activity from the putatively cholinergic motor neurons innervating this ciliary band, perhaps because *Platynereis* larvae will only start feeding much later in development, usually 5-6 days after fertilization.

Several ciliomotor neurons showed biaxonal morphology, which was suggested to be important in ciliated larvae by others (Temereva and Wanninger, 2012, Temereva and Tsitrin, 2014). These neurons span twice the entire body length of the larva, but there is little information regarding them in the literature. To the best of my knowledge, biaxonal motor neurons are uncommon or rare in vertebrates and fly, but are a common feature in the *C. elegans* nervous system. More comparative studies are needed to elucidate the evolutionary origin of biaxonal motor neurons, and understand their functional role, and whether they are ancient motifs of early bilaterian nervous systems.

In both protostomes and deuterostomes with ciliary structures, ciliary regulation by motor neurons expressing serotonin, catecholamine and acetylcholine has been reported many times (Hay-Schmidt, 2000, Stach, 2005, Stach, 2002, Friedrich et al., 2002, Kempf et al., 1997, Wanninger et al., 2005, Croll et al., 1997, Schmidt-Rhaesa et al., 2016, Nezlin, 2000, Raineri, 1995). Thus, my study fits well with other works, although no previous study could combine these neuronal units into a functional circuit. It is still an open question whether these seemingly similar ciliary locomotor systems

originated from a common ancestor or evolved multiple times independently.

On the wireless components of the larval brain

In my second study, I introduced the ANS, a neurosecretory center in the *Platynereis dumerilii* larva. The forte of an EM reconstruction is that it is comprehensive; one can reconstruct every cell at nanometer resolution. Combining this data with gene expression profiles of single cells allowed me to put landmarks on the still unknown map of peptidergic signaling. With the help of the *Platynereis* single-cell transcriptome resource we could uncover a portion of the potential peptidergic communication network in the ANS. With a larger dataset, one could potentially extend the network between the ANS and the rest of the body, and compare different developmental stages or even closely related species. Uncovered network edges (between two non-synaptically connected neurons) can be tested experimentally, as I have shown here with an example of achatin signaling modulating the downstream circuitry.

Important parallels can be drawn between the peptidergic and the synaptic brains. An overall sparse connectivity is thus far a common theme of every connectome study (Eichler et al., 2017, Ryan et al., 2016, Randel et al., 2014, Randel et al., 2015). In my study, the uncovered peptidergic network and the low degree of synaptic connectivity within the ANS suggest a “classical neurosecretory center” with very few synapses. The synapses found in the network mainly cluster to the few interneurons that are interconnected among themselves and project the ciliary photoreceptors’ signal to other brain regions. This suggests that the ANS is a semi-closed peptidergic network, and most peptidergic connections occur within the ANS. The large number of peptide receptors expressed within the ANS compared to the rest of the brain supports this conclusion. Taken together with other works (Campbell et al., 2017), neurosecretory centers show an unexpected level of complexity with their own “small world rules”.

One of the most exciting implications of this finding is the potential for combinatorial signaling. Neurons expressing multiple peptides and receptors can receive and release signals in a combinatorial manner, similar to transcriptional regulators (Munsterberg et al., 1995, Flores et al., 2000), thus a small number of peptides can create a large variety of unique signals. This potential for signaling complexity within the ANS goes beyond

the conventional definition of neuroendocrine centers, where cells release messenger molecules to the surrounding body upon neuronal input.

The overall neuronal anatomy of the *Platynereis* larva, i.e. a small sensory-neurosecretory center, the dual peptidergic and synaptic signaling, and the projection interneurons that connect to the rest of the nervous system, make the ANS a small yet sophisticated organ with which to study early nervous system origins. I found that in *Platynereis* the ANS is both neurosecretory and is synaptically connected to the locomotor system, similar to the apical sensory center's proposed mode of signaling in the bilaterian forebrain theory (Tosches and Arendt, 2013). My data support this chimeric brain model, which proposes the dual evolutionary origin of the bilaterian nervous system. The ANS is an apical, photosensory-neurosecretory subsystem controlling body physiology via the release of neuropeptides. The ANS is also clearly demarcated from the synaptic brain that regulates muscle-based locomotion. If the chimeric bilaterian brain hypothesis stands true, the *Platynereis* ANS is an ideal model for studying the ancient role of neuropeptides and neurohormones in animals. One can use the ANS to model the evolution and development of the vertebrate forebrain (Tessmar-Raible, 2007, Tessmar-Raible et al., 2007).

In the *Platynereis* ANS, we find the ciliary photoreceptors and other sensory neurons expressing the *c-opsin* gene. Ciliary opsins are light-sensitive proteins expressed in both the vertebrate retina (Arendt et al., 2004, Lamb et al., 2007) and in invertebrate ciliary photoreceptors (unpublished data). Previous works (Tosches et al., 2014, Arendt et al., 2004) postulated that the ciliary photoreceptors function in non-visual light detection for regulating circadian cycles in *Platynereis*. I find the idea interesting that one ancient role of apical sensory centers, such as the apical organ in invertebrates, was non-visual light perception to control e.g. circadian rhythms and the release of developmental hormones.

The reconstruction of the *Platynereis* ANS confirmed the existence of many sensory neurons described as the central cells of the *Platynereis* apical organ (Marlow et al., 2014, Fischer et al., 2010). Not all cells of this apical organ (Marlow et al., 2014) project to the ANS neuropil though. Mechanosensory cells in this area bypass this neurosecretory center and synapse on interneurons of a different synaptic circuit. In general, the putative mechanosensory neurons of the three-day-old larva primarily

possess many synapses and seem to lack dense-core vesicles, which would be an indication for peptidergic communication.

I also found that the ANS could regulate the ciliomotor neurons. I could not however find a regulator of the contractile motor system or the somatic motor system. It is however possible that the newly developing contractile motor system in *Platynereis* is also regulated by the ANS later in development (Dockray, 2004, Wicher et al., 2007). From an evolutionary and developmental point of view, ciliary locomotion is more ancient than muscle-based locomotion. Further experiments need to be conducted on older larval stages to test this.

Two studies (Jekely, 2013a, Mirabeau and Joly, 2013) concluded that the urbilaterian ancestor had a nervous system with many ancient peptide receptor pairs that appeared together with the ancient bilaterian body plan. Other studies (Nikitin, 2015, Smith et al., 2014) postulated that neurosecretory cells and peptidergic signaling were already present in the first metazoans and before the first nervous systems. In the primitive chordate amphioxus, the neuronal tube contains mostly synaptic neurons, except in the median portion of the cerebral vesicle, which is populated by the neurosecretory cells (Candiani et al., 2010). Taken together, both *Platynereis* and amphioxus show nervous system centralization with identifiable subsystems (Lacalli and Kelly, 2000). More detailed studies on basal metazoans (Placozoa, sponges, cnidarians, ctenophores) should follow suit to shed light on early nervous system evolution.

In their discussion of “signals without synapses and synapses without signals”, Morgan and Lichtman (Morgan and Lichtman, 2013) suggest that it is not possible to infer the signaling pathways of the brain and neurosecretory signaling from the anatomical wiring diagram of the brain alone. While this is certainly true, conversely, the connectome of the nervous system is a complete experiment (one can look at all possible connections), and provided me invaluable information and landmarks during the reconstruction of synaptic and non-synaptic wiring of the ANS. It is more reliable to map the neuronal chemical partners via peptide receptor pairs and transcriptome data, and overlay this network of real and potential signaling partners on an independently reconstructed neuron network. Overlaying the diagram of the peptidergic network on the synaptic network created through EM reconstruction does not confirm a functional connection between neurons, but it helps to make sense of the data and design experiments

accordingly. I want to emphasize here that the peptidergic connectome, similar to the synaptic connectome, does not replace physiological and pharmacological experiments. EM reconstruction of high-resolution, three-dimensional, static maps of nervous systems are the first step towards dynamic maps of active neuronal processes. They are more than the modern day‘s sparse labeling of Golgi stain (Golgi, 1898a, Golgi, 1898b, Ramón y Cajal, 1889b, Ramón y Cajal, 1889a) as they contain quantitative information on wiring patterns between neuron classes. They serve as diagrams and models that help us to understand and marvel at the complexity of nervous systems. They are also the frameworks of future experiments to test functional connections and peer into the details of how brains work.

References

ACHIM, K., PETTIT, J. B., SARAIVA, L. R., GAVRIOUCHKINA, D., LARSSON, T., ARENDT, D. & MARIONI, J. C. 2015. High-throughput spatial mapping of single-cell RNA-seq data to tissue of origin. *Nature Biotechnology,* 33**,** 503-U215.

ACKERMANN, C. F. 2003. *Markierung der Zelllinien im Embryo von Platynereis. .* University of Mainz.

ANDERSON, P. A. V., THOMPSON, L. F. & MONEYPENNY, C. G. 2004. Evidence for a common pattern of peptidergic innervation of cnidocytes. *Biological Bulletin,* 207**,** 141-146.

ARENDT, D., TESSMAR-RAIBLE, K., SNYMAN, H., DORRESTEIJN, A. W. & WITTBRODT, J. 2004. Ciliary photoreceptors with a vertebrate-type opsin in an invertebrate brain. *Science,* 306**,** 869-71.

ARKETT, S. A., MACKIE, G. O. & SINGLA, C. L. 1987. Neuronal Control of Ciliary Locomotion in a Gastropod Veliger (Calliostoma). *Biological Bulletin,* 173**,** 513-526.

ASADULINA, A., PANZERA, A., VERASZTO, C., LIEBIG, C. & JEKELY, G. 2012. Whole-body gene expression pattern registration in Platynereis larvae. *Evodevo,* 3.

AVIDOR-REISS, T., MAER, A. M., KOUNDAKJIAN, E., POLYANOVSKY, A., KEIL, T., SUBRAMANIAM, S. & ZUKER, C. S. 2004. Decoding cilia function: Defining specialized genes required for compartmentalized cilia biogenesis. *Cell,* 117**,** 527-539.

BARGMANN, C. I. 2012. Beyond the connectome: How neuromodulators shape neural circuits. *Bioessays,* 34**,** 458-465.

BAUKNECHT, P. & JEKELY, G. 2015. Large-Scale Combinatorial Deorphanization of Platynereis Neuropeptide GPCRs. *Cell Reports,* 12**,** 684-693.

BAUKNECHT, P. & JEKELY, G. 2017. Ancient coexistence of norepinephrine, tyramine, and octopamine signaling in bilaterians. *Bmc Biology,* 15.

BENTLEY, B., BRANICKY, R., BARNES, C. L., CHEW, Y. L., YEMINI, E., BULLMORE, E. T., VERTES, P. E. & SCHAFER, W. R. 2016. The Multilayer Connectome of Caenorhabditis elegans. *Plos Computational Biology,* 12.

BERKMAN, E. T. & LIEBERMAN, M. D. 2011. What's outside the black box?: The status of behavioral outcomes in neuroscience research. *Psychol Inq,* 22**,** 100-107.

BEYER, J., HADWIGER, M., AL-AWAMI, A., JEONG, W. K., KASTHURI, N., LICHTMAN, J. W. & PFISTER, H. 2013. Exploring the connectome: petascale volume visualization of microscopy data streams. *IEEE Comput Graph Appl,* 33**,** 50-61.

BOCK, D. D., LEE, W. C. A., KERLIN, A. M., ANDERMANN, M. L., HOOD, G., WETZEL, A. W., YURGENSON, S., SOUCY, E. R., KIM, H. S. & REID, R. C. 2011. Network anatomy and in vivo physiology of visual cortical neurons.

Nature, 471**,** 177-U59.
BORST, A. & HAAG, J. 2002. Neural networks in the cockpit of the fly. *Journal of Comparative Physiology a-Neuroethology Sensory Neural and Behavioral Physiology,* 188**,** 419-437.
BORST, A. & HELMSTAEDTER, M. 2015. Common circuit design in fly and mammalian motion vision. *Nat Neurosci,* 18**,** 1067-76.
BRADFORD, W., BUCKHOLZ, A., MORTON, J., PRICE, C., JONES, A. M. & URANO, D. 2013. Eukaryotic G Protein Signaling Evolved to Require G Protein-Coupled Receptors for Activation. *Science Signaling,* 6.
BRODFUEHRER, P. D. & THOROGOOD, M. S. E. 2001. Identified neurons and leech swimming behavior. *Progress in Neurobiology,* 63**,** 371-381.
BYRNE, M., NAKAJIMA, Y., CHEE, F. C. & BURKE, R. D. 2007. Apical organs in echinoderm larvae: insights into larval evolution in the Ambulacraria. *Evolution & Development,* 9**,** 432-445.
CAMPBELL, J. N., MACOSKO, E. Z., FENSELAU, H., PERS, T. H., LYUBETSKAYA, A., TENEN, D., GOLDMAN, M., VERSTEGEN, A. M. J., RESCH, J. M., MCCARROLL, S. A., ROSEN, E. D., LOWELL, B. B. & TSAI, L. T. 2017. A molecular census of arcuate hypothalamus and median eminence cell types. *Nature Neuroscience,* 20**,** 484-496.
CANDIANI, S., MORONTI, L., PENNATI, R., DE BERNARDI, F., BENFENATI, F. & PESTARINO, M. 2010. The synapsin gene family in basal chordates: evolutionary perspectives in metazoans. *Bmc Evolutionary Biology,* 10.
CARDONA, A. 2013. Towards Semi-Automatic Reconstruction of Neural Circuits. *Neuroinformatics,* 11**,** 31-33.
CARDONA, A., SAALFELD, S., SCHINDELIN, J., ARGANDA-CARRERAS, I., PREIBISCH, S., LONGAIR, M., TOMANCAK, P., HARTENSTEIN, V. & DOUGLAS, R. J. 2012. TrakEM2 Software for Neural Circuit Reconstruction. *Plos One,* 7.
CHEN, T. W., WARDILL, T. J., SUN, Y., PULVER, S. R., RENNINGER, S. L., BAOHAN, A., SCHREITER, E. R., KERR, R. A., ORGER, M. B., JAYARAMAN, V., LOOGER, L. L., SVOBODA, K. & KIM, D. S. 2013. Ultrasensitive fluorescent proteins for imaging neuronal activity. *Nature,* 499**,** 295-+.
CHIA, F. S., BUCKLANDNICKS, J. & YOUNG, C. M. 1984. Locomotion of Marine Invertebrate Larvae - a Review. *Canadian Journal of Zoology,* 62**,** 1205-1222.
CHIANG, A. S., LIN, C. Y., CHUANG, C. C., CHANG, H. M., HSIEH, C. H., YEH, C. W., SHIH, C. T., WU, J. J., WANG, G. T., CHEN, Y. C., WU, C. C., CHEN, G. Y., CHING, Y. T., LEE, P. C., LIN, C. Y., LIN, H. H., WU, C. C., HSU, H. W., HUANG, Y. A., CHEN, J. Y., CHIANG, H. J., LU, C. F., NI, R. F., YEH, C. Y. & HWANG, J. K. 2011. Three-dimensional reconstruction of brain-wide wiring networks in Drosophila at single-cell resolution. *Curr Biol,* 21**,** 1-11.
CHIU, I. M., BARRETT, L. B., WILLIAMS, E., STROCHLIC, D. E., LEE, S., WEYER, A. D., LOU, S., BRYMAN, G., ROBERSON, D. P., GHASEMLOU, N., PICCOLI, C., AHAT, E., WANG, V., COBOS, E. J., STUCKY, C. L., MA, Q. F., LIBERLES, S. D. & WOOLF, C. J. 2014. Transcriptional profiling at whole population and single cell levels reveals somatosensory neuron molecular diversity. *Elife,* 3.

CHKLOVSKII, D. B., VITALADEVUNI, S. & SCHEFFER, L. K. 2010. Semi-automated reconstruction of neural circuits using electron microscopy. *Current Opinion in Neurobiology,* 20**,** 667-675.

CONZELMANN, M., OFFENBURGER, S. L., ASADULINA, A., KELLER, T., MUNCH, T. A. & JEKELY, G. 2011. Neuropeptides regulate swimming depth of Platynereis larvae. *Proceedings of the National Academy of Sciences of the United States of America,* 108**,** E1174-83.

CONZELMANN, M., WILLIAMS, E. A., KRUG, K., FRANZ-WACHTEL, M., MACEK, B. & JEKELY, G. 2013a. The neuropeptide complement of the marine annelid Platynereis dumerilii. *Bmc Genomics,* 14.

CONZELMANN, M., WILLIAMS, E. A., TUNARU, S., RANDEL, N., SHAHIDI, R., ASADULINA, A., BERGER, J., OFFERMANNS, S. & JEKELY, G. 2013b. Conserved MIP receptor-ligand pair regulates Platynereis larval settlement. *Proceedings of the National Academy of Sciences of the United States of America,* 110**,** 8224-8229.

COSTA, M., MANTON, J. D., OSTROVSKY, A. D., PROHASKA, S. & JEFFERIS, G. S. 2016. NBLAST: Rapid, Sensitive Comparison of Neuronal Structure and Construction of Neuron Family Databases. *Neuron,* 91**,** 293-311.

CROLL, R. P., JACKSON, D. L. & VORONEZHSKAYA, E. E. 1997. Catecholamine-containing cells in larval and postlarval bivalve molluscs. *Biological Bulletin,* 193**,** 116-124.

DOCKRAY, G. J. 2004. The expanding family of -RFamide peptides and their effects on feeding behaviour. *Experimental Physiology,* 89**,** 229-235.

DRUMMOND, I. A. 2013. The cilium in lights: new views of an ancient organelle. *Bmc Biology,* 11.

EDITORIAL, N. N. 2017a. Focus on human brain mapping. *Nature Neuroscience,* 20**,** 297-297.

EDITORIAL, N. N. 2017b. Fostering reproducible fMRI research. *Nature Neuroscience,* 20**,** 298-298.

EICHLER, K., LI, F., LITWIN-KUMAR, A., PARK, Y., ANDRADE, I., CHNEIDER-MIZELL, C. M. S., SAUMWEBER, T., HUSER, A., ESCHBACH, C., GERBER, B., FETTER, R. D., TRUMAN, J. W., PRIEBE, C. E., ABBOTT, L. F., THUM, A. S., ZLATIC, M. & CARDONA, A. 2017. The complete connectome of a learning and memory centre in an insect brain. *Nature,* 548**,** 175-+.

EKSTRAND, M. I., NECTOW, A. R., KNIGHT, Z. A., LATCHA, K. N., POMERANZ, L. E. & FRIEDMAN, J. M. 2014. Molecular Profiling of Neurons Based on Connectivity. *Cell,* 157**,** 1230-1242.

ELGETI, J. & GOMPPER, G. 2013. Emergence of metachronal waves in cilia arrays. *Proc Natl Acad Sci U S A,* 110**,** 4470-5.

EMMONS, S. W. 2015. The beginning of connectomics: a commentary on White et al. (1986) 'The structure of the nervous system of the nematode Caenorhabditis elegans'. *Philosophical Transactions of the Royal Society B-Biological Sciences,* 370.

FAUBEL, R., WESTENDORF, C., BODENSCHATZ, E. & EICHELE, G. 2016. Cilia-based flow network in the brain ventricles. *Science,* 353**,** 176-8.

FISCHER, A. H. L., HENRICH, T. & ARENDT, D. 2010. The normal development of Platynereis dumerilii (Nereididae, Annelida). *Frontiers in Zoology,* 7.

FLORES, G. V., DUAN, H., YAN, H. J., NAGARAJ, R., FU, W. M., ZOU, Y., NOLL, M. & BANERJEE, U. 2000. Combinatorial signaling in the specification of unique cell fates. *Cell,* 103**,** 75-85.

FRIEDRICH, S., WANNINGER, A., BRUCKNER, M. & HASZPRUNAR, G. 2002. Neurogenesis in the mossy chiton, Mopalia muscosa (Gould) (Polyplacophora): Evidence against molluscan metamerism. *Journal of Morphology,* 253**,** 109-117.

FUJISAWA, T. 2008. Hydra Peptide Project 1993-2007. *Development Growth & Differentiation,* 50**,** S257-S268.

FUXE, K., BORROTO-ESCUELA, D. O., ROMERO-FERNANDEZ, W., ZHANG, W. B. & AGNATI, L. F. 2013. Volume transmission and its different forms in the central nervous system. *Chinese Journal of Integrative Medicine,* 19**,** 323-329.

GILPIN, W., PRAKASH, V. N. & PRAKASH, M. 2017. Vortex arrays and ciliary tangles underlie the feeding-swimming trade-off in starfish larvae. *Nature Physics,* 13**,** 380-386.

GOLGI, C. 1898a. Intorno alla struttura della cellula nervosa. *Boll Soc Med Chir Pavia 13:1–14 Arch Ital Biol 30: 60–70;*

Opera omnia, vol II. Hoepli, Milan pp:643–654, II.

GOLGI, C. 1898b. Sulla struttura della cellula nervosa dei gangli spinali. *Boll Soc Med Chir Pavia,* 13**,** 60–70.

GOTZ, M., WILLIAMS, B. P., BOLZ, J. & PRICE, J. 1995. The Specification of Neuronal Fate - a Common Precursor for Neurotransmitter Subtypes in the Rat Cerebral-Cortex in-Vitro. *European Journal of Neuroscience,* 7**,** 889-898.

GRIMMELIKHUIJZEN, C. J. P., GRAFF, D., KOIZUMI, O., WESTFALL, J. A. & MCFARLANE, I. D. 1991. Neuropeptides in Coelenterates - a Review. *Hydrobiologia,* 216**,** 555-563.

GUERON, S. & LEVIT-GUREVICH, K. 1999. Energetic considerations of ciliary beating and the advantage of metachronal coordination. *Proc Natl Acad Sci U S A,* 96**,** 12240-5.

HADFIELD, M. G., MELESHKEVITCH, E. A. & BOUDKO, D. Y. 2000. The apical sensory organ of a gastropod veliger is a receptor for settlement cues. *Biological Bulletin,* 198**,** 67-76.

HAGMANN, P. 2005. *From diffusion MRI to brain connectomics.* Lausanne: EPFL.

HAY-SCHMIDT, A. 2000. The evolution of the serotonergic nervous system. *Proceedings of the Royal Society B-Biological Sciences,* 267**,** 1071-1079.

HILLE, B. 1994. Modulation of ion-channel function by G-protein-coupled receptors. *Trends Neurosci,* 17**,** 531-6.

JAIN, R., JAVIDAN-NEJAD, C., ALEXANDER-BRETT, J., HORANI, A., CABELLON, M. C., WALTER, M. J. & BRODY, S. L. 2012. Sensory functions of motile cilia and implication for bronchiectasis. *Front Biosci (Schol Ed),* 4**,** 1088-98.

JEKELY, G. 2013a. Global view of the evolution and diversity of metazoan neuropeptide signaling. *Proceedings of the National Academy of Sciences of the United States of America,* 110**,** 8702-8707.

JEKELY, G. 2013b. Mechanism of phototaxis in marine zooplankton and origin of simple visual circuits. *Integrative and Comparative Biology,* 53**,** E103-E103.

JEKELY, G., COLOMBELLI, J., HAUSEN, H., GUY, K., STELZER, E., NEDELEC, F. & ARENDT, D. 2008. Mechanism of phototaxis in marine zooplankton. *Nature,*

456, 395-U62.
JENETT, A., RUBIN, G. M., NGO, T. T., SHEPHERD, D., MURPHY, C., DIONNE, H., PFEIFFER, B. D., CAVALLARO, A., HALL, D., JETER, J., IYER, N., FETTER, D., HAUSENFLUCK, J. H., PENG, H., TRAUTMAN, E. T., SVIRSKAS, R. R., MYERS, E. W., IWINSKI, Z. R., ASO, Y., DEPASQUALE, G. M., ENOS, A., HULAMM, P., LAM, S. C., LI, H. H., LAVERTY, T. R., LONG, F., QU, L., MURPHY, S. D., ROKICKI, K., SAFFORD, T., SHAW, K., SIMPSON, J. H., SOWELL, A., TAE, S., YU, Y. & ZUGATES, C. T. 2012. A GAL4-driver line resource for Drosophila neurobiology. *Cell Rep,* 2, 991-1001.
JIANG, Y., GONG, N. N., HU, X. S., NI, M. J., PASI, R. & MATSUNAMI, H. 2015. Molecular profiling of activated olfactory neurons identifies odorant receptors for odors in vivo. *Nature Neuroscience,* 18, 1446-+.
KATZ, P., GRILLNER, S., WILSON, R., BORST, A., GREENSPAN, R., BUZSAKI, G., MARTIN, K., MARDER, E., KRISTAN, W., FRIEDRICH, R. & CHKLOVSKII, D. 2013. Vertebrate versus invertebrate neural circuits. *Curr Biol,* 23, R504-6.
KEMPF, S. C., PAGE, L. R. & PIRES, A. 1997. Development of serotonin-like immunoreactivity in the embryos and larvae of nudibranch mollusks with emphasis on the structure and possible function of the apical sensory organ. *Journal of Comparative Neurology,* 386, 507-528.
KNIGHT, Z. A., TAN, K., BIRSOY, K., SCHMIDT, S., GARRISON, J. L., WYSOCKI, R. W., EMILIANO, A., EKSTRAND, M. I. & FRIEDMAN, J. M. 2012. Molecular Profiling of Activated Neurons by Phosphorylated Ribosome Capture. *Cell,* 151, 1126-1137.
KONIG, P., KRAIN, B., KRASTEVA, G. & KUMMER, W. 2009. Serotonin Increases Cilia-Driven Particle Transport via an Acetylcholine-Independent Pathway in the Mouse Trachea. *Plos One,* 4.
KUCEYESKI, A., NAVI, B. B., KAMEL, H., RELKIN, N., VILLANUEVA, M., RAJ, A., TOGLIA, J., O'DELL, M. & IADECOLA, C. 2015. Exploring the brain's structural connectome: A quantitative stroke lesion-dysfunction mapping study. *Hum Brain Mapp,* 36, 2147-60.
LACALLI, T. C. & KELLY, S. J. 2000. The infundibular balance organ in amphioxus larvae and related aspects of cerebral vesicle organization. *Acta Zoologica,* 81, 37-47.
LAMB, T. D., COLLIN, S. P. & PUGH, E. N. 2007. Evolution of the vertebrate eye: opsins, photoreceptors, retina and eye cup. *Nature Reviews Neuroscience,* 8, 960-975.
LANG, B. F., O'KELLY, C., NERAD, T., GRAY, M. W. & BURGER, G. 2002. The closest unicellular relatives of animals. *Curr Biol,* 12, 1773-8.
LECHAN, R. M. & TONI, R. 2000. Functional Anatomy of the Hypothalamus and Pituitary. *In:* DE GROOT, L. J., CHROUSOS, G., DUNGAN, K., FEINGOLD, K. R., GROSSMAN, A., HERSHMAN, J. M., KOCH, C., KORBONITS, M., MCLACHLAN, R., NEW, M., PURNELL, J., REBAR, R., SINGER, F. & VINIK, A. (eds.) *Endotext.* South Dartmouth (MA).
LEERGAARD, T. B., HILGETAG, C. C. & SPORNS, O. 2012. Mapping the connectome: multi-level analysis of brain connectivity. *Front Neuroinform,* 6, 14.
LEONARD, J. L. 2000. Identifiable neurons in invertebrates: From invariant cells to

dynamic systems - Preface. *Brain Behavior and Evolution,* 55**,** 233-235.
LIU, F., BAGGERMAN, G., SCHOOFS, L. & WETS, G. 2008. The construction of a bioactive peptide database in Metazoa. *Journal of Proteome Research,* 7**,** 4119-4131.
LODISH, H. F. 2003. *Molecular cell biology,* New York, W.H. Freeman and Company.
LYONS, R. A., SARIDOGAN, E. & DJAHANBAKHCH, O. 2006. The reproductive significance of human Fallopian tube cilia. *Human Reproduction Update,* 12**,** 363-372.
MACKIE, G. O. & STELL, W. K. 1984. Fmrf-Amide-Like Immunoreactivity in the Neurons of Medusae. *American Zoologist,* 24**,** A36-A36.
MALDONADO, M. 2006. The ecology of the sponge larva. *Canadian Journal of Zoology,* 84**,** 175-194.
MARDER, E. 2012. Neuromodulation of Neuronal Circuits: Back to the Future. *Neuron,* 76**,** 1-11.
MARLOW, H., TOSCHES, M. A., TOMER, R., STEINMETZ, P. R., LAURI, A., LARSSON, T. & ARENDT, D. 2014. Larval body patterning and apical organs are conserved in animal evolution. *Bmc Biology,* 12.
MARUYAMA, I., INAGAKI, M. & MOMOSE, K. 1984. The Role of Serotonin in Mucociliary Transport-System in the Ciliated Epithelium of Frog Palatine Mucosa. *European Journal of Pharmacology,* 106**,** 499-506.
MIRABEAU, O. & JOLY, J. S. 2013. Molecular evolution of peptidergic signaling systems in bilaterians. *Proceedings of the National Academy of Sciences of the United States of America,* 110**,** E2028-E2037.
MITCHELL, B., JACOBS, R., LI, J., CHIEN, S. & KINTNER, C. 2007. A positive feedback mechanism governs the polarity and motion of motile cilia. *Nature,* 447**,** 97-U8.
MITCHELL, D. R. 2007. The evolution of eukaryotic cilia and flagella as motile and sensory organelles. *Eukaryotic Membranes and Cytoskeleton: Origins and Evolution,* 607**,** 130-140.
MITGUTSCH, C., HAUSER, F. & GRIMMELIKHUIJZEN, C. J. P. 1999. Expression and developmental regulation of the Hydra-RFamide and Hydra-LWamide preprohormone genes in Hydra: Evidence for transient phases of head formation. *Developmental Biology,* 207**,** 189-203.
MOLYNEAUX, B. J., ARLOTTA, P., MENEZES, J. R. L. & MACKLIS, J. D. 2007. Neuronal subtype specification in the cerebral cortex. *Nature Reviews Neuroscience,* 8**,** 427-437.
MORGAN, J. L. & LICHTMAN, J. W. 2013. Why not connectomics? *Nature Methods,* 10**,** 494-500.
MUNSTERBERG, A. E., KITAJEWSKI, J., BUMCROT, D. A., MCMAHON, A. P. & LASSAR, A. B. 1995. Combinatorial Signaling by Sonic Hedgehog and Wnt Family Members Induces Myogenic Bhlh Gene-Expression in the Somite. *Genes & Development,* 9**,** 2911-2922.
NADIM, F. & BUCHER, D. 2014. Neuromodulation of neurons and synapses. *Curr Opin Neurobiol,* 29**,** 48-56.
NEZLIN, L. P. 2000. Tornaria of hemichordates and other dipleurula-type larvae: a comparison. *Journal of Zoological Systematics and Evolutionary Research,* 38**,** 149-156.

NIELSEN, C. 2004. Trochophora larvae: Cell-lineages, ciliary bands, and body regions. 1. Annelida and mollusca. *Journal of Experimental Zoology Part B-Molecular and Developmental Evolution,* 302B**,** 35-68.

NIELSEN, C. 2005. Trochophora larvae: Cell-lineages, ciliary bands and body regions. 2. Other groups and general discussion. *Journal of Experimental Zoology Part B-Molecular and Developmental Evolution,* 304B**,** 401-447.

NIKITIN, M. 2015. Bioinformatic prediction of Trichoplax adhaerens regulatory peptides. *General and Comparative Endocrinology,* 212**,** 145-155.

NIKOLAEV, S. I., BERNEY, C., FAHRNI, J. F., BOLIVAR, I., POLET, S., MYLNIKOV, A. P., ALESHIN, V. V., PETROV, N. B. & PAWLOWSKI, J. 2004. The twilight of Heliozoa and rise of Rhizaria, an emerging supergroup of amoeboid eukaryotes. *Proceedings of the National Academy of Sciences of the United States of America,* 101**,** 8066-8071.

OHYAMA, T., SCHNEIDER-MIZELL, C. M., FETTER, R. D., ALEMAN, J. V., FRANCONVILLE, R., RIVERA-ALBA, M., MENSH, B. D., BRANSON, K. M., SIMPSON, J. H., TRUMAN, J. W., CARDONA, A. & ZLATIC, M. 2015. A multilevel multimodal circuit enhances action selection in Drosophila. *Nature,* 520**,** 633-9.

OSTERMAN, N. & VILFAN, A. 2011. Finding the ciliary beating pattern with optimal efficiency. *Proc Natl Acad Sci U S A,* 108**,** 15727-32.

PAZOUR, G. J., AGRIN, N., LESZYK, J. & WITMAN, G. B. 2005. Proteomic analysis of a eukaryotic cilium. *J Cell Biol,* 170**,** 103-13.

PENA, J. L. & DEBELLO, W. M. 2010. Auditory Processing, Plasticity, and Learning in the Barn Owl. *Ilar Journal,* 51**,** 338-352.

PERNET, B. & STRATHMANN, R. R. 2011. Opposed Ciliary Bands in the Feeding Larvae of Sabellariid Annelids. *Biological Bulletin,* 220**,** 186-198.

RAINERI, M. 1995. Is a Mollusk an Evolved Bent Metatrochophore - a Histochemical Investigation of Neurogenesis in Mytilus (Mollusca, Bivalvia). *Journal of the Marine Biological Association of the United Kingdom,* 75**,** 571-592.

RAMÓN Y CAJAL, S. 1889a. Nuevas aplicaciones del método de coloración de Golgi. *In:* NATURALES, M. N. D. C. (ed.). Barcelona

RAMÓN Y CAJAL, S. 1889b. Conexión general de los elementos nerviosos. *Medicina Práctica*.

RANDEL, N., ASADULINA, A., BEZARES-CALDERON, L. A., VERASZTO, C., WILLIAMS, E. A., CONZELMANN, M., SHAHIDI, R. & JEKELY, G. 2014. Neuronal connectome of a sensory-motor circuit for visual navigation. *Elife,* 3.

RANDEL, N., SHAHIDI, R., VERASZTO, C., BEZARES-CALDERON, L. A., SCHMIDT, S. & JEKELY, G. 2015. Inter-individual stereotypy of the Platynereis larval visual connectome. *Elife,* 4.

ROLE, L. W. & BERG, D. K. 1996. Nicotinic receptors in the development and modulation of CNS synapses. *Neuron,* 16**,** 1077-85.

RYAN, K., LU, Z. Y. & MEINERTZHAGEN, I. A. 2016. The CNS connectome of a tadpole larva of Ciona intestinalis (L.) highlights sidedness in the brain of a chordate sibling. *Elife,* 5.

SAALFELD, S., CARDONA, A., HARTENSTEIN, V. & TOMANCAK, P. 2009. CATMAID: collaborative annotation toolkit for massive amounts of image data. *Bioinformatics,* 25**,** 1984-1986.

SALATHE, M. 2007. Regulation of mammalian ciliary beating. *Annu Rev Physiol,* 69**,** 401-22.
SATIR, P. 1999. The cilium as a biological nanomachine. *Faseb Journal,* 13**,** S235-S237.
SCHLEGEL, P., TEXADA, M. J., MIROSCHNIKOW, A., SCHOOFS, A., HUCKESFELD, S., PETERS, M., SCHNEIDER-MIZELL, C. M., LACIN, H., LI, F., FETTER, R. D., TRUMAN, J. W., CARDONA, A. & PANKRATZ, M. J. 2016. Synaptic transmission parallels neuromodulation in a central food-intake circuit. *Elife,* 5.
SCHMIDT-RHAESA, A., HARZSCH, S. & PURSCHKE, G. 2016. *Structure & evolution of invertebrate nervous systems,* Oxford ; New York, NY, Oxford University Press.
SCHNEIDER-MIZELL, C. M., GERHARD, S., LONGAIR, M., KAZIMIERS, T., LI, F., ZWART, M. F., CHAMPION, A., MIDGLEY, F. M., FETTER, R. D., SAALFELD, S. & CARDONA, A. 2016. Quantitative neuroanatomy for connectomics in Drosophila. *Elife,* 5.
SHAHIDI, R., WILLIAMS, E. A., CONZELMANN, M., ASADULINA, A., VERASZTO, C., JASEK, S., BEZARES-CALDERON, L. A. & JEKELY, G. 2015. A serial multiplex immunogold labeling method for identifying peptidergic neurons in connectomes. *Elife,* 4.
SHOEMARK, A. & HOGG, C. 2013. Electron tomography of respiratory cilia. *Thorax,* 68**,** 190-191.
SMITH, C. L., VAROQUEAUX, F., KITTELMANN, M., AZZAM, R. N., COOPER, B., WINTERS, C. A., EITEL, M., FASSHAUER, D. & REESE, T. S. 2014. Novel Cell Types, Neurosecretory Cells, and Body Plan of the Early-Diverging Metazoan Trichoplax adhaerens. *Current Biology,* 24**,** 1565-1572.
STACH, T. 2005. Comparison of the serotonergic nervous system among Tunicata: implications for its evolution within Chordata. *Organisms Diversity & Evolution,* 5**,** 15-24.
STACH, T. G. 2002. Evolution of the serotonergic nervous system in Chordata. *Integrative and Comparative Biology,* 42**,** 1317-1317.
STECHMANN, A. & CAVALIER-SMITH, T. 2003. Phylogenetic analysis of eukaryotes using heat-shock protein Hsp90. *Journal of Molecular Evolution,* 57**,** 408-419.
STEIN, W., DELONG, N. D., WOOD, D. E. & NUSBAUM, M. P. 2007. Divergent co-transmitter actions underlie motor pattern activation by a modulatory projection neuron. *European Journal of Neuroscience,* 26**,** 1148-1165.
STRAUSFELD, N. J. & HILDEBRAND, J. G. 1999. Olfactory systems: common design, uncommon origins? *Curr Opin Neurobiol,* 9**,** 634-9.
SUDHOF, T. C. & MALENKA, R. C. 2008. Understanding synapses: past, present, and future. *Neuron,* 60**,** 469-76.
SUGINO, K., HEMPEL, C. M., MILLER, M. N., HATTOX, A. M., SHAPIRO, P., WU, C. Z., HUANG, Z. J. & NELSON, S. B. 2006. Molecular taxonomy of major neuronal classes in the adult mouse forebrain. *Nature Neuroscience,* 9**,** 99-107.
TAKEMURA, S. Y., ASO, Y., HIGE, T., WONG, A., LU, Z., XU, C. S., RIVLIN, P. K., HESS, H., ZHAO, T., PARAG, T., BERG, S., HUANG, G., KATZ, W., OLBRIS, D. J., PLAZA, S., UMAYAM, L., ANICETO, R., CHANG, L. A., LAUCHIE, S.,

OGUNDEYI, O., ORDISH, C., SHINOMIYA, A., SIGMUND, C., TAKEMURA, S., TRAN, J., TURNER, G. C., RUBIN, G. M. & SCHEFFER, L. K. 2017. A connectome of a learning and memory center in the adult Drosophila brain. *Elife,* 6.

TAKEMURA, S. Y., BHARIOKE, A., LU, Z., NERN, A., VITALADEVUNI, S., RIVLIN, P. K., KATZ, W. T., OLBRIS, D. J., PLAZA, S. M., WINSTON, P., ZHAO, T., HORNE, J. A., FETTER, R. D., TAKEMURA, S., BLAZEK, K., CHANG, L. A., OGUNDEYI, O., SAUNDERS, M. A., SHAPIRO, V., SIGMUND, C., RUBIN, G. M., SCHEFFER, L. K., MEINERTZHAGEN, I. A. & CHKLOVSKII, D. B. 2013. A visual motion detection circuit suggested by Drosophila connectomics. *Nature,* 500**,** 175-81.

TAMM, S. L. 2014. Cilia and the life of ctenophores. *Invertebrate Biology,* 133**,** 1-46.

TEMEREVA, E. & WANNINGER, A. 2012. Development of the nervous system in Phoronopsis harmeri (Lophotrochozoa, Phoronida) reveals both deuterostome- and trochozoan-like features. *Bmc Evolutionary Biology,* 12.

TEMEREVA, E. N. & TSITRIN, E. B. 2014. Development and organization of the larval nervous system in Phoronopsis harmeri: new insights into phoronid phylogeny. *Frontiers in Zoology,* 11.

TESSMAR-RAIBLE, K. 2007. The evolution of neurosecretory centers in bilaterian forebrains: Insights from protostomes. *Seminars in Cell & Developmental Biology,* 18**,** 492-501.

TESSMAR-RAIBLE, K., RAIBLE, F., CHRISTODOULOU, F., GUY, K., REMBOLD, M., HAUSEN, H. & ARENDT, D. 2007. Conserved sensory-neurosecretory cell types in annelid and fish forebrain: Insights into hypothalamus evolution. *Cell,* 129**,** 1389-1400.

THIRUMALAI, V. & MARDER, E. 2002. Colocalized neuropeptides activate a central pattern generator by acting on different circuit targets. *Journal of Neuroscience,* 22**,** 1874-1882.

TIAN, L., HIRES, S. A. & LOOGER, L. L. 2012. Imaging neuronal activity with genetically encoded calcium indicators. *Cold Spring Harb Protoc,* 2012**,** 647-56.

TOMER, R., DENES, A. S., TESSMAR-RAIBLE, K. & ARENDT, D. 2010. Profiling by Image Registration Reveals Common Origin of Annelid Mushroom Bodies and Vertebrate Pallium. *Cell,* 142**,** 800-809.

TOSCHES, M. A. & ARENDT, D. 2013. The bilaterian forebrain: an evolutionary chimaera. *Current Opinion in Neurobiology,* 23**,** 1080-1089.

TOSCHES, M. A., BUCHER, D., VOPALENSKY, P. & ARENDT, D. 2014. Melatonin Signaling Controls Circadian Swimming Behavior in Marine Zooplankton. *Cell,* 159**,** 46-57.

VAN DIJCK, G., VAN HULLE, M. M., HEINEY, S. A., BLAZQUEZ, P. M., MENG, H., ANGELAKI, D. E., ARENZ, A., MARGRIE, T. W., MOSTOFI, A., EDGLEY, S., BENGTSSON, F., EKEROT, C. F., JORNTELL, H., DALLEY, J. W. & HOLTZMAN, T. 2013. Probabilistic Identification of Cerebellar Cortical Neurones across Species. *Plos One,* 8.

WALENTEK, P., BOGUSCH, S., THUMBERGER, T., VICK, P., DUBAISSI, E., BEYER, T., BLUM, M. & SCHWEICKERT, A. 2014. A novel serotonin-secreting cell type regulates ciliary motility in the mucociliary epidermis of

Xenopus tadpoles. *Development,* 141**,** 1526-1533.
WANNINGER, A., KOOP, D. & DEGNAN, B. M. 2005. Immunocytochemistry and metamorphic fate of the larval nervous system of Triphyllozoon mucronatum (Ectoprocta : Gymnolaemata : Cheilostomata). *Zoomorphology,* 124**,** 161-170.
WATANABE, H., FUJISAWA, T. & HOLSTEIN, T. W. 2009. Cnidarians and the evolutionary origin of the nervous system. *Development Growth & Differentiation,* 51**,** 167-183.
WATTS, D. J. & STROGATZ, S. H. 1998. Collective dynamics of 'small-world' networks. *Nature,* 393**,** 440-442.
WHITE, J. G., SOUTHGATE, E., THOMSON, J. N. & BRENNER, S. 1986. The Structure of the Nervous-System of the Nematode Caenorhabditis-Elegans. *Philosophical Transactions of the Royal Society of London Series B-Biological Sciences,* 314**,** 1-340.
WICHER, D., DERST, C., GAUTIER, H., LAPIED, B., HEINEMANN, S. H. & AGRICOLA, H. J. 2007. The satiety signaling neuropeptide perisulfakinin inhibits the activity of central neurons promoting general activity. *Frontiers in Cellular Neuroscience,* 1.
WILLIAMS, E. A., VERASZTÓ, C., JASEK, S., CONZELMANN, M., SHAHIDI, R., BAUKNECHT, P. & JÉKELY, G. 2017. Synaptic and peptidergic connectome of a neurosecretory centre in the annelid brain. *bioRxiv*.
WORTHINGTON, W. C., JR. & CATHCART, R. S., 3RD 1963. Ependymal cilia: distribution and activity in the adult human brain. *Science,* 139**,** 221-2.
YOUNG, C. M., SEWELL, M. A. & RICE, A. P. M. E. 2003. Atlas of Marine Invertebrate Larvae. *Aquaculture Research,* 34**,** 437-437.
ZANTKE, J., BANNISTER, S., RAJAN, V. B. V., RAIBLE, F. & TESSMAR-RAIBLE, K. 2014. Genetic and Genomic Tools for the Marine Annelid Platynereis dumerilii. *Genetics,* 197**,** 19-31.
ZANTKE, J., ISHIKAWA-FUJIWARA, T., ARBOLEDA, E., LOHS, C., SCHIPANY, K., HALLAY, N., STRAW, A. D., TODO, T. & TESSMAR-RAIBLE, K. 2013. Circadian and circalunar clock interactions in a marine annelid. *Cell Rep,* 5**,** 99-113.

Appendix

eLIFE elifesciences.org

RESEARCH ARTICLE

Ciliomotor circuitry underlying whole-body coordination of ciliary activity in the *Platynereis* larva

Csaba Verasztó, Nobuo Ueda, Luis A Bezares-Calderón, Aurora Panzera, Elizabeth A Williams, Réza Shahidi, Gáspár Jékely*

Max Planck Institute for Developmental Biology, Tübingen, Germany

Abstract Ciliated surfaces harbouring synchronously beating cilia can generate fluid flow or drive locomotion. In ciliary swimmers, ciliary beating, arrests, and changes in beat frequency are often coordinated across extended or discontinuous surfaces. To understand how such coordination is achieved, we studied the ciliated larvae of *Platynereis dumerilii*, a marine annelid. *Platynereis* larvae have segmental multiciliated cells that regularly display spontaneous coordinated ciliary arrests. We used whole-body connectomics, activity imaging, transgenesis, and neuron ablation to characterize the ciliomotor circuitry. We identified cholinergic, serotonergic, and catecholaminergic ciliomotor neurons. The synchronous rhythmic activation of cholinergic cells drives the coordinated arrests of all cilia. The serotonergic cells are active when cilia are beating. Serotonin inhibits the cholinergic rhythm, and increases ciliary beat frequency. Based on their connectivity and alternating activity, the catecholaminergic cells may generate the rhythm. The ciliomotor circuitry thus constitutes a stop-and-go pacemaker system for the whole-body coordination of ciliary locomotion.

DOI: 10.7554/eLife.26000.001

***For correspondence:** gaspar.jekely@tuebingen.mpg.de

Competing interests: The authors declare that no competing interests exist.

Funding: See page 21

Received: 13 February 2017
Accepted: 14 May 2017
Published: 16 May 2017

Reviewing editor: Piali Sengupta, Brandeis University, United States

Introduction

Multiciliated surfaces characterised by many beating cilia are widespread in eukaryotes. Such surfaces can effectively generate flow in many different contexts, including the driving of solute transport in reef corals (***Shapiro et al., 2014***), moving mucus and particles in mucociliary epithelia (***Kramer-Zucker et al., 2005***; ***Walentek et al., 2014***), driving the cerebrospinal fluid (***Faubel et al., 2016***), or moving the ovum in the mammalian oviduct (***Halbert et al., 1989***). Multiciliated surfaces can also drive locomotion, as in ciliates, colonial green algae, or marine invertebrate larvae (***Tamm, 1972***; ***Chia et al., 1984***; ***Brumley et al., 2015***).

A universal feature of multiciliated surfaces is the long-range beat synchronisation of individual cilia into metachronal waves (***Tamm, 1984***; ***Brumley et al., 2012***; ***Knight-Jones, 1954***; ***Tamm, 1972***). Theoretical studies indicate that metachronal waves are energetically efficient and have a higher efficiency of flow generation than non-metachronal beating (***Osterman and Vilfan, 2011***; ***Gueron and Levit-Gurevich, 1999***; ***Elgeti and Gompper, 2013***). Metachronal coordination requires the orientation of ciliary beating planes during development (***Mitchell et al., 2007***; ***Park et al., 2008***; ***Mitchell et al., 2009***; ***Guirao et al., 2010***; ***Vladar et al., 2012***; ***Kunimoto et al., 2012***). If cilia are oriented, synchronisation emerges by hydrodynamic coupling as adjacent cilia engage by flow (***Brumley et al., 2014***; ***Elgeti and Gompper, 2013***). In addition, basal body coupling can also contribute to beat synchronisation as demonstrated in green algae (***Wan and Goldstein, 2016***).

However, biophysical mechanisms alone cannot explain all aspects of ciliary beat synchronisation. For example, the flow-networks generated by ependymal cilia show complex reorganisation that is

eLife digest The oceans contain a wide variety of microscopic organisms including bacteria, algae and animal larvae. Many of the microscopic animals that live in water use thousands of beating hair-like projections called cilia instead of muscles to swim around in the water. Understanding how these animals move will aid our understanding of how ocean processes, such as the daily migration of plankton to and from the surface of the water, are regulated.

The larvae of a ragworm called *Platynereis* use cilia to move around. Like other animals, *Platynereis* has a nervous system containing neurons that form networks to control the body. It is possible that the nervous system is involved in coordinating the activity of the cilia to allow the larvae to manoeuvre in the water, but it was not clear how this could work.

Here, Veraszto et al. investigated how *Platynereis* is able to swim. The experiments show that the larvae can coordinate their cilia so that they all stop beating at the same time and fold into to the body. Then the larvae can stimulate all of their cilia to resume beating. Veraszto et al. used a technique called electron microscopy to study how the nervous system connects to the cilia. This revealed that several giant neurons span the entire length of the larva and connect to cells that bear cilia. When these neurons were active, all the cilia in the body closed. When a different group of neurons in the larva was active, all of the cilia resumed beating. Together, these two groups of neurons were ultimately responsible for the swimming motions of the larvae.

Together, the findings of Veraszto et al. show that a few neurons in the nervous system of the larvae provide a sophisticated system for controlling how the larvae swim around. This suggests that the microscopic animals found in marine environments are a lot more sophisticated than previously appreciated. A next challenge is to find out how the neurons that control cilia connect to the rest of the animal's nervous system and how different cues influence when the larva swims or stops swimming. This would help us understand how the environment influences the distribution of animal larvae in the oceans and how this may change in the future.

DOI: 10.7554/eLife.26000.002

under circadian regulation (***Faubel et al., 2016***). In mucociliary surfaces, changes in ciliary beat frequency are coordinated to regulate flow rates. Some of these changes are due to locally secreted diffusible molecules, including serotonin (***Maruyama et al., 1984***; ***König et al., 2009***; ***Walentek et al., 2014***) and neuropeptides (***Conductier et al., 2013***). However, long-range ciliary coordination is often under neuronal control (***Doran et al., 2004***; ***Tamm, 2014***; ***Arkett et al., 1987***; ***Kuang and Goldberg, 2001***).

Ciliary swimmers display the most elaborate forms of neuronal ciliary coordination. In the ctenophore *Pleurobrachia*, prey-capture triggers a rapid synchronised beating of all eight ciliary comb-rows resulting in fast forward swimming (***Tamm, 2014***). In gastropod veliger larvae, the normal beating of velar cilia is periodically interrupted by coordinated, velum-wide ciliary arrests, triggered by calcium-spikes (***Arkett et al., 1987***). Similarly, annelid larvae show regular and coordinated arrests of the entire prototroch ciliary band (***Conzelmann et al., 2011***). Such coordinated changes in ciliary activity, often triggered throughout the whole body, require neuronal control.

The neuronal circuits coordinating whole-body ciliary activity have not been described in any animal. Here we reconstruct and functionally analyse the complete ciliomotor circuitry in the planktonic nectochaete larva of the marine annelid *Platynereis dumerilii*. *Platynereis* has emerged as a powerful model to study neural cell types and development (***Tomer et al., 2010***; ***Marlow et al., 2014***; ***Tessmar-Raible et al., 2007***) and the whole-body circuit bases of larval behaviour, including conical-scanning and visual phototaxis (***Jékely et al., 2008***; ***Randel et al., 2014***). *Platynereis* nectochaete larvae (***Fischer et al., 2010***) have three trunk segments and use segmentally arranged ciliary bands to swim and muscles to turn while swimming (***Randel et al., 2014***) or to crawl on the substrate. Ciliary beating is also under neuromodulatory control and can be influenced by several neuropeptides and melatonin (***Conzelmann et al., 2011***; ***Tosches et al., 2014***).

We used whole-body connectomics, transgenic neuron labelling, and calcium imaging to reconstruct and functionally analyse the entire ciliomotor system in *Platynereis* larvae. We identified a ciliomotor system consisting of interconnected catecholaminergic, cholinergic, and serotonergic

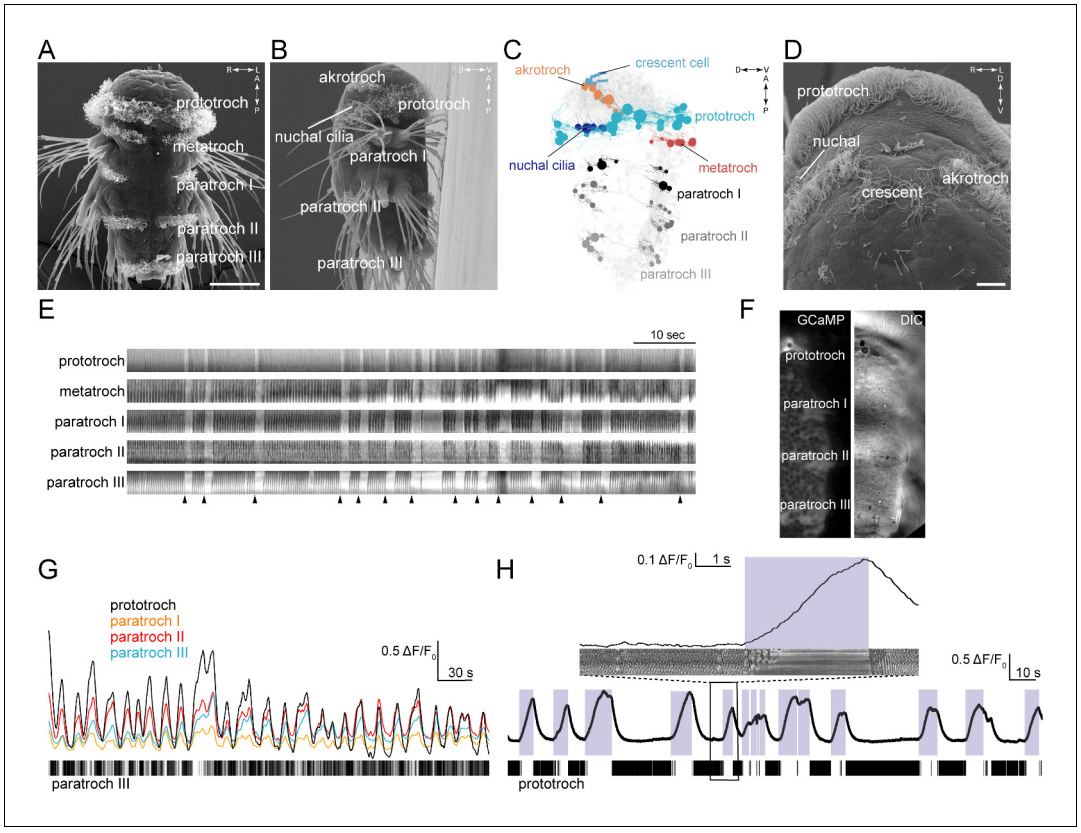

Figure 1. Coordinated ciliary beating and arrests in *Platynereis* larvae. (**A–B,D**) Scanning electron micrographs of 72 hr-post-fertilization larvae, (**A**) ventral view, (**B**) lateral view, (**D**) anterior view, close up. The structures dorsal to the crescent cell are non-motile sensory cilia. (**C**) Serial TEM reconstruction of ciliary band cells, lateral view. Nuclei of ciliary band cells are shown as spheres. The nervous system (brain and ventral nerve cord) is shown in light grey. (**E**) Kymographs of spontaneous ciliary activity from an immobilized 72 hr-post-fertilization larva. Arrowheads indicate the beginning of ciliary arrests. (**F**) Ventral view of the left half of a 72 hr-post-fertilization larva in a calcium-imaging experiment (left panel) with the corresponding differential interference contrast (DIC) image (right panel). (**G**) GCaMP6s signal from the prototroch and paratroch ciliary bands. A kymograph of ciliary activity in paratroch III is shown below. (**H**) GCaMP6s signal recorded from the prototroch of a 48 hr-post-fertilization larva at 45 frames per second. White areas in the kymograph correspond to periods of arrest. The boxed area is shown enlarged in the inset. Scale bars, 50 μm (**A**), 10 μm (**D**).

DOI: 10.7554/eLife.26000.003

ciliomotor neurons. These neurons form a pacemaker system responsible for the whole-body coordination of alternating episodes of ciliary arrests and ciliary beating to regulate larval swimming.

Results

Coordinated beating and arrests of segmentally arranged locomotor cilia

Platynereis nectochaete larvae have segmentally arranged locomotor ciliated cells that form distinct ciliated fields (***Figure 1A–D***). The main ciliary band (prototroch) is located between the head and the trunk. The head has two patches of locomotor cilia (akrotroch) and multiciliated cells that cover the olfactory pit of the nuchal organs (nuchal cilia). There is also an unpaired multiciliated cell, the crescent cell, located anteriorly in the head in the middle of the sensory region of the apical organ. The three chaetigerous (with chaetae) trunk segments each have four fields of cilia forming the paratroch ciliary bands (paratroch I-III). There is an additional non-chaetigerous cryptic segment between the head and the trunk segments (***Steinmetz et al., 2011***) that harbours ventrally the metatroch ciliary band. Younger larvae have four posterior telotroch cells that merge with the paratroch III (eight

Video 1. Coordinated arrests of cilia on all ciliary band cells in a 72 hr-post-fertilization *Platynereis* larva. Differential interference contrast (DIC) imaging, recorded and played at 60 frames per second (fps).
DOI: 10.7554/eLife.26000.004

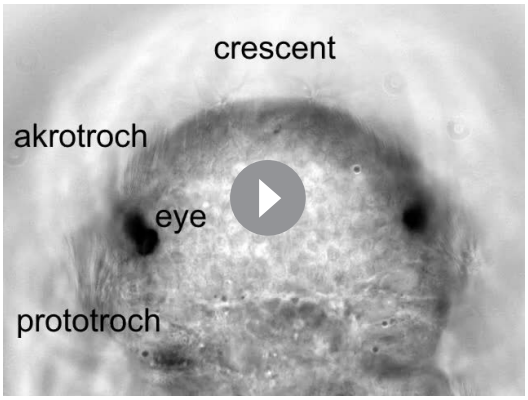

Video 2. Coordinated arrests of akrotroch and paratroch but not crescent cilia. DIC imaging of cilia in the *Platynereis* larval head. Recorded and played at 30 fps.
DOI: 10.7554/eLife.26000.005

cells) during development to form a posterior ciliary band of 12 cells (***Starunov et al., 2015***) (referred to as paratroch III).

To investigate beat coordination across the ciliary bands in *Platynereis*, we imaged ciliary activity of mechanically immobilized 3-day-old nectochaete larvae. We found that spontaneous arrests of ciliary beating occurred synchronously across all ciliary bands (***Figure 1A–E*** and ***Video 1***). Cilia first resumed beating in the prototroch followed in synchrony by the paratroch cilia (with a delay of 19 ± 3 msec relative to the prototroch cilia). Arrests of prototroch cilia were also in synchrony with arrests in the akrotroch (***Video 2***) and the nuchal cilia (data not shown).

We next combined differential interference contrast (DIC) imaging with calcium imaging using a ubiquitously expressed fluorescent calcium indicator, GCaMP6s. In *Platynereis* larvae, regular arrests are triggered by bursts of spikes that can be recorded from the ciliary band cells (***Conzelmann et al., 2011***; ***Tosches et al., 2014***). With calcium imaging, we detected periodic synchronous increases in calcium signals in cells of each ciliary band that corresponded with the arrests of cilia (***Figure 1G***, ***Video 3***).

The only cilia that did not beat and arrest synchronously were the cilia of the crescent cell (***Figure 1D***). Although calcium signals also increase in the crescent cell simultaneously with the other multiciliated cells (data not shown), the cilia of this cell were beating when the other cilia were arrested (***Video 2***). Crescent cilia stopped beating after the locomotor cilia resumed beating (***Video 2***). The crescent cell has a lower

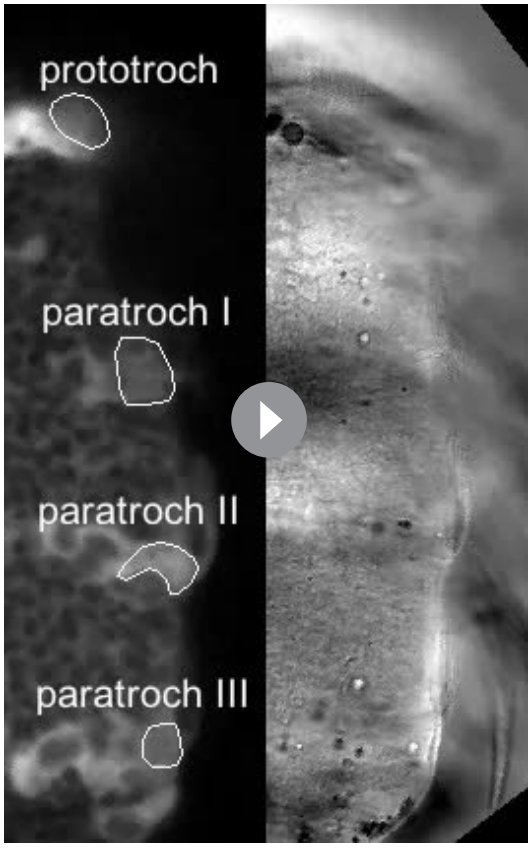

Video 3. Calcium and DIC imaging of ciliary bands in a 72 hr-post-fertilization *Platynereis* larva. The GCaMP6s signal (left panel) and DIC signal (right panel) are shown for the left side of the larva (ventral view). Regions of interest used to record calcium signals are indicated. Recorded at 3 fps, played at 25 fps.
DOI: 10.7554/eLife.26000.006

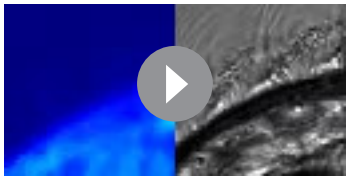

Video 4. Calcium and DIC imaging of the ciliary band in a 48 hr-post-fertilization *Platynereis* larva. The video was recorded at 45 fps, here only every 10th frame is shown at 45 fps.
DOI: 10.7554/eLife.26000.007

density of cilia that beat more irregularly and do not organise into metachronal waves (***Video 2*** and ***Figure 1D***).

To investigate in more detail how intracellular calcium concentrations $[Ca^{2+}]_i$ in the prototroch cells relate to the arrests of cilia, we imaged calcium activity in close-ups from the prototroch cells at higher frame rates (***Video 4***). We found that ciliary activity did not correlate with the absolute levels of $[Ca^{2+}]_i$, but with the time derivative of calcium $d[Ca^{2+}]_i/dt$ (***Figure 1H***). As long as calcium levels increase, the cilia are arrested. As soon as calcium levels start to drop, the cilia resume their metachronal beating. A similar case was reported in sea urchin sperm where $d[Ca^{2+}]_i/dt$ rather than absolute $[Ca^{2+}]_i$ controls ciliary waveform during chemotaxis (***Alvarez et al., 2012***).

Connectomic reconstruction of the ciliomotor circuitry

To understand the mechanism of ciliary beat synchronisation across ciliary bands and to get a comprehensive view of ciliomotor circuits in the *Platynereis* larva, we employed serial-section transmission electron microscopy (ssTEM). We used a whole-body ssTEM dataset of a 3 day old larva (***Randel et al., 2015***; ***Shahidi et al., 2015***; ***Shahidi and Jékely, 2017***) to identify and reconstruct all neurons innervating ciliary band cells.

First, we identified all multiciliated cells in this larva ***(Figure 1C***).There are 23 cells in the prototroch that are arranged in an anterior and posterior tier, with one unpaired cell in the position of 11 o'clock (***Randel et al., 2014***). In the head, there are eight akrotroch cells, six ciliated cells in the nuchal organs, and an unpaired crescent cell. The metatroch consists of eight cells. In the first, second, and third trunk segments there are eight, 14, and 12 paratroch cells, respectively.

We next identified and reconstructed all neurons that were presynaptic to any of the multiciliated cells in the larva. We define these neurons as ciliomotor neurons. Combining transgenic labelling, immunohistochemistry, and serial multiplex immunogold labelling (siGOLD) (***Shahidi et al., 2015***), we could assign a neurotransmitter and/or a neuropeptide to most of the ciliomotor neurons. We identified three main ciliomotor systems, consisting of either cholinergic, serotonergic, or mixed catecholaminergic/peptidergic neurons. We describe these in detail below.

The cholinergic circuitry

We identified 11 cholinergic ciliomotor neurons in the larva (***Figure 2***, ***Figure 2—figure supplement 1***). These include the previously described six ventral decussating cholinergic motorneurons (vMNs, including MN^{r1}, MN^{r2}, MN^{r3}, MN^{l1}, MN^{l2}, MN^{l3}) and two rhabdomeric photoreceptor cells of the

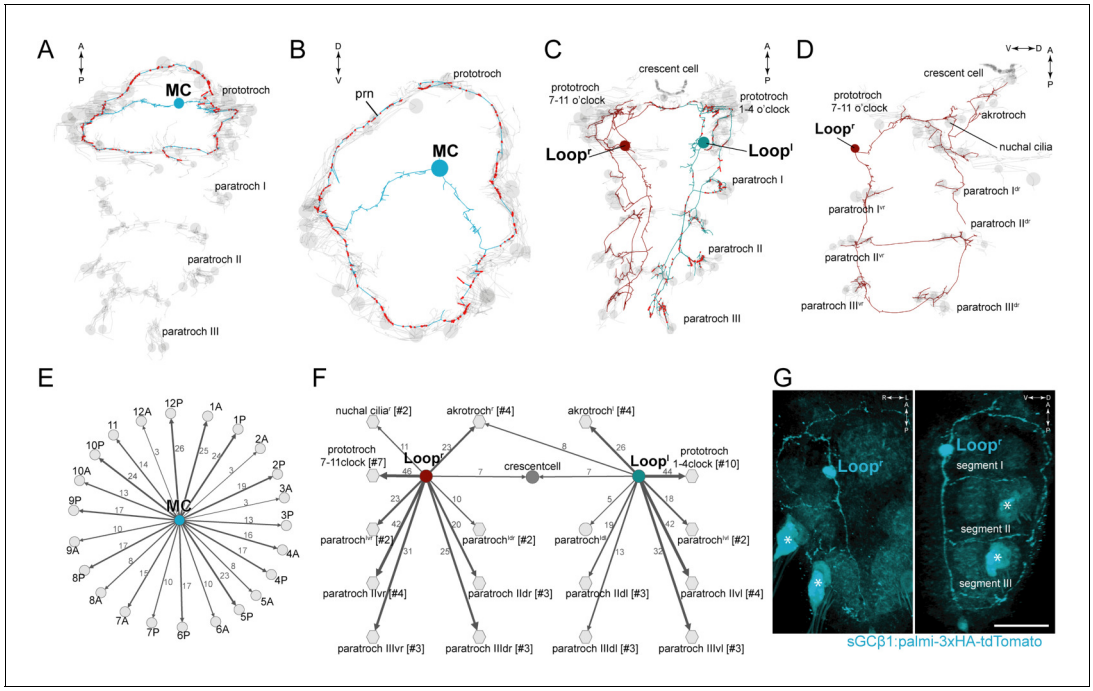

Figure 2. Anatomy and connectivity of biaxonal cholinergic ciliomotor neurons. (**A**) ssTEM reconstruction of the MC neuron (blue), ventral view. Ciliated cells are shown in grey. Circles represent position of cell body, lines represent axonal track. Presynaptic sites along the axon are marked in red. (**B**) The MC neuron in anterior view. (**C**) ssTEM reconstruction of the Loop neurons, ventral view. (**D**) The right Loop neuron in lateral view. (**E**) Synaptic connectivity of the MC neuron and the prototroch cells. (**F**) Synaptic connectivity of the Loop neurons and ciliary band cells. (**G**) Transgenic labelling of the right Loop neuron with an *sGCβ1:palmi-3xHA-tdTomato* construct. Expression was detected with anti-HA antibody staining. Right panel: ventral view, left panel: lateral view. Asterisks indicate background signal in the spinning glands. In the network graphs, nodes represent individual or grouped cells, as indicated by the numbers in square brackets. The edges show the direction of signalling from presynaptic to postsynaptic cells. Edges are weighted by the number of synapses. The number of synapses is indicated on the edges. Scale bar, 40 μm (**G**). Abbreviation: prn, prototroch ring nerve.

DOI: 10.7554/eLife.26000.008

The following figure supplements are available for figure 2:

Figure supplement 1. Anatomy and connectivity of eyespotPRC^{R3}, ventral MN, and MN^{ant} ciliomotor neurons.

DOI: 10.7554/eLife.26000.009

Figure supplement 2. sGCbeta1 is a cholinergic marker.

DOI: 10.7554/eLife.26000.010

larval eyespots (eyespotPRC^{R3}) (***Figure 2—figure supplement 1***) (***Randel et al., 2014***, ***2015***; ***Jékely et al., 2008***). In addition to these neurons, we found three large biaxonal ciliomotor neurons, including a single ciliomotor neuron in the head, the MC neuron, and two trunk ciliomotor neurons that we call the Loop neurons (***Figure 2A–D***, ***Video 5***).

The MC neuron has its soma in the centre of the larval head and projects two axons that run left and right towards the ciliary band. The axons branch at the prototroch and form dorsal and ventral branches that run along the prototroch ring nerve, a nerve running at the inside of the prototroch ring. The MC neuron is the most synapse-rich neuron in the entire *Platynereis* larval connectome (unpublished results) (***Randel et al., 2015***; ***Shahidi et al., 2015***; ***Randel et al., 2014***). We identified 341 presynaptic sites in the MC neuron. 335 of these target the ciliated cells of the prototroch ciliary band. The MC neuron is the only neuron in the body that is presynaptic to each of the 23 prototroch cells (3–25 synapses per prototroch cell) (***Figure 2B,E***).

The somas of the Loop neurons are located in the first trunk segment. These neurons project one axon anteriorly and one posteriorly (***Figure 2C,D***, ***Video 5***). The anterior axon joins the prototroch ring nerve and continues in the dorsal side of the larva where it runs posteriorly along a thin dorsal nerve. The posterior axon runs at the lateral edge of the ventral nerve cord, spans all three trunk segments and in the third segment runs to the dorsal side where it turns anteriorly. The anterior and

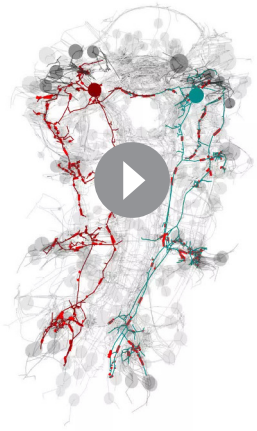

Video 5. The Loop ciliomotor neurons. ssTEM reconstruction of the Loop^{l} and Loop^{r} neurons. Ciliary bands and the ventral nerve cord are shown in grey. Synapses are marked in red.
DOI: 10.7554/eLife.26000.011

posterior axons meet on the dorsal side. The Loop neurons thus loop around the entire body spanning the head and three segments in both the ventral and dorsal side. The Loop neurons have additional side branches in the head and in every segment. These project to and synapse on cells of the different ciliary bands. A single Loop neuron synapses on every ipsilateral paratroch cell, the akrotroch, the ciliated cells of the nuchal organ, and the lateral cells of the prototroch (***Figure 2F***). The Loop neurons also synapse on the crescent cell and represent its only synaptic input. Overall, the two Loop neurons innervate all locomotor ciliary fields in the larva, with the exception of the metatroch where we could not find any synaptic input at either side in the reconstructed specimen. In the prototroch, only some of the most dorsally and ventrally located prototroch cells (at 5, 6, and 12 o'clock position) lack synaptic input from the Loop neurons (***Figure 2F***).

The anatomy and connectivity of the ventral cholinergic motorneurons (vMN) and the eyespot photoreceptors have already been described (***Jékely et al., 2008***; ***Randel et al., 2014***, ***2015***). We include them here for completion, and because we now have a more complete and revised reconstruction of the large intersegmental vMNs (***Figure 2—figure supplement 1***).

The vMNs form three left-right pairs (***Figure 2—figure supplement 1***). One pair (MN^{r1} and MN^{l1}) projects to the ventral nerve chord and innervates ventral paratroch cells and ventral longitudinal muscles. The second pair (MN^{r2} and MN^{l2}) projects dorsally and posteriorly along the trunk dorsal nerve and innervates lateral prototroch cells, dorsal paratroch cells, and dorsal longitudinal muscles. (Note that we swapped the name of MN^{l1} and MN^{l2} relative to (***Randel et al., 2015***) to reflect bilateral pairs). The third pair (MN^{r3} and MN^{l3}) is a purely ciliomotor pair (no muscle targets). Both cells synapse on lateral prototroch cells (only the posterior ring) and project to the ventral nerve cord.

The eyespotPRC^{R3} cells synapse on two ipsilateral prototroch cells of the posterior prototroch belt (***Jékely et al., 2008***; ***Randel et al., 2013***), representing two of the three direct sensory-ciliomotor neurons in the larva (***Figure 2—figure supplement 1***) (see below).

The cholinergic identity of the above neurons is supported by pharmacological experiments and by the expression of cholinergic markers (***Jékely et al., 2008***; ***Randel et al., 2014***; ***Tosches et al., 2014***; ***Denes et al., 2007***) (***Figure 2—figure supplement 2***). To further test this at the single neuron level, we developed a transgenic reporter construct for cholinergic neurons. We could not obtain a working promoter construct for the canonical cholinergic markers *vesicular acetylcholine transporter* (*VAChT*) and *choline acetyltransferase* (*ChAT*), however, we identified a *soluble guanylyl cyclase-β* gene (*sGCβ1*) that coexpresses with *ChAT* as determined by in situ hybridisation combined with whole-body gene expression registration (***Asadulina et al., 2012***) (***Figure 2—figure supplement 2***). We cloned a 12 kB fragment directly upstream of the start site of *sGCβ1* and fused it with a tdTomato fluorescent reporter. The reporter was tagged with three tandem haemagglutinin (HA) tags and a palmitoylation sequence. We used zygote microinjection and mosaic transient transgenesis to label individual cholinergic neurons. In transgenic animals, we could label the Loop neuron (***Figure 2G***) and the ventral MN^{l3} neuron (***Figure 2—figure supplement 2***), as identified by position and morphology, confirming their cholinergic identity. We could not label the MC neuron with this transgene, but its cholinergic identity is supported by *VAChT* expression in the cell body area of this cell (***Figure 2—figure supplement 2***) (***Jékely et al., 2008***) and also by pharmacological evidence (see below).

In addition to these 11 cholinergic cells, there are two biaxonal MN^{ant} cells, described before (***Randel et al., 2015***), that are likely cholinergic. These cells have their cell bodies below the ciliary

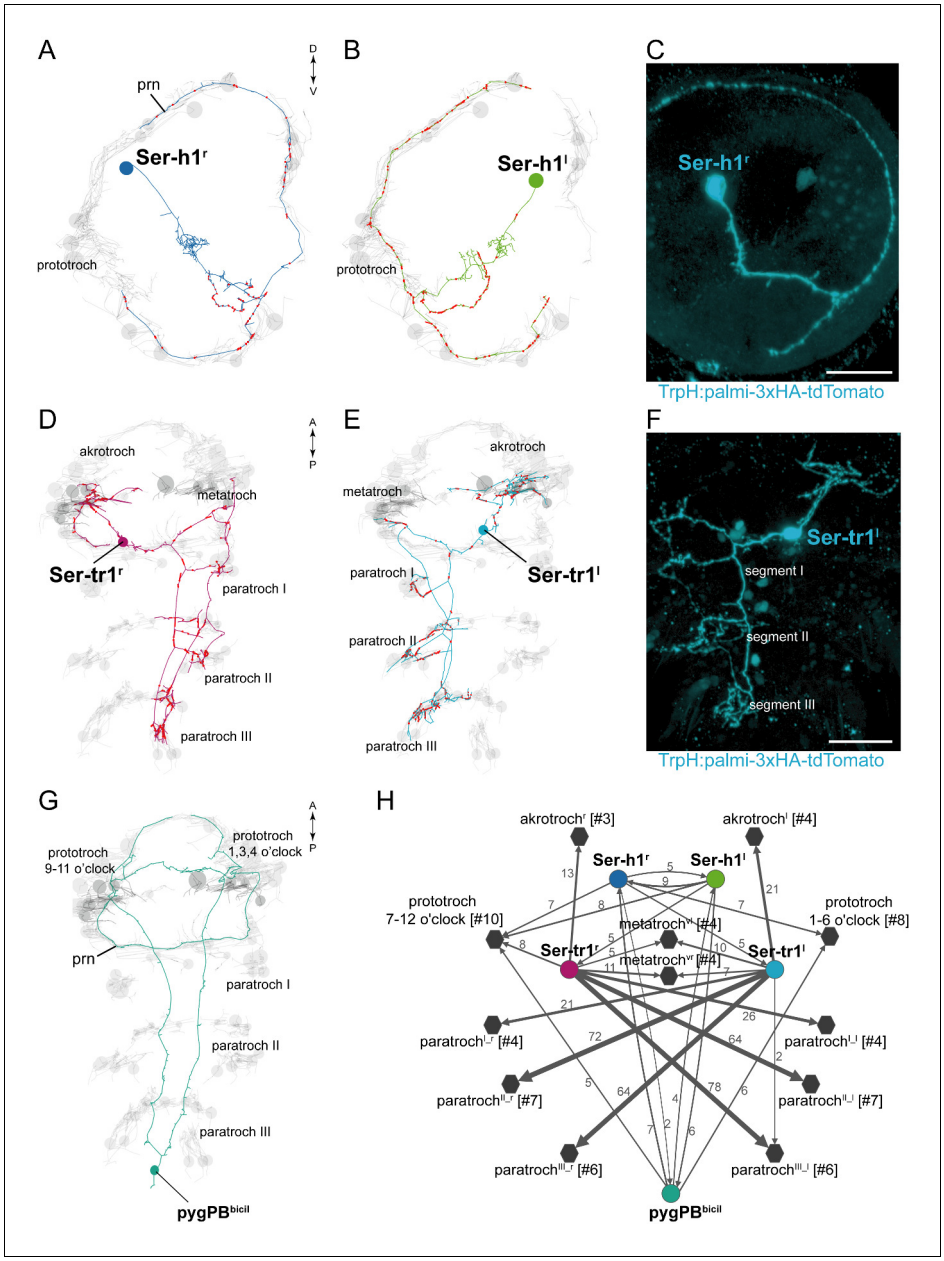

Figure 3. Anatomy and connectivity of serotonergic ciliomotor neurons. (**A–B**) ssTEM reconstruction of the right (**A**) and left (**B**) head serotonergic ciliomotor (Ser-h1) neuron, anterior view. (**C**) Transgenic labelling of the right Ser-h1 neuron with the *TrpH:palmi-3xHA-tdTomato* construct, anterior view. Expression was detected with anti-HA antibody staining. (**D–E**) ssTEM reconstruction of the right (**D**) and left (**E**) trunk serotonergic ciliomotor (Ser-tr1) cell, anterior view. (**F**) Transgenic labelling of the left Ser-tr1 neuron with the *TrpH:palmi-3xHA-tdTomato* construct, ventral view. (**G**) ssTEM reconstruction of the pygPB^{bicil} serotonergic sensory-ciliomotor neuron. Ciliated cells are shown in grey. Circles represent position of cell body, lines represent axonal track. Presynaptic sites along the axon are marked in red. (**H**) Synaptic connectivity of the serotonergic ciliomotor neurons and the ciliary band cells. Nodes represent individual or grouped cells, as indicated by the numbers in square brackets. Edges show the direction of signalling from presynaptic to postsynaptic cells. Edges are weighted by the number of synapses. Synapse number is indicated. Edges with one synapse are not shown. Scale bars, 30 µm (**C, F**). Abbreviation: prn, prototroch ring nerve.

DOI: 10.7554/eLife.26000.012

The following figure supplements are available for figure 3:

Figure supplement 1. Serotonergic neurons in *Platynereis* larvae.

DOI: 10.7554/eLife.26000.013

Figure 3 continued on next page

Figure 3 continued

Figure supplement 2. Parallel axons of the Loop and Ser-tr1 neurons.
DOI: 10.7554/eLife.26000.014

photoreceptor cells in a region of *VAChT* expression, but we could not verify their cholinergic identity at a single-cell resolution. The MN^{ant} cells form synapses on the contralateral half of the prototroch, the metatroch, and the paratrochs (***Randel et al., 2015***) (***Figure 2—figure supplement 1***).

The serotonergic circuitry

We identified five serotonergic ciliomotor neurons in the larva (***Figure 3***). There are two serotonergic ciliomotor neurons in the head (Ser-h1), with their somas lateral to the ciliary photoreceptor cells (***Figure 3A,B*** and ***Figure 3—figure supplement 1***). These neurons cross the midline and project along the contralateral side of the ciliary band, forming several synapses on the ciliated cells. The Ser-h1 cells also synapse reciprocally on each other in the brain neuropil.

In the trunk, there are two large serotonergic biaxonal neurons (Ser-tr1) with their somas in the first segment, near the somas of the cholinergic Loop neurons, anterior to the first commissure of the ventral nerve cord (***Figure 3D,E*** and ***Figure 3—figure supplement 1***). The Ser-tr1 and the Loop neurons represent the largest neurons in the entire *Platynereis* connectome (between 1,600–1,850 µm total cable length each). One of the axons of the Ser-tr1 cells projects anteriorly and innervates ipsilateral prototroch cells. The other axon crosses the midline in the first segment and its axon loops around the body, running in close proximity to the axons of the contralateral Loop neuron. The Ser-tr1 neurons also innervate every paratroch cell as well as the metatroch (***Figure 3H***). The axons of the Ser-tr1 neurons run parallel to the axons of the Loop neurons throughout the body and are ultrastructurally distinct from the Loop neurons. The Ser-tr1 axons are characterised by a less electron-dense cytoplasm and the lack of dense core vesicles (abundant in the Loop neurons) (***Figure 3—figure supplement 2***).

The Ser-tr1 cells were identified as serotonergic by comparing cell body positions and neuron

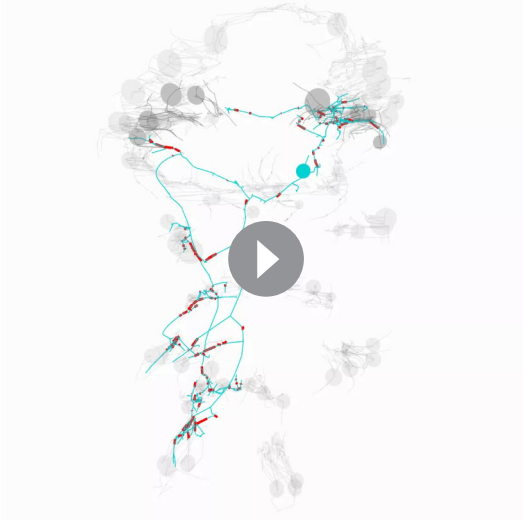

Video 6. The Ser-tr1 ciliomotor neurons. ssTEM reconstruction of the Ser-$tr1^{l}$ and Ser-$tr1^{r}$ neurons. Ciliary bands are shown in grey. The metatroch is shown in darker grey, synapses are marked in red.
DOI: 10.7554/eLife.26000.015

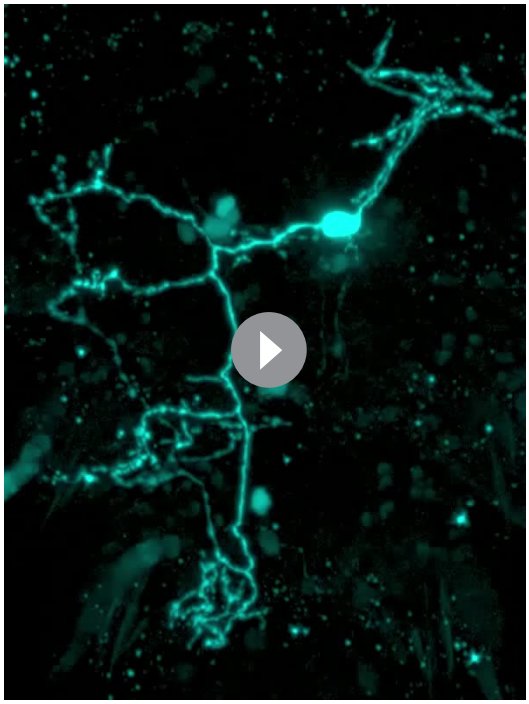

Video 7. The Ser-$tr1^{l}$ neuron labelled by transient transgenesis. The *TrpH:palmy-3xHA-tdTomato* was used to label the Ser-$tr1^{l}$ neuron. The reporter was visualised by anti-HA antibody staining.
DOI: 10.7554/eLife.26000.016

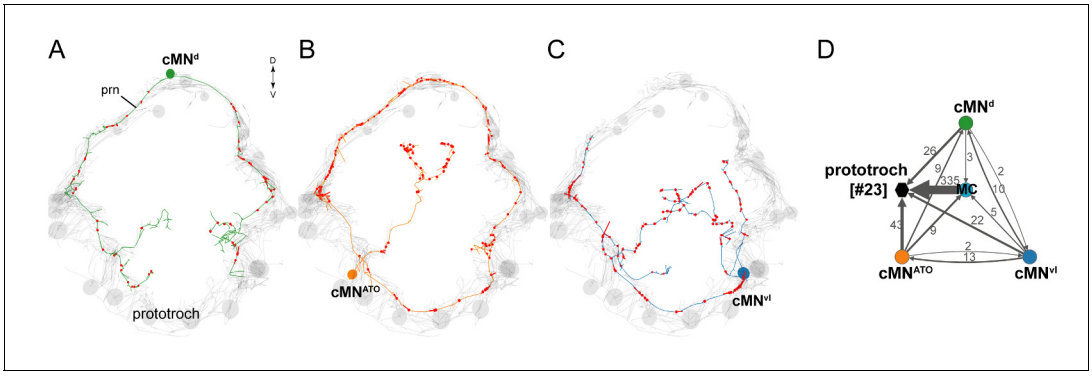

Figure 4. Anatomy and connectivity of catecholaminergic/peptidergic ciliomotor neurons. (**A–C**) ssTEM reconstruction of the cMN^{d} (green) (**A**), cMN^{ATO} (orange) (**B**), and cMN^{vl} (blue) (**C**) ciliomotor neurons, anterior view. Ciliated cells are shown in grey. Circles represent position of cell bodies, lines represent axonal tracks. Presynaptic sites along the axon are marked in red. (**D**) Synaptic connectivity of the cMN neurons with the prototroch and the MC cell. Nodes represent individual or grouped cells, as indicated by the numbers in square brackets. Edges show the direction of signalling from presynaptic to postsynaptic cells. Edges are weighted by the number of synapses and indicate the direction of signalling. Synapse number is indicated. Abbreviation: prn, prototroch ring nerve.

DOI: 10.7554/eLife.26000.017

The following figure supplement is available for figure 4:

Figure supplement 1. Catecholaminergic and neuropeptide marker expression in cMN neurons.

DOI: 10.7554/eLife.26000.018

morphologies to cells stained with a serotonin antibody in 2-day-old and 3-day-old larvae (***Figure 3—figure supplement 1***) (***Fischer et al., 2010***). We also used mosaic transient transgenesis with a construct containing a 5 kB upstream regulatory sequence of the *tryptophan hydroxylase* gene (*TrpH*), a marker of serotonergic neurons. We could label both the head Ser-h1 neurons and the Ser-tr1 cells (***Figure 3C,F***). The unique morphology of these cells and the correspondence of the TEM reconstruction (***Video 6***, ***Video 7***) to the transgenic labelling confirm the serotonergic identity of these cells.

We also identified a giant serotonergic sensory-motor neuron (pygPB^{bicil}) with a cell body in the pygidium and a unique morphology (***Figure 3G***). This cell has two sensory cilia and two axons that run anterior along the ventral nerve chord. The axons then innervate the prototroch cilia in the head and send a branch to the anterior nervous system. The pygPB^{bicil} neuron is identifiable by serotonin immunolabeling (***Figure 3—figure supplement 1***) and also expresses the neuropeptide FMRFamide as determined by serial multiplex immunogold (siGOLD) labelling (***Shahidi et al., 2015***). This cell, together with the eyespot photoreceptor cells, is the third sensory neuron that directly synapses on ciliated cells.

Catecholaminergic and peptidergic ciliomotor neurons

There are three molecularly distinct, asymmetric peptidergic cells (cMN^{vl}, cMN^{d}, cMN^{ATO}) with their cell bodies at the level of the prototroch ciliary band (***Figure 4***). (cMN^{vl} was referred to in [***Shahidi et al., 2015***] as cMN$^{PDF\text{-}vcl1}$). The two ventral-lateral cells (cMN^{vl}, cMN^{ATO}) express *tyrosine hydroxylase*, a marker of dopaminergic neurons (***Figure 4—figure supplement 1***). The cMN^{ATO} cell also expresses *dopamine-β-hydroxylase*, indicating that it is noradrenergic (***Figure 4—figure supplement 1***).

The cMN cells express different combinations of neuropeptides. The neurons cMN^{vl} and cMN^{d} express pigment dispersing factor (PDF), as determined by siGOLD (***Shahidi et al., 2015***). The cMN^{ATO} cell expresses allatotropin and its full morphology is revealed by immunostaining with an allatotropin antibody (***Figure 4—figure supplement 1***). The cMN^{vl} neuron also expresses FLamide and FVamide, cMN^{ATO} expresses DLamide, and cMN^{d} expresses the neuropeptides L11, and LYamide, as revealed by immunostainings (***Conzelmann et al., 2011***) and in situ hybridisation (***Figure 4—figure supplement 1***). The cMN cells synapse on prototroch cells and the MC cell and also synapse reciprocally among themselves (***Figure 4D***).

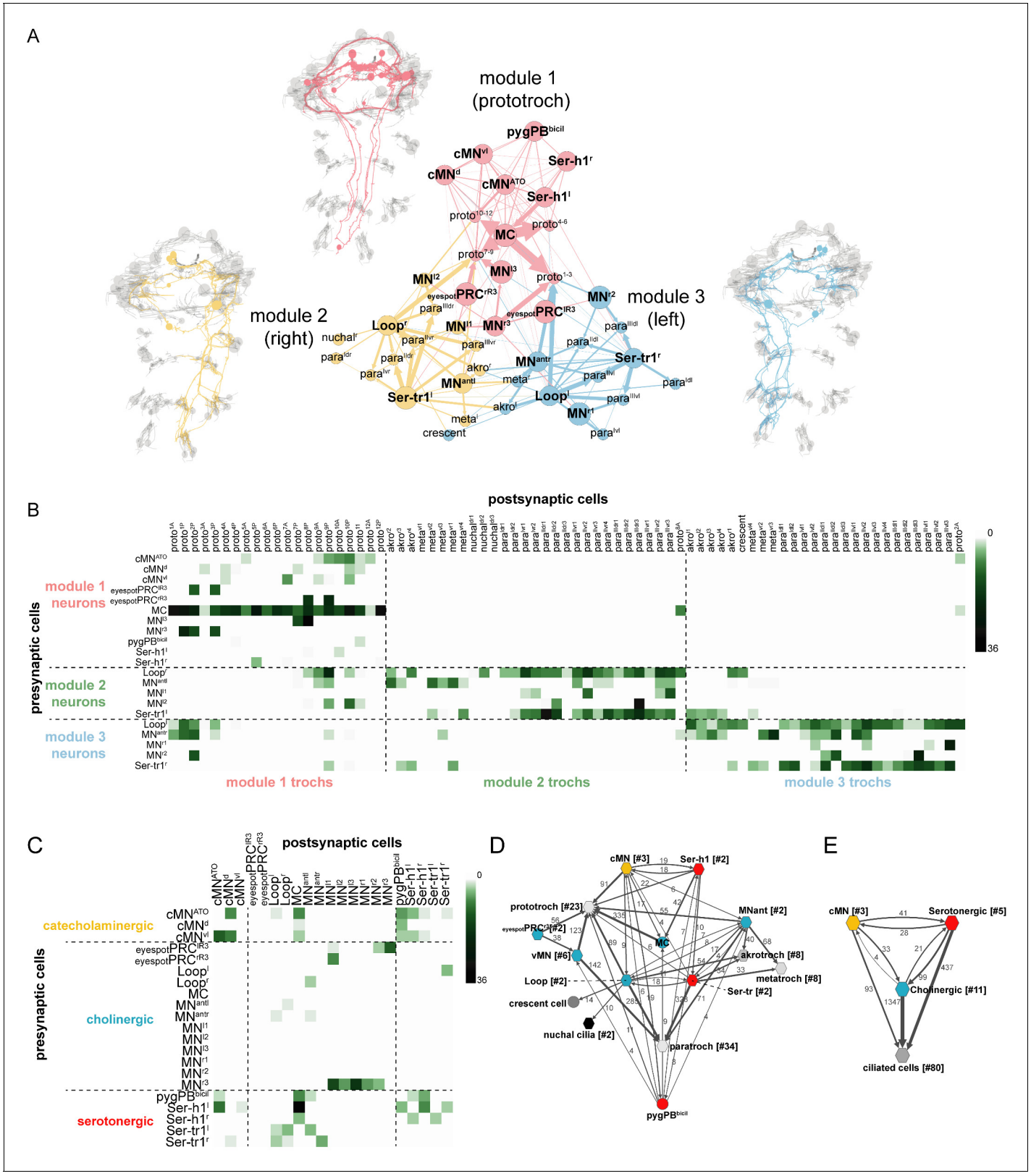

Figure 5. Overall connectivity of ciliomotor neurons and ciliary bands. (**A**) Synaptic connectivity graph of all ciliomotor neurons and ciliary band cells. The network is partitioned into three modules. The neurons belonging to each module are shown in the anatomical reconstructions. The ciliary band cells are grouped into anatomical units. (**B**) Matrix representation of the connectivity of ciliomotor neurons to all ciliated cells. Colour intensity is proportional to the number of synapses. (**C**) Matrix representation of the connectivity of ciliomotor neurons amongst themselves. Colour intensity is

Figure 5 continued on next page

Figure 5 continued

proportional to the number of synapses. (**D–E**) Graph representations of the ciliomotor circuit. Nodes with <4 synapses are not shown. In (**D**) nodes are grouped by cell type (teal, cholinergic; red, serotonergic; orange, cMN; grey, ciliated cells). In (**E**) all cMN, serotonergic, cholinergic neurons, and ciliary band cells are represented as one node each. In (**D, E**) edges with <4 synapses are not shown. Abbreviations: proto, prototroch; meta, metatroch; para, paratroch; akro, akrotroch.

DOI: 10.7554/eLife.26000.019

Overall connectivity of the ciliomotor system

To analyse the overall connectivity of the ciliomotor system (***Video 8***, ***Supplementary file 1***), we next performed modularity analysis to identify more strongly connected communities of cells (***Blondel et al., 2008***). We could subdivide the network of ciliomotor neurons and multiciliated cells into three communities each containing cells that were more strongly connected among each other (***Figure 5A***). The three modules can be distinguished primarily based on the ciliated cells they contain (***Figure 5B*** and ***Supplementary file 1***). Module 1 includes ciliomotor neurons that only innervate prototroch cells (MC, cMN, Ser-h1, and pygPB^{bicil}, MN^{l3}, MN^{r3}, eyespotPRC^{R3}, and most prototroch cells). Module 2 is composed of the right (ipsilaterally-projecting) Loop^{r} neuron and the left (contralaterally projecting) Ser-tr1^{l}, MN^{antl}, MN^{l1}, and MN^{l2} neurons. These neurons share ciliated target cells that are primarily on the right body side (***Figure 5A,B***). Module 3 includes neurons providing innervation primarily to cilia on the left body side (Loop^{l}, Ser-tr1^{r}, MN^{antr}, MN^{r1}, and MN^{r2}). Module 2 and 3 thus contain the corresponding set of left-right neuron pairs and their ciliary targets.

There are also many interconnections between ciliomotor neurons expressing distinct transmitters (cholinergic, serotonergic, and catecholaminergic/peptidergic) (***Figure 5C–E***). The cMN neurons are presynaptic to the MC neuron, the MN^{ant} and the Loop neurons, and show reciprocal connectivity with the Ser-h1 and pygPB^{bicil} cells. The serotonergic and cholinergic systems are also interconnected. The Ser-h1 cells are presynaptic to the MC neuron and the Ser-tr1 and Loop neurons are reciprocally connected. The pygPB^{bicil} neuron is also presynaptic to the MC cell (***Figure 5C–E***).

Rhythmic activation of cMN neurons in and out of phase with ciliary arrests

To functionally characterise the ciliomotor system, we performed calcium-imaging experiments in immobilized larvae ubiquitously expressing GCaMP6s. Since 3-day-old larvae are difficult to immobilize without compromising neuronal activity, we used 2-day-old larvae for activity imaging. At this stage, the musculature is not yet well developed. However, several ciliomotor neurons are already present as evidenced by immunostaining or in situ hybridisation (cMN, serotonergic, cholinergic cells) (***Figure 3—figure supplement 1***, ***Figure 4—figure supplement 1***).

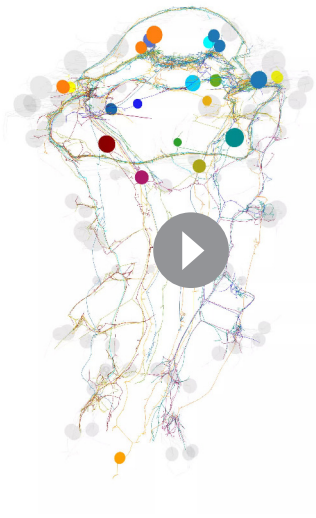

Video 8. The entire ciliomotor circuit of the *Platynereis* larva. Neuron reconstructions of all ciliomotor neurons.

DOI: 10.7554/eLife.26000.020

Calcium imaging revealed that the cMN neurons display spontaneous rhythmic activity patterns. The somas of the cMN cells are close to the prototroch cells at unique positions allowing their unambiguous identification. We found that the cMN^{vl} and cMN^{d} neurons showed rhythmic increases in the GCaMP signal in synchrony with the ciliary band (***Figure 6***). In contrast, the activity of the cMN^{ATO} was negatively correlated with the two other cMN neurons and the ciliary band (***Figure 6C,D,F***, ***Figure 6—source data 1***). We could detect the rhythmic activation of the cMN neurons in larvae from 24 hr-post-fertilisation (hpf) onwards.

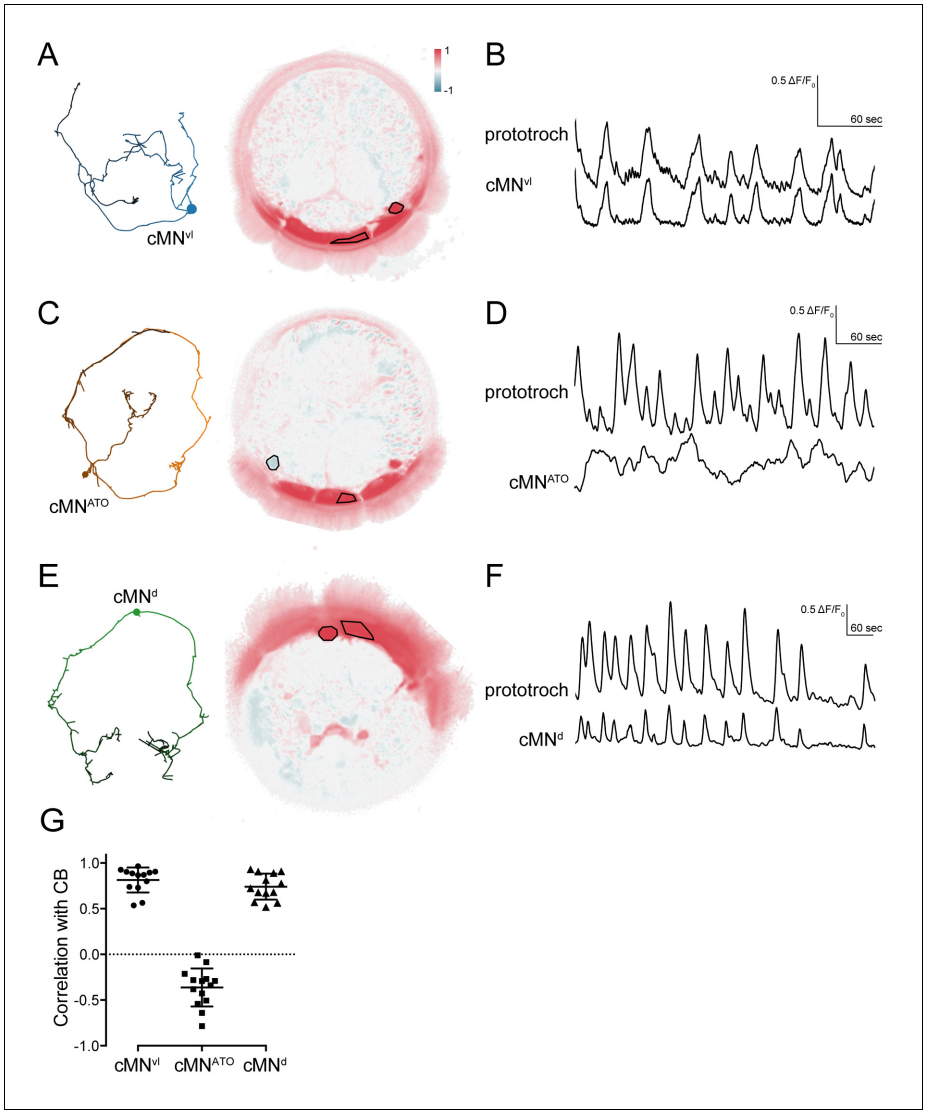

Figure 6. Activity of cMN neurons. (**A**) ssTEM reconstruction (left) and correlation (Pearson's r) map of neuronal activity (right) of cMN^{vl}, anterior view. Correlation values were calculated relative to cMN^{vl} (outlined). (**B**) Calcium-imaging trace of cMN^{vl} and the prototroch (**C**) ssTEM reconstruction (left) and correlation (Pearson's r) map of neuronal activity (right) of cMN^{ATO}. Correlation values were calculated relative to the prototroch (outlined). (**D**) Calcium imaging trace of cMN^{ATO} and the prototroch. (**E**) ssTEM reconstruction (left) and correlation (Pearson's r) map of neuronal activity (right) of cMN^{d}. Correlation values were calculated relative to cMN^{d} (outlined). (**F**) Calcium-imaging trace of cMN^{d} and the prototroch. (**G**) Correlation of GCaMP signals of cMN neurons with GCaMP signals measured from the prototroch ciliary band (CB). Data points represent measurements from different larvae, n > 12 larvae. Mean and standard deviation are shown. All sample medians are different from 0 with p-values≤0.0002 as determined by Wilcoxon Signed Rank Test.

DOI: 10.7554/eLife.26000.021

The following source data is available for figure 6:

Source data 1. Source data for ***Figure 6G*** with correlation values of neuronal activity.

DOI: 10.7554/eLife.26000.022

The MC and loop neurons trigger coordinated ciliary arrests

Next, we imaged the activity of the cholinergic MC and Loop neurons. We could identify the MC neuron based on its position and biaxonal morphology as revealed by the GCaMP signal (***Video 9***). We found that the activity of the MC neuron was periodic and strongly correlated with the activity of the prototroch cells and with ciliary arrests (***Figure 7A,D***, ***Figure 7—source data 1***). Recording from

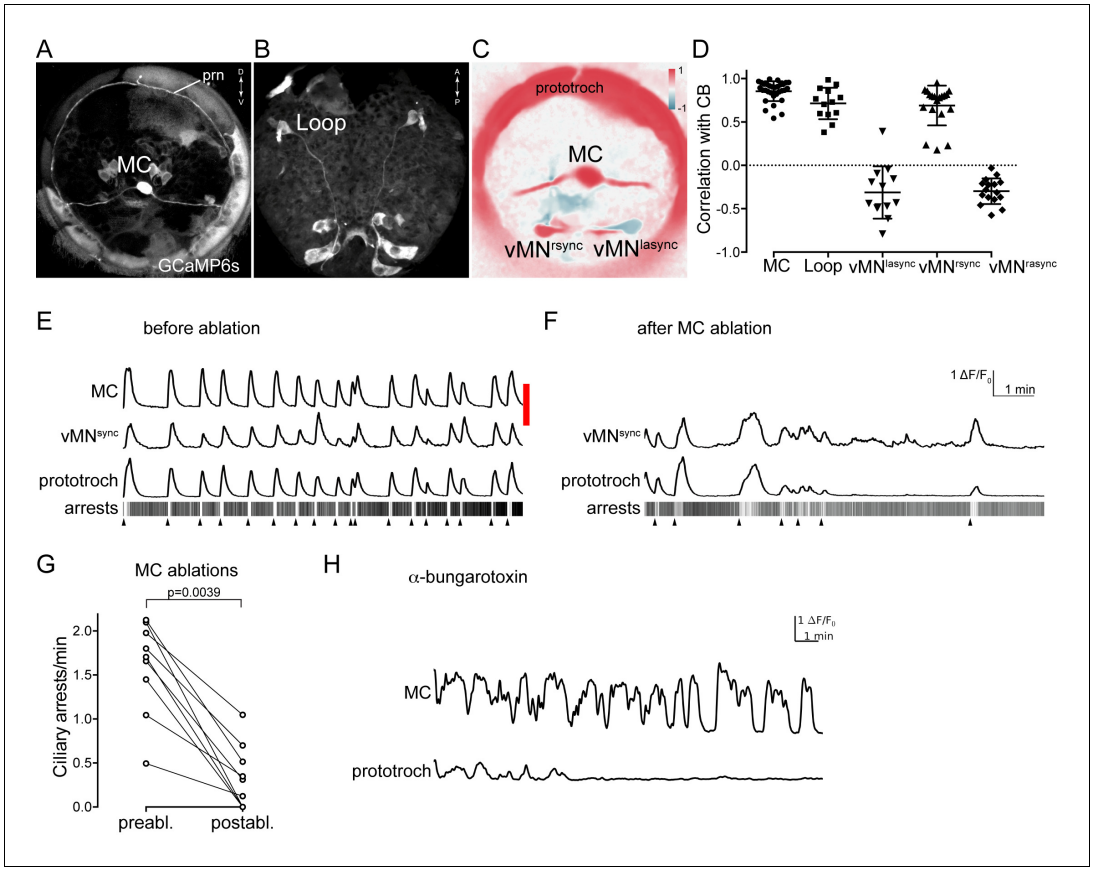

Figure 7. Activity of cholinergic neurons. (**A–B**) GCaMP6s signal revealing cell morphologies of the active MC (anterior view) (**A**) and Loop (ventral/posterior view) (**B**) neurons in 2 days-post-fertilisation larvae. (**C**) Correlation (Pearson's r) map of neuronal activity of the MC, vMN^{sync} and vMN^{async} neurons. Correlation values were calculated relative to the MC neuron. (**D**) Correlation of GCaMP signals of cholinergic neurons with GCaMP signals measured from the prototroch ciliary band (CB). Data points represent measurements from different larvae, n > 12 larvae. Mean and standard deviation are shown. All sample medians are different from 0 with p-values≤0.0034 as determined by Wilcoxon Signed Rank Test. (**E–F**) Effect of MC neuron ablation on prototroch activity and ciliary closures. Red bar represents the time of the ablation. GCaMP signals in the MC neuron, in a vMN^{sync} neuron, and in the prototroch before (**E**) and after (**F**) MC neuron ablation. (**G**) Number of ciliary arrests in the prototroch before and after MC neuron ablation. (**H**) Calcium signals measured from the MC neuron and the prototroch following the addition of 50 µM alpha-bungarotoxin. Abbreviation: prn, prototroch ring nerve.

DOI: 10.7554/eLife.26000.023

The following source data and figure supplements are available for figure 7:

Source data 1. Source data for ***Figure 7D*** with correlation values of neuronal activity.

DOI: 10.7554/eLife.26000.024

Source data 2. Source data for ***Figure 7G*** with ciliary closures before and after MC neuron ablation.

DOI: 10.7554/eLife.26000.025

Figure supplement 1. Characterisation of MC neuron activity.

DOI: 10.7554/eLife.26000.026

Figure 7–figure supplement source data 1. Source data for ***Figure 7—figure supplement 1A*** with calcium imaging data of the MC neuron from 96 individual larvae.

DOI: 10.7554/eLife.26000.027

Figure supplement 2. Effect of MC neuron ablation on prototroch activity and ciliary closures.

DOI: 10.7554/eLife.26000.028

96 different larvae (***Figure 7—figure supplement 1***, ***Figure 7—figure supplement 1—source data 1***) followed by Fourier analysis of the calcium signals revealed a median cycle length of 71 s of the

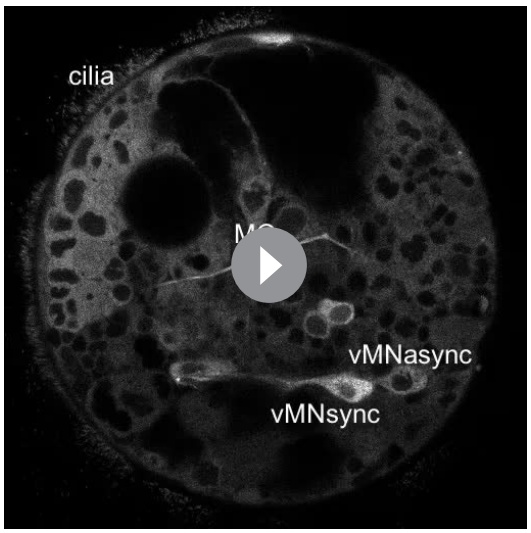

Video 9. Calcium imaging of the MC neuron in a 30 hr-post-fertilisation larva. Ubiquitously expressed GCaMP6s was used to image neuronal activity. The MC neuron, a vMN^{sync}, a vMN^{async} neuron, and prototroch cilia are labelled. The video was recorded at 1.5 fps and is shown at 45 fps.
DOI: 10.7554/eLife.26000.029

periodic activation of the MC neuron. In 43% of larvae the MC neuron had a cycle length between 50–100 s (***Figure 7—figure supplement 1***).

In the trunk, we also identified two cells in the first segment that were activated synchronously with the ciliary band cells and thus the MC neuron (though not imaged simultaneously for technical reasons). These two trunk cells had somas in the approximate position of the two Loop neurons with ipsilaterally projecting axons, and could thus be identified as the Loop neurons (***Figure 7B,D***, see also ***Figure 8—figure supplement 1A***).

In the connectome graph, the Loop and the MC neurons provide the main cholinergic motor input to the ciliary bands. Their coordinated activation and high number of synapses suggest that these cells are responsible for triggering the coordinated arrests of locomotor cilia across the body. To test this experimentally, we focused on the MC cell. First, we ablated the MC cell with a pulsed laser in 1–1.5 days-post-fertilisation larvae. MC-cell ablation eliminated the rhythmic activity in the prototroch cells and thus most ciliary arrests (***Figure 7E,F*** and ***Figure 7—figure supplement 2***, ***Figure 7—source data 2***). This shows that the MC cell is essential for triggering the rhythmic arrests of the prototroch cilia. To test whether acetylcholine is involved in rhythm generation and triggering ciliary arrests, we incubated larvae in alpha-bungarotoxin, a specific blocker of nicotinic acetylcholine receptors. When we imaged alpha-bungarotoxin-treated larvae, we observed the decoupling of the activity of the MC neuron and the ciliary band. While the MC neuron continued to rhythmically activate, the calcium signals were progressively reduced and then disappeared in the ciliary band (***Figure 7H***). Ciliary arrests were also eliminated (data not shown). This indicates that cholinergic signalling is not required for the generation of the neuronal rhythm but is required for ciliary arrests.

The ventral cholinergic motorneurons (vMN) were previously shown to rhythmically activate, and were suggested to trigger ciliary arrests (***Tosches et al., 2014***). To directly correlate the activity of these cells to ciliary activity we imaged from the ventral MN cells and the prototroch cells simultaneously. We could identify three ventral MN cells that were activated either synchronously or asynchronously (designated vMN^{sync} and vMN^{async}) with the ciliary band (***Figure 7C–E***). We cannot unambiguously link these three cells to the six ventral MN cells identified by EM, but based on cell body positions and their distinct cell lineage as identified by blastomere injections (***Tosches et al., 2014***), the ventral-most cells likely correspond to MN^{r3} and MN^{l3}. Following MC neuron ablation, the activity of the prototroch correlated with the activity of the vMN^{sync} neuron suggesting that this cholinergic neuron can maintain a lower rate of prototroch activation.

Serotonergic neuron activity is anti-correlated with cholinergic neuron activity

The cholinergic and serotonergic ciliomotor neurons have many synaptic connections, suggesting that their activity is interdependent (***Figure 5***). Correlation analysis of the calcium-imaging videos revealed that the head serotonergic cells (Ser-h1), identified by position and morphology, showed anti-correlated activity with the ciliated cells and the MC neuron (***Figure 8A,B,E***, ***Figure 8—source data 1***).

In the ventral nerve cord, we also identified two neurons whose activity was anti-correlated with the activity of the ciliary band. (***Figure 8C–E***). The GCaMP signal did not reveal the axonal morphology of these neurons, but their cell-body position corresponded to the position of the Ser-tr1 cells.

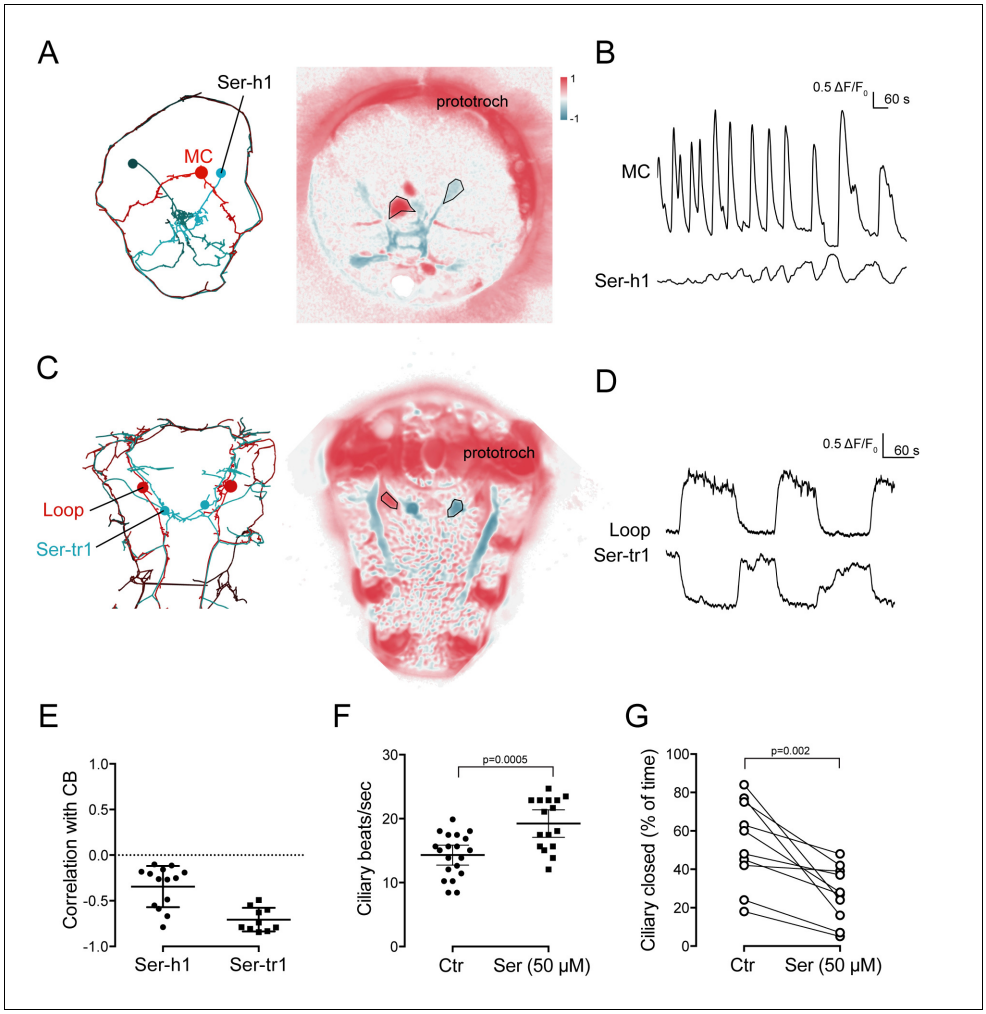

Figure 8. Activity of serotonergic neurons. (**A**) ssTEM reconstruction (left) and correlation (Pearson's r) map of neuronal activity (right) of the Ser-h1 neurons, anterior view. Correlation values were calculated relative to the MC neuron (outlined). (**B**) Calcium signals measured from a Ser-h1 neuron and the MC cell. (**C**) ssTEM reconstruction (left) and neuronal activity correlation (right) of the Ser-tr1 neurons, ventral view. Correlation values were calculated relative to the Loop neuron (outlined). (**D**) Calcium signals measured from a Ser-tr1 neuron and a Loop neuron. (**E**) Correlation of GCaMP signals of serotonergic neurons with GCaMP signals measured from the prototroch ciliary band (CB). Data points represent measurements from different larvae, n > 9. Mean and standard deviation are shown. All sample medians are different from 0 with p-values≤0.002 as determined by Wilcoxon Signed Rank Test. (**F**) Ciliary beat frequency of prototroch cilia in the absence and presence of serotonin. (**G**) Ciliary closures of prototroch cilia in the absence and presence of serotonin. P-values of an unpaired (**F**) and paired (**G**) t-test are shown. In (**F**,**G**) n > 9 larvae. Samples in (**F**,**G**) passed the D'Agostino and Pearson omnibus normality test (alpha = 0.05).

DOI: 10.7554/eLife.26000.030

The following source data and figure supplement are available for figure 8:

Source data 1. Source data for ***Figure 8E*** with correlation values of neuronal activity.

DOI: 10.7554/eLife.26000.031

Source data 2. Source data for ***Figure 8F***.

DOI: 10.7554/eLife.26000.032

Source data 3. Source data for ***Figure 8G***.

DOI: 10.7554/eLife.26000.033

Figure supplement 1. In vivo labelling of a Ser-tr1 cell by photoactivation during calcium imaging.

DOI: 10.7554/eLife.26000.034

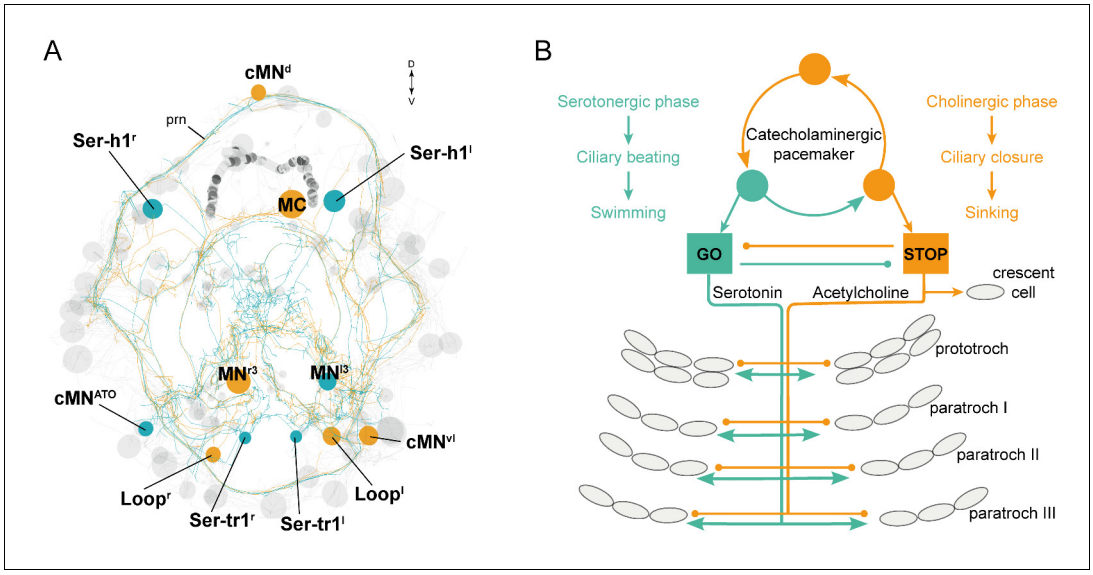

Figure 9. The stop-and-go ciliomotor system of the *Platynereis* larva. (**A**) ssTEM reconstruction of ciliomotor neurons that are activated synchronously (orange) and asynchronously (teal) with the ciliary bands. (**B**) Schematic of the circuitry, consisting of a pacemaker system, as well as cholinergic and serotonergic ciliomotor neurons that span the entire body and innervate all multiciliated cells. Abbreviation: prn, prototroch ring nerve.
DOI: 10.7554/eLife.26000.035

To directly test the identity of these cells, we performed in vivo photoactivation experiments. We co-injected GCaMP mRNA with an mRNA encoding a photoactivatable mCherry fluorescent protein (PAmCherry1). During calcium imaging, we identified the Ser-tr1 candidate neuron based on its activity and then photoactivated PAmCherry1 in this neuron. The larvae were subsequently fixed and stained for serotonin. In all cases (n = 11 larvae) we labelled the serotonergic Ser-tr1 neuron, together with a few out-of-focus cells that were labelled more weakly (***Figure 8—figure supplement 1***).

To further explore how serotonin influences ciliary activity, we treated larvae with serotonin. Serotonin increased ciliary beat frequency and inhibited ciliary arrests compared to untreated larvae (***Figure 8F,G***, ***Figure 8—source data 2***, ***Figure 8—source data 3***).

Discussion

The three-segmented *Platynereis* larva has many distinct cell groups with locomotor cilia that efficiently propel the larva in water. Periods of swimming are interrupted by ciliary arrests. Here we investigated how spontaneous ciliary arrests and beating are coordinated across ciliated fields.

With whole-body connectomics and calcium imaging, we described the anatomy, connectivity, and activity of the entire ciliomotor system in the *Platynereis* larva. In trochophore larvae, which do not yet have a functioning musculature, this system represents the entire motor part of the nervous system.

One of the most fascinating aspects of this ciliomotor system is its rhythmic pattern of activation consisting of two alternating phases. In one phase, a dopaminergic, a peptidergic, and several cholinergic neurons are active together with the ciliary band cells. In the other phase, anti-correlated with the cholinergic rhythm, one noradrenergic neuron and the serotonergic neurons are active. Our connectome and imaging data indicate the rhythm is generated by the interactions of the ciliomotor neurons themselves. This is supported by the presence of many and often reciprocal synaptic connections between the ciliomotor motorneurons. We cannot exclude the possibility that interneurons connecting distinct ciliomotor neurons are involved in the generation of the rhythmic pattern and the synchronisation of ciliomotor activity. We could identify such interneurons in the connectome (unpublished results). However, we could not observe rhythmic activity for any of these interneurons by calcium imaging.

We could subdivide the ciliomotor circuit into three connectivity modules. All three modules contain both serotonergic and cholinergic neurons and have largely non-overlapping ciliary targets (prototroch, left and right ciliated fields, respectively). Module 1 is special in that besides the serotonergic and cholinergic neurons it also contains the three unpaired peptidergic cMN neurons, two of which are also catecholaminergic. These neurons are likely involved in the generation of the rhythmic pattern. Three observations support this. First, together with the MC neuron, the cMN cells are the first neurons that show a rhythmic pattern during development. Second, they contain three cells with distinct transmitter profiles suggesting the possibility of antagonistic reciprocal signalling. Third, they are presynaptic or reciprocally connected with all the other ciliomotor neurons. For example, the cMN neurons are presynaptic to both the MC and the Loop neurons that are not themselves directly connected, yet activate synchronously. We can also exclude a role for cholinergic neurons in rhythm generation since blocking cholinergic transmission did not eliminate the rhythmic activation of the MC neuron. The precise delineation of the pacemaker neurons will require further cell ablation studies.

The function of the rhythmically active ciliomotor circuitry is to trigger the coordinated arrests of all cilia in the body and likely to trigger the coordinated resumption of beating. Targeted neuron ablation revealed a critical role for the cholinergic MC neuron in coordinated arrests of prototroch cilia suggesting that this neuron relays the rhythmic activation of the cMN neurons to trigger arrests. Our imaging and connectome data suggest that the MC neuron together with the two Loop neurons is able to trigger coordinated, body-wide ciliary arrests. These three cells innervate all multiciliated cells in the body (with the exception of the metatroch). Arrests of metatroch cilia may be triggered by the MN^{ant} neurons, the only putatively cholinergic neurons that innervate the metatroch. The metatroch is a special ciliary band that in some feeding trochophore larvae beats in opposition to the prototroch to collect food particles (***Rouse, 1999***; ***Pernet and Strathmann, 2011***). The distinct pattern of innervation for the metatroch may reflect the unique evolutionary history of this ciliary band.

The crescent cell represents another specialised multiciliated cell. This cell shows a beat pattern alternating with the beating of locomotor cilia. Crescent cilia thus beat when the larvae do not swim. The only synaptic contacts to the crescent cell come from the Loop neurons. The crescent cell also shows increases in calcium signals, in synchrony with the ciliary bands. However, crescent cilia respond differently to stimulation than locomotor cilia and start beating instead of arresting. The crescent cell is in the middle of the apical organ, a sensory area. Beating of the crescent cilia may serve to generate water flow to facilitate chemosensory sampling in the apical organ, similar to the role of cilia-generated flows in olfaction in fish (***Reiten et al., 2017***).

Parallel and upstream to the cholinergic system, we identified four serotonergic ciliomotor neurons that also collectively innervate all ciliary bands. Serotonergic cells are also presynaptic to the cholinergic cells and serotonin application suppresses closures and increases ciliary beat frequency. Determining the site of serotonin action would require further studies. One possibility is that serotonin influences the pacemaker activity thereby indirectly affecting closures. Serotonin may also act directly on ciliated cells via serotonergic synapses to increase beat frequency. The activation of the serotonergic cells corresponds to periods of swimming and thus these cells are likely responsible for the resumption of beating.

The monoamines and neuropeptides we mapped to the ciliomotor neurons may act at synapses or extrasynaptically (***Bentley et al., 2016***). Understanding the details of signalling will require the identification of the receptor expressing cells. We recently characterised several neuropeptide receptors, adrenergic receptors and other monoamine receptors in *Platynereis* (***Bauknecht and Jékely, 2017***, ***2015***). We also developed a method to dissect chemical connectivity of neuropeptide signalling with cellular resolution (***Williams et al., 2017***). These approaches will help to dissect the mechanisms of rhythm generation and the modulation of the rhythm and ciliary activity.

What is the relevance of coordinated ciliary arrests for larval behaviour? It was shown that in freely-swimming *Platynereis* larvae the alternation of periods of upward swimming (when cilia beat) and sinking (when cilia are arrested) is important for maintaining a constant depth in the water column of the negatively buoyant larvae (***Conzelmann et al., 2011***). It is remarkable that the *Platynereis* larval nervous system exhibits a rhythmic autonomic activity already in the 1-day-old stage, when the nervous system only consists of <20 differentiated neurons. This ongoing activity is present in all larvae and is not induced by sensory input. Early larval behaviour is thus best described in operant

terms (**Brembs, 2017**). This autonomic activity can then be modified by sensory input. Several neuromodulators, including neuropeptides and melatonin were shown to either inhibit or induce ciliary arrests, and thereby shift larvae upwards or downwards in the water column (**Conzelmann et al., 2011**, **2013**; **Tosches et al., 2014**). Many neuropeptides are expressed in sensory-neurosecretory cells, suggesting that sensory cues can influence larval swimming by neuroendocrine signalling (**Conzelmann et al., 2013**; **Tessmar-Raible et al., 2007**). The serotonergic and cholinergic ciliomotor neurons are also postsynaptic to functionally distinct sensory neuron pathways that can trigger ciliary arrests or induce swimming by synaptic signalling (unpublished results).

The ciliomotor system we describe here represents a novel pacemaker motor circuit that forms a stop-and-go system for ciliary swimming (**Figure 9**). Remarkably, some of the neurons in this circuit (Loop and Ser-tr1 neurons) span twice the entire body length to coordinately regulate segmental cilia. Furthermore, many cells have a biaxonal morphology, a feature that is very rare in *Platynereis* neurons belonging to other circuits (**Randel et al., 2014**; **Shahidi et al., 2015**). Comparative morphological studies using histological techniques suggest that similar ciliomotor systems, sometimes with large biaxonal neurons (**Temereva and Wanninger, 2012**), are widespread in ciliated larvae. Serotonergic neurons innervating ciliary bands have been described in several groups (**Hay-Schmidt, 2000**), including annelid (**Voronezhskaya et al., 2003**), mollusc (**Friedrich et al., 2002**; **Kempf et al., 1997**), phoronid (**Temereva and Wanninger, 2012**), and bryozoan larvae (**Wanninger et al., 2005**), and likely represent an ancestral character in lophotrochozoans (**Wanninger et al., 2005**). Serotonergic innervation of ciliary bands is also present in deuterostomes, including echinoderm and hemichordate larvae (**Hay-Schmidt, 2000**). Likewise, catecholamine-containing processes innervate ciliary bands in mollusc (**Croll et al., 1997**), phoronid (**Hay-Schmidt, 1990b**), echinoderm, hemichordate (**Dautov and Nezlin, 1992**; **Nezlin, 2000**), and nemertean larvae (**Hay-Schmidt, 1990a**). Cholinergic nerves also often associate with ciliary bands in echinoderm, hemichordate (**Dautov and Nezlin, 1992**; **Nezlin, 2000**), and mollusc larvae (**Raineri, 1995**).

One intriguing (although controversial) scenario is that ciliated larvae and their nervous systems, including the apical sensory organ (**Marlow et al., 2014**) and the ciliomotor systems, are homologous across bilaterians or even eumetazoans. If this is the case, this could mean that the *Platynereis* ciliomotor system represents an ancient system that evolved close to the origin of the nervous system (**Jékely, 2011**). The internal coordination of multiciliated surfaces may thus have been one of the early functions of nervous systems (**Jékely et al., 2015**). In-depth comparative studies are needed to understand how larval locomotor systems are related and whether ciliary coordination has a common origin or evolved multiple times independently.

Materials and methods

Animal culture and behavioural experiments

Platynereis dumerilii larvae were reared at 18˚C in a 16 hr light 8 hr dark cycle until the behavioural experiments. Occasionally animals were kept overnight at 10˚C to slow down growth. Larvae were raised to sexual maturity according to established breeding procedures (**Hauenschild and Fischer, 1969**). We found that nectochaete larvae showed very similar ciliary activity to trochophore larvae, but younger larvae displayed fewer muscle contractions. For this reason, we often used younger animals for recordings. Experiments were conducted at 22˚C, most often between 36 and 52 hr-post-fertilisation.

In situ hybridization and immunohistochemistry

Whole mount in situ hybridization, and confocal imaging of the animals were performed as described previously (**Asadulina et al., 2012**). Immunostainings were done as described in (**Conzelmann and Jékely, 2012**) with modifications. The custom-made *Platynereis* allatotropin antibody was described in (**Shahidi et al., 2015**). Larvae were fixed with 4% formaldehyde in PTW (PBS + 0.1% Tween-20) for 15 min at room temperature and rinsed three times with PTW. Larvae were blocked in PTWST (PTW, 5% sheep serum, 0.1% Triton-X 100) at room temperature, incubated overnight in 1:250 rabbit anti-HA antibody (rabbit, RRID: AB_1549585) and 1:250 anti acetylated-tubulin antibody (mouse, RRID: AB_477585) in PTWST. Larvae were washed five times for 20–60 min

in PTW, blocked for 1 hr in PTWST at room temperature and incubated for 2 hr at room temperature in anti-mouse Alexa Fluor-488 1:250 (goat, RRID: AB_2534069) and anti-rabbit Alexa Fluor-633 1:250 (goat, RRID: AB_2535731), in PTWST. Larvae were washed five times for 20–60 min in PTW and transferred gradually to 97% 2,2'-thiodiethanol (TDE) (166782, Sigma-Aldrich, St. Louis, USA) in steps of 25% TDE/PTW dilutions. For the whole-mount in situ and immunostaining samples we generated projections using Imaris 8.0.2 (Bitplane, Zürich).

Connectome reconstruction, neuron and network visualisation

Neuron reconstruction, visualization, and synapse annotation were done in Catmaid (***Schneider-Mizell et al., 2016***; ***Saalfeld et al., 2009***) as described before (***Randel et al., 2015***; ***Shahidi et al., 2015***). The ciliomotor neurons described here include all neurons that form at least five synapses combined on any of the multiciliated cells in the whole larval body. Six neurite fragments could not be linked to a cell body, these were omitted from the analyses.

Neurons were named based on transmitter content or morphology and position, (e.g., dorsal ciliomotor, cMN^{d}, ventral left ciliomotor, cMN^{vl}). The ciliated troch cells were named following the morphological literature. We numbered prototroch cells based on their position (e.g. 2 o'clock) and whether they belong to the anterior or posterior prototroch ring (e.g., $proto^{5P}$ is the posterior prototroch cell at 5 o'clock position in the ring). We grouped paratroch cells from the same larval segment into four clusters, based on their position (e.g., $para^{IIIvl1}$ is a paratroch cell in the third segment in the ventral-left cluster). Cells are labelled based on body side of their soma (left $^{[l]}$ or right $^{[r]}$).

Network analyses were done in Catmaid (RRID:SCR_006278) and Gephi 0.8.2 (RRID:SCR_004293). Modules were detected in Gephi with an algorithm described in (***Blondel et al., 2008***) with randomization on, using edge weights and a resolution of 1.4. Force-field-based clustering was performed using the Force Atlas 2 Plugin.

Cable length was measured in Catmaid using skeleton smoothing with Gaussian convolution with a sigma of 6 µm.

Imaging

Ciliary beating and ciliary arrests were imaged with a Zeiss Axioimager microscope (Carl Zeiss, Jena, Germany) and a DMK 21BF04 camera (The Imaging Source, Bremen, Germany) at 60 frames per second. Experiments were done at room temperature in filtered natural seawater. Larvae were immobilized between a slide and a coverslip spaced with adhesive tape. Calcium-imaging experiments were performed with GCaMP6s (***Chen et al., 2013***) mRNAs (1000 µg/µL) injected in one-cell stage as described previously (***Randel et al., 2014***). Injected larvae were mounted following the same protocol as ciliary beating experiments. Confocal images were taken on an Olympus Fluoview-1200 (with a UPLSAPO 60X water-immersion objective, NA 1.2), and a Leica TCS SP8 (with a 40X water-immersion objective, NA 1.1) confocal microscopes. Movies were acquired with a temporal resolution between 0.8 and 45 Hz. Responses to drugs were imaged 5–20 min after application to the bath and without any change of imaging settings.

Laser ablation

Laser ablation was performed on the Olympus FV1200 confocal microscope equipped with a SIM scanner (Olympus Corporation, Tokyo, Japan), as described in (***Randel et al., 2014***). Larvae were immobilized between a slide and a coverslip. A 351 nm pulsed laser (Teem Photonics, Grenoble, France) at 90–95% power was used, coupled via air to the SIM scanner for controlled ablation in a region of interest (ROI). 95% corresponds to a beam power of 297.5 µwatts as measured with a microscope slide power sensor (S170C; Thorlabs, Newton, USA).

Photoactivation

PAmCherry1 (Addgene plasmid 31928) was cloned into a *Platynereis* expression vector (pUC57-T7-RPP2-(NLS)pPAmCherry1) (***Randel et al., 2014***) with an NLS-tag before the N-terminus. PAmCherry1 RNA was synthesized in vitro and co-injected with GCaMP6s RNA. Photoactivation in a region of interest was performed with a 405 nm laser (0.2% power) with 2–3 200 msec pulses using the SIM scanner of an Olympus FV12000 confocal microscope. Photo-activated larvae were

recovered from the slide, fixed and processed for immunostaining with serotonin (rabbit, RRID: AB_572263) and acetylated tubulin (mouse, RRID: AB_477585) antibodies.

Data analysis and image registration

GCaMP6s movies were analysed with FIJI (***Schindelin et al., 2012***) (RRID:SCR_002285) and a custom Python script, as described in (***Gühmann et al., 2015***) with modifications (***Verasztó, 2017***). The same ROI was used to quantify fluorescence before and after drug application. Data are presented as $\Delta F/F_0$. For the calculation of the normalized $\Delta F/F_0$ with a time-dependent baseline, F_0 was set as the minimum standard deviation of fluorescence in a 10-frame-window in every experiment. Videos were motion-corrected in FIJI with moco (***Dubbs et al., 2016***) and Descriptor based registration (https://github.com/fiji/Descriptor_based_registration). Correlation analyses and fast Fourier transformation to compute the discrete Fourier transform of activation sequences were done using FIJI and Python scripts (***Verasztó, 2017***; a copy is archived at https://github.com/elifesciences-publications/Veraszto_et_al_2017). We only analysed segments of videos without movement artefacts. The ROI was defined manually and was correlated with every pixel of the time-series. Finally, a single image was created with the Pearson correlation coefficients and a [−1, 1] heatmap plot with two colours.

Acknowledgements

We thank Sara Mendes for cloning the palmitoylation tag into the reporter vector. We thank Markus Conzelmann for generating antibodies, and Christian Liebig for help with microscopy. The research leading to these results received funding from the European Research Council under the European Union's Seventh Framework Programme (FP7/2007-2013)/European Research Council Grant Agreement 260821. This project is supported by the Marie Curie ITN 'Neptune', GA 317172, funded under the FP7, PEOPLE Work Programme of the European Commission. This project is supported by the DFG - Deutsche Forschungsgemeinschaft (Reference no. JE 777/3–1).

Additional information

Funding

Funder	Grant reference number	Author
Deutsche Forschungsgemeinschaft	777/3-1	Gáspár Jékely
Max-Planck-Gesellschaft	Open-access funding	Gáspár Jékely
European Commission	GA 317172	Gáspár Jékely

The funders had no role in study design, data collection and interpretation, or the decision to submit the work for publication.

Author contributions

CV, Conceptualization, Data curation, Software, Formal analysis, Validation, Investigation, Visualization, Methodology, Writing—review and editing; NU, LAB-C, Investigation, Visualization, Methodology, Writing—review and editing; AP, Investigation, Visualization, Methodology; EAW, Investigation, Methodology, Writing—review and editing; RS, Resources, Investigation, Visualization, Methodology, Writing—review and editing; GJ, Conceptualization, Data curation, Formal analysis, Supervision, Funding acquisition, Validation, Investigation, Visualization, Writing—original draft, Project administration, Writing—review and editing

Author ORCIDs

Csaba Verasztó, http://orcid.org/0000-0001-6295-7148
Luis A Bezares-Calderón, http://orcid.org/0000-0001-6678-6876
Gáspár Jékely, 0000-0001-8496-9836

Additional files

Supplementary files

• Supplementary file 1. Synaptic connectivity matrix of ciliomotor neurons and multiciliated cells.
DOI: 10.7554/eLife.26000.036

Major datasets

The following previously published dataset was used:

Author(s)	Year	Dataset title	Dataset URL	Database, license, and accessibility information
Shahidi et. al	2017	Full-body serial TEM dataset of a Platynereis nectochaete larva	https://neurodata.io/	

References

Alvarez L, Dai L, Friedrich BM, Kashikar ND, Gregor I, Pascal R, Kaupp UB. 2012. The rate of change in Ca(2+) concentration controls sperm chemotaxis. *The Journal of Cell Biology* **196**:653–663. doi: 10.1083/jcb.201106096, PMID: 22371558

Arkett SA, Mackie GO, Singla CL. 1987. Neuronal control of ciliary locomotion in a gastropod veliger (*CALLIOSTOMA*). *The Biological Bulletin* **173**:513–526. doi: 10.2307/1541697

Asadulina A, Panzera A, Verasztó C, Liebig C, Jékely G. 2012. Whole-body gene expression pattern registration in Platynereis larvae. *EvoDevo* **3**:27. doi: 10.1186/2041-9139-3-27, PMID: 23199348

Bauknecht P, Jékely G. 2015. Large-Scale combinatorial deorphanization of Platynereis neuropeptide GPCRs. *Cell Reports* **12**:684–693. doi: 10.1016/j.celrep.2015.06.052, PMID: 26190115

Bauknecht P, Jékely G. 2017. Ancient coexistence of norepinephrine, tyramine, and octopamine signaling in bilaterians. *BMC Biology* **15**:6. doi: 10.1186/s12915-016-0341-7, PMID: 28137258

Bentley B, Branicky R, Barnes CL, Chew YL, Yemini E, Bullmore ET, Vértes PE, Schafer WR. 2016. The multilayer connectome of Caenorhabditis elegans. *PLoS Computational Biology* **12**:e1005283. doi: 10.1371/journal.pcbi.1005283, PMID: 27984591

Blondel VD, Guillaume J-L, Lambiotte R, Lefebvre E. 2008. Fast unfolding of communities in large networks. *Journal of Statistical Mechanics: Theory and Experiment* **2008**:P10008. doi: 10.1088/1742-5468/2008/10/P10008

Brembs B. 2017. Operant behavior in model systems. In: *Reference Module in Neuroscience and Biobehavioral Psychology*. Elsevier. doi: 10.1016/B978-0-12-809324-5.21032-8

Brumley DR, Polin M, Pedley TJ, Goldstein RE. 2012. Hydrodynamic synchronization and metachronal waves on the surface of the colonial alga Volvox carteri. *Physical Review Letters* **109**:268102. doi: 10.1103/PhysRevLett.109.268102, PMID: 23368623

Brumley DR, Wan KY, Polin M, Goldstein RE. 2014. Flagellar synchronization through direct hydrodynamic interactions. *eLife* **3**:e02750. doi: 10.7554/eLife.02750, PMID: 25073925

Brumley DR, Polin M, Pedley TJ, Goldstein RE. 2015. Metachronal waves in the flagellar beating of Volvox and their hydrodynamic origin. *Journal of the Royal Society Interface* **12**:20141358. doi: 10.1098/rsif.2014.1358, PMID: 26040592

Chen TW, Wardill TJ, Sun Y, Pulver SR, Renninger SL, Baohan A, Schreiter ER, Kerr RA, Orger MB, Jayaraman V, Looger LL, Svoboda K, Kim DS. 2013. Ultrasensitive fluorescent proteins for imaging neuronal activity. *Nature* **499**:295–300. doi: 10.1038/nature12354, PMID: 23868258

Chia F-S, Buckland-Nicks J, Young CM. 1984. Locomotion of marine invertebrate larvae: a review. *Canadian Journal of Zoology* **62**:1205–1222. doi: 10.1139/z84-176

Conductier G, Brau F, Viola A, Langlet F, Ramkumar N, Dehouck B, Lemaire T, Chapot R, Lucas L, Rovère C, Maitre P, Hosseiny S, Petit-Paitel A, Adamantidis A, Lakaye B, Risold PY, Prévot V, Meste O, Nahon JL, Guyon A. 2013. Melanin-concentrating hormone regulates beat frequency of ependymal cilia and ventricular volume. *Nature Neuroscience* **16**:845–847. doi: 10.1038/nn.3401, PMID: 23708141

Conzelmann M, Offenburger SL, Asadulina A, Keller T, Münch TA, Jékely G. 2011. Neuropeptides regulate swimming depth of Platynereis larvae. *PNAS* **108**:E1174–E1183. doi: 10.1073/pnas.1109085108, PMID: 22006315

Conzelmann M, Jékely G. 2012. Antibodies against conserved amidated neuropeptide epitopes enrich the comparative neurobiology toolbox. *EvoDevo* **3**:23. doi: 10.1186/2041-9139-3-23, PMID: 23020891

Conzelmann M, Williams EA, Tunaru S, Randel N, Shahidi R, Asadulina A, Berger J, Offermanns S, Jékely G. 2013. Conserved MIP receptor-ligand pair regulates Platynereis larval settlement. *PNAS* **110**:8224–8229. doi: 10.1073/pnas.1220285110, PMID: 23569279

Croll RP, Jackson DL, Voronezhskaya EE. 1997. Catecholamine-containing cells in larval and postlarval bivalve molluscs. *The Biological Bulletin* **193**:116–124. doi: 10.2307/1542757

Dautov SS, Nezlin LP. 1992. Nervous system of the Tornaria larva (Hemichordata: enteropneusta). a histochemical and ultrastructural study. *The Biological Bulletin* **183**:463–475. doi: 10.2307/1542023

Denes AS, Jékely G, Steinmetz PR, Raible F, Snyman H, Prud'homme B, Ferrier DE, Balavoine G, Arendt D. 2007. Molecular architecture of annelid nerve cord supports common origin of nervous system centralization in bilateria. *Cell* **129**:277–288. doi: 10.1016/j.cell.2007.02.040, PMID: 17448990

Doran SA, Koss R, Tran CH, Christopher KJ, Gallin WJ, Goldberg JI. 2004. Effect of serotonin on ciliary beating and intracellular calcium concentration in identified populations of embryonic ciliary cells. *Journal of Experimental Biology* **207**:1415–1429. doi: 10.1242/jeb.00924, PMID: 15010492

Dubbs A, Guevara J, Yuste R. 2016. Moco: fast Motion Correction for calcium Imaging. *Frontiers in Neuroinformatics* **10**:6. doi: 10.3389/fninf.2016.00006, PMID: 26909035

Elgeti J, Gompper G. 2013. Emergence of metachronal waves in cilia arrays. *PNAS* **110**:4470–4475. doi: 10.1073/pnas.1218869110, PMID: 23487771

Faubel R, Westendorf C, Bodenschatz E, Eichele G. 2016. Cilia-based flow network in the brain ventricles. *Science* **353**:176–178. doi: 10.1126/science.aae0450, PMID: 27387952

Fischer AH, Henrich T, Arendt D. 2010. The normal development of platynereis dumerilii (nereididae, annelida). *Frontiers in Zoology* **7**:31. doi: 10.1186/1742-9994-7-31, PMID: 21192805

Friedrich S, Wanninger A, Brückner M, Haszprunar G. 2002. Neurogenesis in the mossy chiton, mopalia muscosa (gould) (polyplacophora): evidence against molluscan metamerism. *Journal of Morphology* **253**:109–117. doi: 10.1002/jmor.10010, PMID: 12112126

Gueron S, Levit-Gurevich K. 1999. Energetic considerations of ciliary beating and the advantage of metachronal coordination. *PNAS* **96**:12240–12245. doi: 10.1073/pnas.96.22.12240, PMID: 10535905

Guirao B, Meunier A, Mortaud S, Aguilar A, Corsi JM, Strehl L, Hirota Y, Desoeuvre A, Boutin C, Han YG, Mirzadeh Z, Cremer H, Montcouquiol M, Sawamoto K, Spassky N. 2010. Coupling between hydrodynamic forces and planar cell polarity orients mammalian motile cilia. *Nature Cell Biology* **12**:341–350. doi: 10.1038/ncb2040, PMID: 20305650

Gühmann M, Jia H, Randel N, Verasztó C, Bezares-Calderón LA, Michiels NK, Yokoyama S, Jékely G. 2015. Spectral tuning of phototaxis by a Go-Opsin in the rhabdomeric eyes of Platynereis. *Current Biology* **25**:2265–2271. doi: 10.1016/j.cub.2015.07.017, PMID: 26255845

Halbert SA, Becker DR, Szal SE. 1989. Ovum transport in the rat oviductal ampulla in the absence of muscle contractility. *Biology of Reproduction* **40**:1131–1136. doi: 10.1095/biolreprod40.6.1131, PMID: 2775809

Hauenschild C, Fischer A. 1969. *Platynereis Dumerilii. Mikroskopische Anatomie, Fortpflanzung, Entwicklung*. Stuttgart: Gustav Fischer Verlag.

Hay-Schmidt A. 1990a. Catecholamine-containing, serotonin-like and neuropeptide FMRFamide-like immunoreactive cells and processes in the nervous system of the Pilidium larva (Nemertini). *Zoomorphology* **109**:231–244. doi: 10.1007/BF00312190

Hay-Schmidt A. 1990b. Distribution of catecholamine-containing, serotonin-like and neuropeptide FMRFamide-like immunoreactive neurons and processes in the nervous system of the actinotroch larva of phoronis muelleri (phoronida). *Cell and Tissue Research* **259**:105–118. doi: 10.1007/BF00571435

Hay-Schmidt A. 2000. The evolution of the serotonergic nervous system. *Proceedings of the Royal Society B: Biological Sciences* **267**:1071–1079. doi: 10.1098/rspb.2000.1111, PMID: 10885511

Jékely G, Colombelli J, Hausen H, Guy K, Stelzer E, Nédélec F, Arendt D. 2008. Mechanism of phototaxis in marine zooplankton. *Nature* **456**:395–399. doi: 10.1038/nature07590, PMID: 19020621

Jékely G. 2011. Origin and early evolution of neural circuits for the control of ciliary locomotion. *Proceedings of the Royal Society B: Biological Sciences* **278**:914–922. doi: 10.1098/rspb.2010.2027, PMID: 21123265

Jékely G, Keijzer F, Godfrey-Smith P. 2015. An option space for early neural evolution. *Philosophical Transactions of the Royal Society B: Biological Sciences* **370**:20150181. doi: 10.1098/rstb.2015.0181, PMID: 26554049

Kempf SC, Page LR, Pires A. 1997. Development of serotonin-like immunoreactivity in the embryos and larvae of nudibranch mollusks with emphasis on the structure and possible function of the apical sensory organ. *The Journal of Comparative Neurology* **386**:507–528. doi: 10.1002/(SICI)1096-9861(19970929)386:3<507::AID-CNE12>3.0.CO;2-7, PMID: 9303432

Knight-Jones E. 1954. Relations between metachronism and the direction of ciliary beat in metazoa. *Journal of Cell Science* **95**:503–521.

Kramer-Zucker AG, Olale F, Haycraft CJ, Yoder BK, Schier AF, Drummond IA. 2005. Cilia-driven fluid flow in the zebrafish pronephros, brain and Kupffer's vesicle is required for normal organogenesis. *Development* **132**:1907–1921. doi: 10.1242/dev.01772, PMID: 15790966

Kuang S, Goldberg JI. 2001. Laser ablation reveals regulation of ciliary activity by serotonergic neurons in molluscan embryos. *Journal of Neurobiology* **47**:1–15. doi: 10.1002/neu.1011, PMID: 11257609

Kunimoto K, Yamazaki Y, Nishida T, Shinohara K, Ishikawa H, Hasegawa T, Okanoue T, Hamada H, Noda T, Tamura A, Tsukita S. 2012. Coordinated ciliary beating requires Odf2-mediated polarization of basal bodies via basal feet. *Cell* **148**:189–200. doi: 10.1016/j.cell.2011.10.052, PMID: 22265411

König P, Krain B, Krasteva G, Kummer W. 2009. Serotonin increases cilia-driven particle transport via an acetylcholine-independent pathway in the mouse Trachea. *PLoS One* **4**:e4938. doi: 10.1371/journal.pone.0004938, PMID: 19290057

Marlow H, Tosches MA, Tomer R, Steinmetz PR, Lauri A, Larsson T, Arendt D. 2014. Larval body patterning and apical organs are conserved in animal evolution. *BMC Biology* **12**:7. doi: 10.1186/1741-7007-12-7, PMID: 24476105

Maruyama I, Inagaki M, Momose K. 1984. The role of serotonin in mucociliary transport system in the ciliated epithelium of frog palatine mucosa. *European Journal of Pharmacology* **106**:499–506. doi: 10.1016/0014-2999(84)90053-0, PMID: 6335099

Mitchell B, Jacobs R, Li J, Chien S, Kintner C. 2007. A positive feedback mechanism governs the polarity and motion of motile cilia. *Nature* **447**:97–101. doi: 10.1038/nature05771, PMID: 17450123

Mitchell B, Stubbs JL, Huisman F, Taborek P, Yu C, Kintner C. 2009. The PCP pathway instructs the planar orientation of ciliated cells in the Xenopus larval skin. *Current Biology* **19**:924–929. doi: 10.1016/j.cub.2009.04.018, PMID: 19427216

Nezlin LP. 2000. Tornaria of hemichordates and other dipleurula-type larvae: a comparison*. *Journal of Zoological Systematics and Evolutionary Research* **38**:149–156. doi: 10.1046/j.1439-0469.2000.383144.x

Osterman N, Vilfan A. 2011. Finding the ciliary beating pattern with optimal efficiency. *PNAS* **108**:15727–15732. doi: 10.1073/pnas.1107889108, PMID: 21896741

Park TJ, Mitchell BJ, Abitua PB, Kintner C, Wallingford JB. 2008. Dishevelled controls apical docking and planar polarization of basal bodies in ciliated epithelial cells. *Nature Genetics* **40**:871–879. doi: 10.1038/ng.104, PMID: 18552847

Pernet B, Strathmann RR. 2011. Opposed ciliary bands in the feeding larvae of sabellariid annelids. *The Biological Bulletin* **220**:186–198. doi: 10.1086/BBLv220n3p186, PMID: 21712227

Raineri M. 1995. Is a mollusc an evolved bent metatrochophore? A histochemical investigation of neurogenesis in Mytilus (mollusca: bivalvia). *Journal of the Marine Biological Association of the United Kingdom* **75**:571–592. doi: 10.1017/S0025315400039023

Randel N, Bezares-Calderón LA, Gühmann M, Shahidi R, Jékely G. 2013. Expression dynamics and protein localization of rhabdomeric opsins in Platynereis larvae. *Integrative and Comparative Biology* **53**:7–16. doi: 10.1093/icb/ict046, PMID: 23667045

Randel N, Asadulina A, Bezares-Calderón LA, Verasztó C, Williams EA, Conzelmann M, Shahidi R, Jékely G. 2014. Neuronal connectome of a sensory-motor circuit for visual navigation. *eLife* **3**:e02730. doi: 10.7554/eLife.02730, PMID: 24867217

Randel N, Shahidi R, Verasztó C, Bezares-Calderón LA, Schmidt S, Jékely G. 2015. Inter-individual stereotypy of the Platynereis larval visual connectome. *eLife* **4**:e08069. doi: 10.7554/eLife.08069, PMID: 26061864

Reiten I, Uslu FE, Fore S, Pelgrims R, Ringers C, Diaz Verdugo C, Hoffman M, Lal P, Kawakami K, Pekkan K, Yaksi E, Jurisch-Yaksi N. 2017. Motile-Cilia-Mediated flow improves sensitivity and temporal resolution of olfactory computations. *Current Biology* **27**:166–174. doi: 10.1016/j.cub.2016.11.036, PMID: 28041793

Rouse GW. 1999. Trochophore concepts: ciliary bands and the evolution of larvae in spiralian metazoa. *Biological Journal of the Linnean Society* **66**:411–464. doi: 10.1111/j.1095-8312.1999.tb01920.x

Saalfeld S, Cardona A, Hartenstein V, Tomancak P. 2009. CATMAID: collaborative annotation toolkit for massive amounts of image data. *Bioinformatics* **25**:1984–1986. doi: 10.1093/bioinformatics/btp266, PMID: 19376822

Schindelin J, Arganda-Carreras I, Frise E, Kaynig V, Longair M, Pietzsch T, Preibisch S, Rueden C, Saalfeld S, Schmid B, Tinevez JY, White DJ, Hartenstein V, Eliceiri K, Tomancak P, Cardona A. 2012. Fiji: an open-source platform for biological-image analysis. *Nature Methods* **9**:676–682. doi: 10.1038/nmeth.2019, PMID: 22743772

Schneider-Mizell CM, Gerhard S, Longair M, Kazimiers T, Li F, Zwart MF, Champion A, Midgley FM, Fetter RD, Saalfeld S, Cardona A. 2016. Quantitative neuroanatomy for connectomics in Drosophila. *eLife* **5**:e12059. doi: 10.7554/eLife.12059, PMID: 26990779

Shahidi R, Williams EA, Conzelmann M, Asadulina A, Verasztó C, Jasek S, Bezares-Calderón LA, Jékely G. 2015. A serial multiplex immunogold labeling method for identifying peptidergic neurons in connectomes. *eLife* **4**:e11147. doi: 10.7554/eLife.11147, PMID: 26670546

Shahidi R, Jékely G. 2017. Full-body serial TEM dataset of a Platynereis nectochaete larva. https://neurodata.io/

Shapiro OH, Fernandez VI, Garren M, Guasto JS, Debaillon-Vesque FP, Kramarsky-Winter E, Vardi A, Stocker R. 2014. Vortical ciliary flows actively enhance mass transport in reef corals. *PNAS* **111**:13391–13396. doi: 10.1073/pnas.1323094111, PMID: 25192936

Starunov VV, Dray N, Belikova EV, Kerner P, Vervoort M, Balavoine G. 2015. A metameric origin for the annelid pygidium? *BMC Evolutionary Biology* **15**:25. doi: 10.1186/s12862-015-0299-z, PMID: 25880037

Steinmetz PR, Kostyuchenko RP, Fischer A, Arendt D. 2011. The segmental pattern of otx, gbx, and hox genes in the annelid Platynereis dumerilii. *Evolution & Development* **13**:72–79. doi: 10.1111/j.1525-142X.2010.00457.x, PMID: 21210944

Tamm SL. 1972. Cillary motion in *Paramecium*. A scanning electron microscope study. *The Journal of Cell Biology* **55**:250–255. doi: 10.1083/jcb.55.1.250, PMID: 4569410

Tamm SL. 1984. Mechanical synchronization of ciliary beating within comb plates of ctenophores. *The Journal of Experimental Biology* **113**:401–408. PMID: 6151964

Tamm SL. 2014. Cilia and the life of ctenophores. *Invertebrate Biology* **133**:1–46. doi: 10.1111/ivb.12042

Temereva E, Wanninger A. 2012. Development of the nervous system in Phoronopsis harmeri (Lophotrochozoa, Phoronida) reveals both deuterostome- and trochozoan-like features. *BMC Evolutionary Biology* **12**:121. doi: 10.1186/1471-2148-12-121, PMID: 22827441

Tessmar-Raible K, Raible F, Christodoulou F, Guy K, Rembold M, Hausen H, Arendt D. 2007. Conserved sensory-neurosecretory cell types in annelid and fish forebrain: insights into hypothalamus evolution. *Cell* **129**:1389–1400. doi: 10.1016/j.cell.2007.04.041, PMID: 17604726

Tomer R, Denes AS, Tessmar-Raible K, Arendt D. 2010. Profiling by image registration reveals common origin of annelid mushroom bodies and vertebrate pallium. *Cell* **142**:800–809. doi: 10.1016/j.cell.2010.07.043, PMID: 20813265

Tosches MA, Bucher D, Vopalensky P, Arendt D. 2014. Melatonin signaling controls circadian swimming behavior in marine zooplankton. *Cell* **159**:46–57. doi: 10.1016/j.cell.2014.07.042, PMID: 25259919

Verasztó C. 2017. ImageJ and Python Scripts for the Analysis of Platynereis Calcium Imaging Data. *Github*. https://github.com/JekelyLab/Veraszto_et_al_2017 bfb4615

Vladar EK, Bayly RD, Sangoram AM, Scott MP, Axelrod JD. 2012. Microtubules enable the planar cell polarity of airway cilia. *Current Biology* **22**:2203–2212. doi: 10.1016/j.cub.2012.09.046, PMID: 23122850

Voronezhskaya EE, Tsitrin EB, Nezlin LP. 2003. Neuronal development in larval polychaete phyllodoce maculata (Phyllodocidae). *The Journal of Comparative Neurology* **455**:299–309. doi: 10.1002/cne.10488, PMID: 12483683

Walentek P, Bogusch S, Thumberger T, Vick P, Dubaissi E, Beyer T, Blum M, Schweickert A. 2014. A novel serotonin-secreting cell type regulates ciliary motility in the mucociliary epidermis of Xenopus tadpoles. *Development* **141**:1526–1533. doi: 10.1242/dev.102343, PMID: 24598162

Wan KY, Goldstein RE. 2016. Coordinated beating of algal flagella is mediated by basal coupling. *PNAS* **113**: E2784–E2793. doi: 10.1073/pnas.1518527113, PMID: 27140605

Wanninger A, Koop D, Degnan BM. 2005. Immunocytochemistry and metamorphic fate of the larval nervous system of triphyllozoon mucronatum (Ectoprocta: gymnolaemata: cheilostomata). *Zoomorphology* **124**:161–170. doi: 10.1007/s00435-005-0004-7

Williams EA, Verasztó C, Jasek S, Conzelmann M, Shahidi R, Bauknecht P, Jékely G. 2017. Synaptic and peptidergic connectome of a neurosecretory centre in the annelid brain. *BioRxiv*. http://biorxiv.org/content/early/2017/03/08/115204.

Synaptic and peptidergic connectome of a neurosecretory centre in the annelid brain

Elizabeth A. Williams[1], Csaba Verasztó[1], Sanja Jasek[1], Markus Conzelmann[1], Réza Shahidi[1], Philipp Bauknecht[1], and Gáspár Jékely[1*]

[1]Max Planck Institute for Developmental Biology, Spemannstrasse 35, 72076 Tübingen, Germany.

*Correspondence to: gaspar.jekely@tuebingen.mpg.de.

Abstract

Neurosecretory centres in animal brains use peptidergic signalling to influence physiology and behaviour. Understanding neurosecretory centre function requires mapping cell types, synapses, and peptidergic networks. Here we use electron microscopy and gene expression mapping to analyse the synaptic and peptidergic connectome of an entire neurosecretory centre. We mapped 78 neurosecretory neurons in the brain of larval *Platynereis dumerilii*, a marine annelid. These neurons form an anterior neurosecretory organ expressing many neuropeptides, including hypothalamic peptide orthologues and their receptors. Analysis of peptide-receptor pairs revealed sparsely connected networks linking specific neuronal subsets. We experimentally analysed one peptide-receptor pair and found that a neuropeptide can couple neurosecretory and synaptic brain signalling. Our study uncovered extensive non-synaptic signalling within a neurosecretory centre and its connection to the synaptic brain.

Introduction

Nervous system signalling occurs either at synapses or via secreted diffusible chemicals that signal to target cells expressing specific receptors. Synapse-level connectomics using electron microscopy allows mapping synaptic networks, but fails to reveal non-synaptic signalling. In addition to acting in a neuroendocrine fashion, non-synaptic volume transmission by neuropeptides and monoamines can have neuromodulatory effects on synaptic signalling (Bargmann 2012; Marder 2012). Overlaying synaptic and peptidergic maps is challenging and requires knowledge of the expression of the modulators and their specific receptors as well as synaptic connections. Such mapping has only been achieved for relatively simple circuits, such as the stomatogastric nervous system of crustaceans where synaptic connections are known and the effect of neuropeptides and the activation of single peptidergic neurons can be analysed experimentally (Stein et al. 2007; Thirumalai and Marder 2002; Blitz et al. 1999). Likewise, connectome reconstructions combined with cellular-resolution neuropeptide and receptor mapping allow the dissection of peptidergic signalling in *Drosophila* (Schlegel et al. 2016). In *Caenorhabditis elegans*, the spatial mapping of monoamines and neuropeptides and their G

protein-coupled receptors (GPCRs) revealed interconnected networks of synaptic and non-synaptic signalling (Bentley et al. 2016).

Neurosecretory centres, such as the vertebrate hypothalamus and the insect ring gland, found in the anterior brain of many animals show exceptionally high levels of neuropeptide expression (Herget and Ryu 2015; Siegmund and Korge 2001; Campbell et al. 2017) suggesting extensive non-synaptic signalling. These centres coordinate many processes in physiology, behaviour, and development, including growth, feeding, and reproduction (Sakurai et al. 1998; Bluet-Pajot et al. 2001; Sternson et al. 2013). The combined analysis of synaptic and peptidergic networks is particularly challenging using single marker approaches for neurosecretory centres that express dozens of neuropeptides. To fully understand their function, a global mapping of peptidergic networks within these brain regions and how they connect to the rest of the nervous system is required.

Here, we analyse synaptic and peptidergic signalling in the anterior neurosecretory centre in larval *Platynereis dumerilii*, a marine annelid. Annelid and other marine larvae have an anterior sensory centre, the apical organ, involved in the detection of various environmental cues (Hadfield et al. 2000; Conzelmann et al. 2013; Page 2002; Chia and Koss 1984). The apical organ is neurosecretory and expresses diverse neuropeptides that are thought to regulate various aspects of larval behaviour and physiology, including the induction of larval settlement and metamorphosis (Mayorova et al. 2016; Thorndyke et al. 1992; Tessmar-Raible et al. 2007; Conzelmann et al. 2011; Marlow et al. 2014). Apical organs have a conserved molecular fingerprint across marine larvae, suggesting that they represent a conserved sensory-neuroendocrine structure (Marlow et al. 2014). The apical organ area or apical nervous system (ANS) in *Platynereis* larvae shows molecular similarities to other neuroendocrine centres, including the pars intercerebralis in insects and the vertebrate hypothalamus, suggesting a common ancestry (Tessmar-Raible et al. 2007; Steinmetz et al. 2010; Conzelmann et al. 2013). Molecular and developmental similarities in various protostomes and deuterostomes further suggest a more widespread conservation of neuroendocrine centres (Hartenstein 2006; Wirmer et al. 2012; Tessmar-Raible 2007). The study of marine invertebrate larval apical organs could thus inform about the evolution of neuroendocrine cell types and signalling mechanisms in metazoans.

Platynereis larvae represent a powerful system to analyse gene expression and synaptic connectivity in a whole-body context, allowing linking distinct neuropeptides and other molecules to single neurons (Asadulina et al. 2012; Williams and Jékely 2016; Shahidi et al. 2015; Achim et al. 2015; Pettit et al. 2014; Vergara et al. 2017). To understand how synaptic and peptidergic signalling is integrated in the *Platynereis* ANS, we combine serial section electron microscopy with the cellular analysis of neuropeptide signalling. This combined analysis revealed extensive non-synaptic peptidergic signalling networks within the ANS distinguishing this area from the rest of the nervous system. Through connectomics and functional studies we also reveal how this endocrine region can interact with the synaptic nervous system by peptidergic modulation of the ciliomotor circuitry.

Results

Ultrastructural reconstruction of the anterior neurosecretory centre

To comprehensively map a neurosecretory area with ultrastructural detail, we focused on the larvae of *Platynereis*. Due to their small size, the larvae are amenable to whole-body connectomic analysis (Randel et al. 2015; Shahidi et al. 2015). We used a full-body serial electron microscopy dataset of a 3-day-old larva (Randel et al. 2015) and reconstructed its entire apical neurosecretory nervous system (Figure 1A-D). *Platynereis* and other annelids have an anterior neurosecretory plexus containing the projections of peptidergic sensory-neurosecretory neurons (Tessmar-Raible et al. 2007; Aros et al. 1977). The neurosecretory plexus forms an anatomically and ultrastructurally distinct area that can be clearly distinguished from other neuropils, including the adjacent optic and nuchal organ neuropils (Randel et al. 2014; Shahidi et al. 2015) (Figure 1D). Neurites in this area have a high number of dense-core vesicles and very few synapses (Figure 1E, F). Classic neurotransmitter synapses can be identified by large clusters of clear synaptic vesicles in the axons, while peptidergic synapses appear as smaller clusters of dense core vesicles (Randel et al. 2014; Shahidi et al. 2015). We reconstructed all neurons that project to this region (Figure 1B, Supplement 1 to figure 1, Video 1) and identified 70 sensory neurons and eight projection interneurons, the latter project in and out of the neurosecretory plexus. Most of the sensory neurons are bilaterally symmetric pairs with distinct axonal projection patterns, except for a few asymmetric neurons (Supplement 1 to figure 1). The sensory neurons have diverse apical sensory specializations. Based on these morphological criteria we could distinguish at least 20 different sensory cell types with likely different sensory functions. For example, there are four ciliary photoreceptor cells (cPRC)(Arendt et al. 2004) with highly extended ciliary membranes, one asymmetric neuron with five sensory cilia ($SN^{YFa5cil}$), a pair of neurons with two long parallel cilia (SN^{WLD1}), a pair with long branched sensory cilia (SN^{NS29}), and three uniciliary neurons that are part of the nuchal organ (SN^{nuchNS}), a putatively chemosensory annelid organ (Purschke 1997). Twenty-five uniciliated neurons (23 SN^{DLSO} cells, $SN^{PDF\text{-}dcl2}$, and $SN^{PDF\text{-}dcr3}$) are part of a dorsolateral sensory cluster (Supplement 1 to figure 1). Most of the sensory neurons have axonal projections that are extensively branched within the neurosecretory plexus (Supplement 1 to figure 1) and that are filled with dense-core vesicles (Figure 1F). The pairs of left-right symmetric sensory neurons project to similar areas of the neurosecretory plexus revealing a fine-scale organization within the plexus (Figure 1G and Supplement 1 to figure 1, Video 1). We refer to all neurons that project to the neurosecretory plexus as the apical nervous system (ANS).

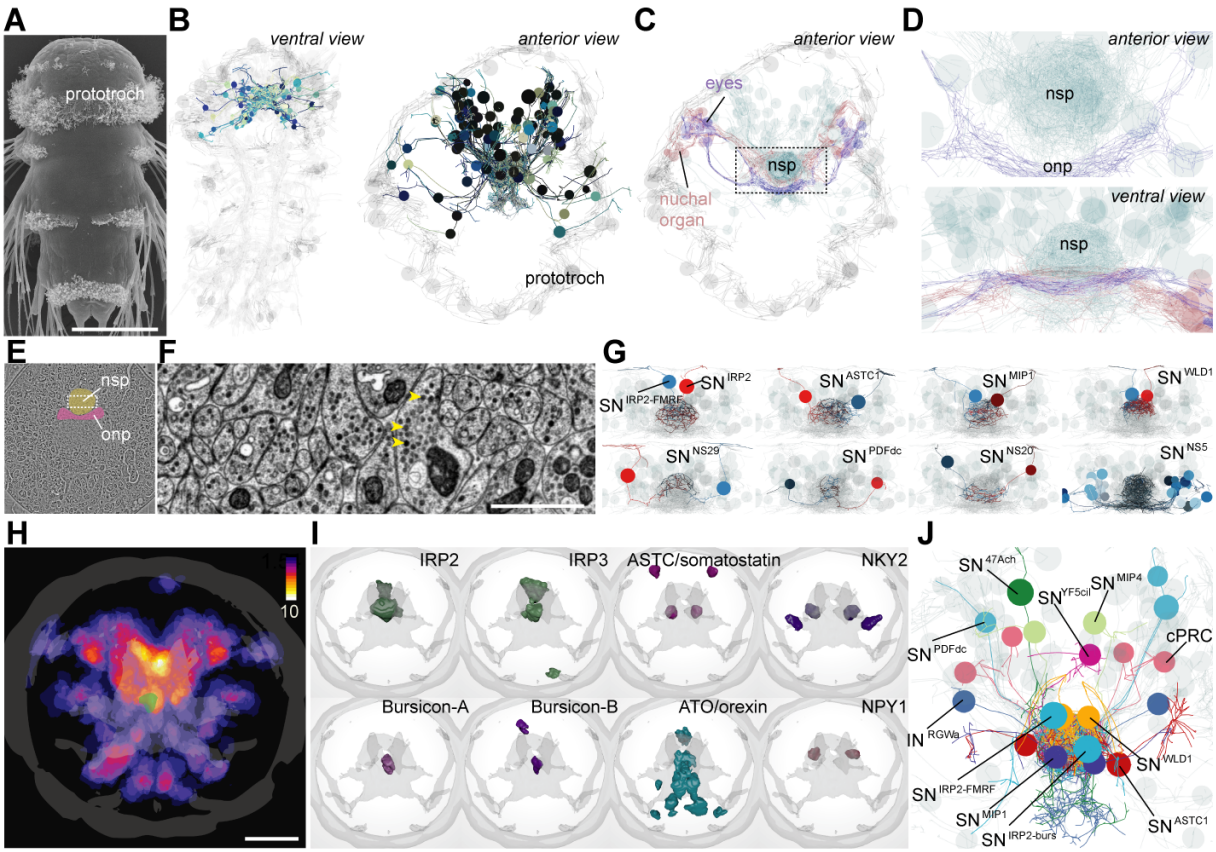

Figure 1. EM reconstruction and mapping of proneuropeptide expression in the apical nervous system of *Platynereis* larvae. (**A**) Scanning electron micrograph of a 3-day-old *Platynereis* larva. (**B**) Reconstructed apical nervous system neurons (ANS) (shades of blue) in a full body transmission electron microscopy (TEM) dataset of a 3-day-old larva, shown against a framework of reconstructed ciliated cells and axonal scaffold (light grey). Axons and dendrites appear as lines and cell body positions are represented by spheres. (**C**) ANS neurons project to an apical neurosecretory plexus in the centre of the head, which forms a small sphere dorsal and apical to the optic neuropil and nuchal organ neuropil. (**D**) Close-up view of neurosecretory plexus indicated by box in C. (**E**) TEM image of a section in the larval head. The neurosecretory plexus and the optic neuropil are highlighted. Boxed area is shown in F. (**F**) Close-up view of the neurosecretory plexus. Yellow arrowheads point at dense core vesicles. (**G**) Examples of bilaterally symmetric pairs of sensory neurons that innervate different regions of the neurosecretory plexus in the reconstructed ANS (grey), ventral view. (**H**) Heat map of the expression of 48 proneuropeptides in the 2-day-old *Platynereis* larva, apical view, projected on a reference scaffold of cilia and axonal scaffold (grey). Colour scheme indicates number of different proneuropeptides expressed in a cell. An apical FMRFamide-expressing neuron of the ANS ($SN^{IRP2\text{-}FMRF}$) is overlaid for spatial reference (green). (**I**) Examples of average gene expression patterns of individual proneuropeptides from the 2-day proneuropeptide expression atlas. (**J**) TEM reconstruction of the 3-day-old larval ANS showing neurons that could be assigned specific proneuropeptide expression based on position and sensory cilia morphology. Abbreviations: nsp, apical neurosecretory plexus; onp, optic neuropil. Scale bars: A, 70 µm; H, 30 µm; F, 1 µm.

Comprehensive mapping of neuropeptide expression in *Platynereis* larvae

The *Platynereis* larval ANS is known to express many neuropeptides, including vasotocin, FMRFamide, and myoinhibitory peptide (Tessmar-Raible et al. 2007; Conzelmann et al. 2011; Conzelmann et al. 2013). To comprehensively analyse neuropeptide expression in the whole larva, we used whole-mount *in situ* hybridization for 51 *Platynereis* proneuropeptides (of 98 total (M Conzelmann et al. 2013)). We used image registration to spatially map all neuropeptide expressions to a common nuclear reference template (Asadulina et al. 2012). We summed all binarized average expression domains and found that the region with the highest proneuropeptide expression corresponds to the ANS (Figure 1H, Figure 1 – source data 1). Some voxels in the map coexpress up to 10 different neuropeptides. Neuropeptides that were expressed in the ANS include two *Platynereis* insulin-like peptides (IRP2, IRP3), two bursicons (bursicon-A, -B), achatin, myoinhibitory peptide (MIP), and several homologs of hypothalamic peptides (Mirabeau and Joly 2013; Jékely 2013) including NPY (three homologs, NPY1, NPY4, NKY2), orexin/allatotropin, tachykinin, galanin/allatostatin-A, and allatostatin-C/somatostatin (Figure 1I and Supplement 2 to figure 1).
The acetylated tubulin antibody we used to counterstain the *in situ* samples labels cilia and axonal scaffold. With this counterstaining signal, we correlated neurons expressing specific proneuropeptides and with distinct ciliation to sensory ANS neurons reconstructed from EM data (Figure 1J and Supplement 3 to figure 1). For other ANS neurons (SN^{PDFdc}, IN^{RGW}) we assigned neuropeptides based on direct immunogold labelling on the same EM series (Shahidi et al. 2015). Overall, we mapped neuropeptide expression to 25 reconstructed ANS neurons, including sensory neurons coexpressing IRP2 and FMRFamide ($SN^{IRP2\text{-}FMRF}$), IRP2 and bursicon ($SN^{IRP2\text{-}burs}$), or expressing ASTC/somatostatin (SN^{ASTC1}) (Figure 1J and Supplement 3 to Figure).

Low level of synaptic connectivity within the ANS

We next analysed how the ANS neurons are synaptically connected. We found that most neurons have no or only very few synapses (Figure 2, Supplementary table 1). 33% of the neurons have 0-2 synapses despite highly branched axonal projections filled with dense core vesicles (Figure 2). This suggests that these neurons predominantly use volume transmission. The synapses we identified in most neurons contained dense-core vesicles, indicative of their peptidergic nature. The four cPRCs, an asymmetric sensory neuron (SN^{47Ach}), and the 8 projection neurons have the highest number of synapses. In addition, 15 ANS sensory neurons have 10 or more peptidergic synapses. The cPRCs express a cholinergic marker (Jékely et al. 2008) and contain large synapses with clear vesicles. The other sensory cells have ultrastructurally distinct, small peptidergic synapses characterized by dense core vesicles clustering at the membrane (Figure 2).

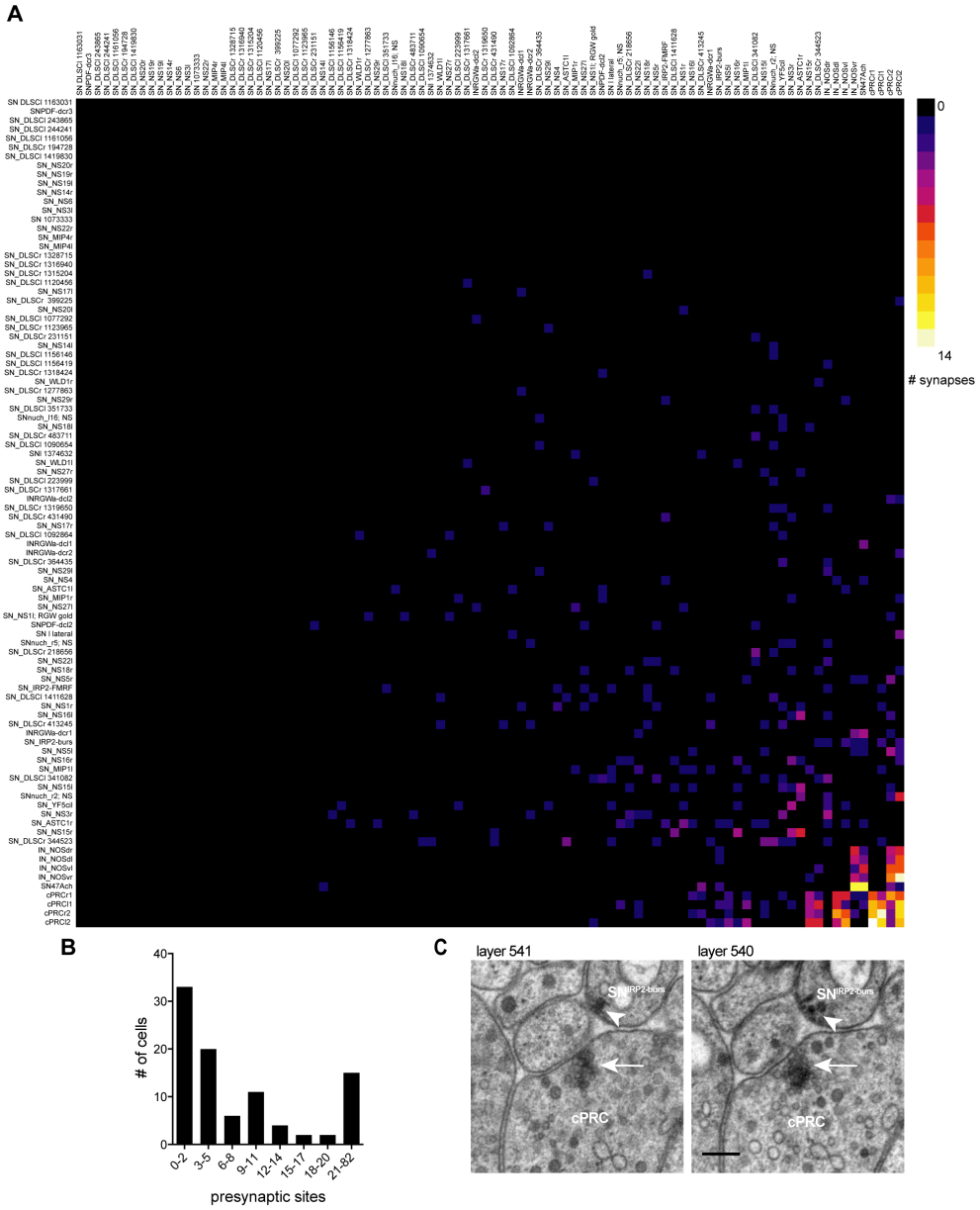

Figure 2.
Low level of synaptic connectivity of ANS neurons. (**A**) Full matrix of synaptic connectivity of ANS neurons. With the exception of the ciliary photoreceptors, a few sensory cells, and the IN^{NOS} interneurons, the ANS shows very sparse synaptic connectivity. (**B**) Histogram of the number of presynaptic sites in ANS neurons. (**C**) Comparison of a cholinergic synapse of a ciliary photoreceptor (arrow) to a peptidergic synapse of the $SN^{IRP2\text{-}burs}$ cell (arrowhead). Two consecutive sections are shown. Scale bar in (**C**), 200 nm.

Analysis of peptidergic signalling networks in the ANS

The high number of neuropeptides expressed in the ANS and the low degree of synaptic connectivity of the cells prompted us to further analyse peptidergic signalling networks in the *Platynereis* larva. We used two resources: an experimentally determined list of *Platynereis* neuropeptide GPCRs (Bauknecht and Jékely 2015) and a spatially-mapped single-cell transcriptome dataset (Achim et al. 2015). The GPCR list included 18 deorphanized

neuropeptide receptors, to which we added a further three deorphanized neuropeptide receptors. We deorphanized a GnRH receptor activated by both *Platynereis* GnRH1 and GnRH2 (M Conzelmann et al. 2013), and second receptors for vasotocin and myomodulin (Supplement 1 to figure 3). The single-cell transcriptome data consisted of cells of the head (episphere) of 2-day-old larvae. The cells were mostly neurons (Achim et al. 2015).

To comprehensively analyse potential peptide-receptor signalling networks, we first created a virtual larval brain with cells arranged in an approximate spatial map (Figure 3A, Supplement 2 to figure 3, Supplementary Table 1, Figure 3 – source data 1, Figure 3 – source data 2). To this virtual map, we mapped the expression of all proneuropeptides and deorphanized receptors (Figure 3C, D). The combined expression of 80 proneuropeptides showed a similar pattern to the *in situ* map with a highly peptidergic group of cells in the ANS region, as defined by the endocrine marker genes *Phc2*, *dimmed*, *Otp* and *nk2.1* (Conzelmann et al. 2013; Tessmar-Raible et al. 2007) (Figure 3B). Given the high level of peptide expression in the ANS, the mapping of peptidergic signalling networks will mostly reveal potential signalling partners within this region or from the ANS to the rest of the brain. Most GPCR expression was also concentrated in the ANS in peptidergic cells. Several cells expressed a unique combination of up to 9 GPCRs (Figure 3D).

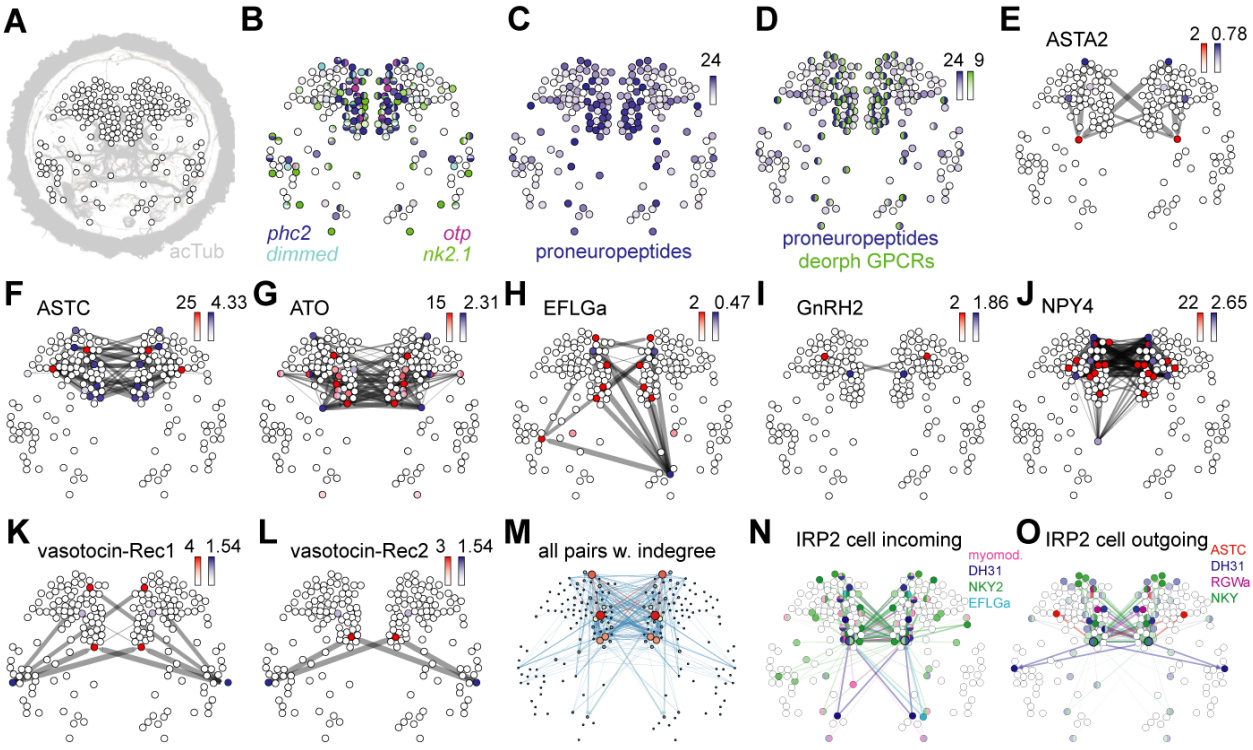

Figure 3. Mapping the peptidergic connectome in the *Platynereis* larval head. (**A**) Positions of cells (nodes) from single cell RNA-Seq from 2-day-old larvae placed in an approximate spatial map, projected on an acetylated tubulin immunostaining (grey, anterior view). Samples with predicted bilateral symmetry were represented as two mirror image nodes in the map. (**B**) Expression of neuroendocrine marker genes projected on the single cell map. Colour intensity of nodes reflects magnitude of normalized $\log_{10}$ gene expression. (**C**) Map of combined expression of 80 proneuropeptides expressed in each single cell sample.

(**D**) Map of combined expression of 80 proneuropeptides and 23 deorphanized GPCRs expressed in each single cell sample. (**E–L**) Connectivity maps of individual neuropeptide-GPCR pairs, coloured by weighted in-degree (red) and proneuropeptide $\log_{10}$ normalized expression (blue). Arrows indicate direction of signalling. Arrow thickness determined by geometric mean of $\log_{10}$ normalized proneuropeptide expression of signalling cell and $\log_{10}$ normalized GPCR expression of corresponding receiving cell. (**M**) Connectivity map of all possible known neuropeptide-GPCR signalling, colour and node size represent weighted in-degree. (**N**) Connectivity map of an IRP2-expressing cell with incoming neuropeptide signals. (**O**) Connectivity map of an IRP2-expressing cell with outgoing neuropeptide signals.

We also used the spatially mapped single cell transcriptome data to map the expression of different types of sensory receptor genes in the opsin and transient receptor potential (Trp) channel families. These receptor genes are known for their function in the detection and transduction of light/pain/temperature/mechanical stimuli (Terakita 2005; Moran et al. 2004). Neurons in the ANS of 2-day-old larvae express diverse combinations of these genes (Supplement 3 to figure 3). This supports our conclusion from the morphological data that these neurons are responsible for detecting a variety of different environmental cues.
Coexpression analysis with small neurotransmitter synthesis enzymes revealed 1 cell (1% of total) with only neurotransmitter markers but no neuropeptide, 76 (71% of total) purely peptidergic cells, and 21 cells that coexpress small transmitters and neuropeptides (19.6% of total)(Supplement 4 to figure 3). The remaining 9 cells expressed neither neuropeptides nor neurotransmitter markers and thus are likely non-neuronal cells (8.4% of total). Strikingly, 2 ANS cells coexpress up to 24 different proneuropeptides. Based on specific neuropeptide expression and the spatial mapping we could correlate 15 cells to ANS cells reconstructed from EM data (Supplementary Table 1). This was possible despite the two resources being derived from different larval stages, because many ANS cells are already differentiated in 2-day-old larvae and readily identifiable between stages.
To establish peptidergic signalling networks, we treated peptide-expressing cells as source nodes and GPCR-expressing cells as target nodes. We define edge weights in the directed graphs as the geometric mean of normalized proneuropeptide expression in the source and normalized GPCR expression in the target. This way, we also consider the expression level of peptides and receptors. Receptor expression can correlate with neurophysiological sensitivity to a neuropeptide (Garcia et al. 2015; Root et al. 2011). For each peptide-receptor pair, we projected these networks onto the virtual map (Figure 3E-L, Supplement 4 to figure 3, Figure 3 – source data 3). The chemical connectivity maps of individual ligand-receptor pairs show very sparse and specific chemical wiring. On average, less than 1% of all potential connections are realized (0.8% graph density averaged for all peptide-receptor pairs). Single cells expressing many different neuropeptides generally link to non-overlapping target nodes by each peptide-receptor channel (Figure 3O and Supplement 4 to figure 3Q). Conversely, multiple signals can converge on one cell that expresses more than one GPCR (Figure 3N).
The combined multichannel peptidergic connectome of 23 receptor-ligand pairs forms a single network with an average clustering coefficient of 0.49 and an average minimum path length of 1.54, forming a small-world network (Watts and Strogatz 1998). Analysis of the combined network revealed highly connected components, including nodes that can act as both source and target as potential mediators of peptide cascades (Figure 3N, O). The three neuron types with the highest weighted in-degree and authority value include a pair of dorsal sensory neurons, a central

pair of IRP2 neurons, and a pair of RGWamide-expressing neurons (Figure 3M and Figure 4A). The IRP2 neurons are under the influence of an NPY peptide and EFLGamide, the *Platynereis* homolog of thyrotropin-releasing hormone (Bauknecht and Jékely 2015) and express 20 different proneuropeptides.

Projection interneurons connect the peptidergic ANS to the synaptic nervous system

The RGWamide-expressing neurons express two NPY receptors (NPY4 and NKY) and an achatin receptor, and 17 proneuropeptides, but no markers for small neurotransmitters. By position and RGWamide-expression we identified these cells as IN^{RGW} projection neurons. We also identified cells that likely correspond to IN^{NOS} projection neurons, based on RYamide expression and expression of *nitric oxide synthase* (unpublished results). The four IN^{RGW} projection interneurons as well as the four IN^{NOS} projection interneurons have a distinct anatomy (Figure 4B). They lack dendrites or cilia and their axons are extensively branched in the neurosecretory plexus and project out of this area to a ventral neuropil. Here the IN^{RGW} cells form many peptidergic synapses on two serotonergic ciliomotor neurons (Ser-h1)(Figure 4C) that are activate during periods of ciliary beating (Verasztó et al. 2017). The IN^{NOS} cells only synapse on the IN^{RGW} cells in the ventral neuropil. The IN^{RGW} neurons also receive synapses in the ventral neuropil area from two non-ANS neurons. These neurons (cMN^{vl} and the serotonergic $pygPB^{bicil}$) belong to the ciliomotor circuit of the larva (Figure 3D-F). From the ANS, the IN^{RGW} projection neurons receive small transmitter synapses from the cPRC cells, mixed clear and dense core vesicle synapses from the SN^{47Ach} neuron in the ventral neuropil, and peptidergic synapses from three other ANS sensory neurons in the neurosecretory plexus (Figure 4, Supplementary Table 1). The distinct anatomy and connectivity as well as the high authority values of the projection neurons in the peptidergic network indicate that these cells are important in relaying peptidergic signals from the ANS to the rest of the brain.

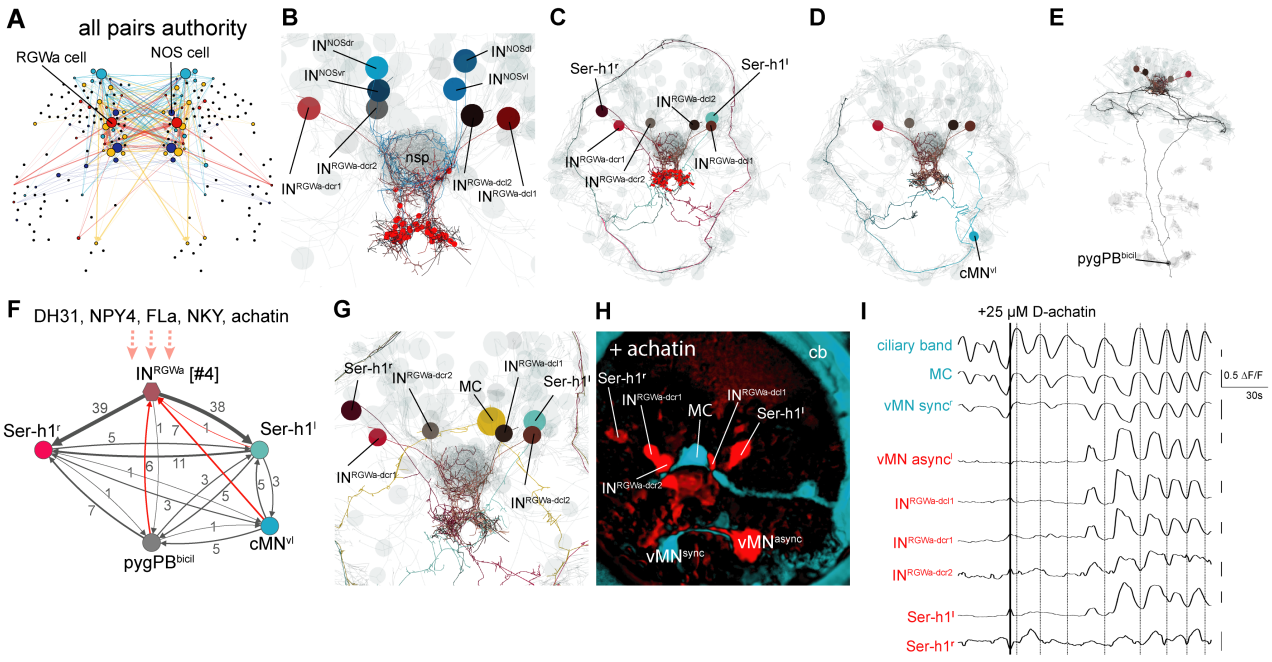

Figure 4. Projection neurons connect the ANS to the synaptic nervous system. (**A**) Connectivity map of all possible known neuropeptide-GPCR signalling, colours represent modules defined by randomized community detection analysis in Gephi and node size represents authority. (**B**) Reconstructed IN^{RGWa} projection neurons (ANS) (shades of brown) in a full body transmission electron microscopy (TEM) dataset of a 3-day-old larva, shown against a framework of reconstructed ANS neurons (light grey). Axons and dendrites appear as lines and cell body positions are represented by spheres. (**C**) TEM reconstruction of IN^{RGWa} projection neurons and Ser-h1 serotonergic neurons. Red spheres indicated IN^{RGWa} presynaptic sites. (**D**) TEM reconstruction of IN^{RGWa} projection neurons and a presynaptic ciliomotor neuron, cMN^{vl}. (**E**) TEM reconstruction of IN^{RGWa} neurons and a presynaptic serotonergic sensory neuron, $pygPD^{bicil}$. (**F**) Synaptic connectivity graph of IN^{RGWa}, Ser-h1, $pygPD^{bicil}$, and cMN^{vl} neurons. Synaptic inputs from the synaptic nervous system to the IN^{RGWa} neuron are in red. Peptidergic inputs to the IN^{RGWa} neurons are indicated with dashed arrows. (**G**) TEM reconstruction of IN^{RGWa} projection neurons, Ser-h1 neurons, and the cholinergic ciliomotor MC neuron, anterior view (**H**) Confocal microscopy image of correlated pixels of GcAMP6s signal in a 2-day-old *Platynereis* larva after the addition of 25 µM D-achatin neuropeptide, anterior view. Cells showing correlated activity with the serotonergic neurons (red) and the MC cell (cyan) are shown. $IN^{RGWa\text{-}dcl2}$ could not be identified in this larva and is likely obscured by the MC cell and/or $IN^{RGWa\text{-}dcl1}$. (**I**) Neuronal activity patterns of individually identified neurons in a 2-day-old larva treated with 25 µM achatin.

To test how these neurons respond to neuropeptides, we used calcium-imaging experiments. The IN^{RGW} and IN^{NOS} neurons express 7 deorphanized GPCRs (Figure 4F), including a receptor for achatin that is specifically activated by achatin peptide containing a D-amino acid (Bauknecht and Jékely 2015). When we treated larvae with D-achatin, four neurons in the ANS were rhythmically activated. These neurons correspond by position to the IN^{RGW} cells (Figure 4I). The rhythmic activation was in-phase with the activation of the Ser-h1 neurons and a ventral motorneuron (vMN^{async}), but out of phase with the main cholinergic motorneuron of the head

ciliary band, the MC neuron (readily identifiable by calcium imaging (Verasztó et al. 2017)). We could not observe a similar effect upon L-achatin treatment (data not shown). *Platynereis* larvae have a cholinergic and a serotonergic circuit that oscillate out-of-phase. The cholinergic phase arrests the cilia and the serotonergic phase correlates with ciliary beating (Verasztó et al. 2017). Correlation analysis of neuronal activity patterns revealed that D-achatin coupled the activity of the IN^{RGW} cells to the serotonergic cells, and increased the negative correlation between the activity patterns of serotonergic neurons and the MC neuron (Figure 4I and Supplement 1 to Figure 4). This provides an example of how peptidergic signalling in the ANS could recruit neurons to a rhythmically active circuit, enhance the rhythm, and thereby potentially influence locomotor activity.

Discussion

Here we presented a comprehensive anatomical description of the ANS in the *Platynereis* larva. We combined this with the cellular-resolution mapping of neuropeptide signalling components to analyse potential peptidergic signalling networks. The use of scRNA-seq has a great potential to reveal such signalling networks but also has limitations. For example, we could only score proneuropeptide and receptor mRNA expression and not protein expression levels, peptide release, or the degree of neuronal activation. We also only analysed a relatively small single-cell dataset derived from the head of the larva and thus could not investigate long-range neuroendocrine signalling from the larval episphere to the rest of the body. The first analyses we present here can be extended when more data become available and can also be applied to other species (e.g., (Campbell et al. 2017)). Nevertheless, our approach can reveal all potential peptidergic connections and allows the development of hypotheses on peptidergic signalling that can be experimentally tested, as we have shown here for achatin.

We found that the *Platynereis* larval ANS has a low degree of synaptic connectivity, a strong neurosecretory character, and shows a high diversity of neuropeptide expression. This suggests that the ANS is wired primarily chemically and not synaptically. We identified very specific peptidergic links that connect only a small subset of ANS neurons. Strikingly, it is not only the proneuropeptides that are expressed with high diversity in the ANS, but also their receptors, suggesting that most peptidergic signalling in the brain occurs within the ANS. A high diversity of neuropeptide receptor expression has also been reported for the mouse hypothalamus (Campbell et al. 2017). These observations suggest that there is more extensive peptidergic integration within these centres than was previously appreciated. Neurosecretory centres may thus also function as chemical brains wired by neuropeptide signalling where the specificity is derived not from direct synaptic connections but by peptide-receptor matching. Given a high enough number of specific peptide-receptor pairs and allowing the possibility of combinatorial signalling, it is theoretically possible to wire arbitrarily complex neural networks. This extends the concept of neurosecretory centres as organs that release peptides to influence external downstream targets.

An anatomically and molecularly distinct ‘chemical’ and ‘synaptic’ brain as we found in the *Platynereis* larva may have originated early in the evolution of the nervous system. This idea is consistent with the chimeric brain hypothesis, which posits the fusion of a neurosecretory and a synaptic nervous system early in animal evolution (Tosches and Arendt 2013). The neurosecretory part of the brain is directly sensory in *Platynereis*, possibly reflecting an ancestral condition for neurosecretory centres (Tessmar-Raible et al. 2007; Hartenstein 2006). The ANS

also connects to the motor parts of the synaptic nervous system by specific projection neurons that are under peptidergic control. This connection may allow the translation of environmental cues that had been integrated by the chemical brain into locomotor output.
Neuropeptides are ideal molecules for chemical signalling due to their small size and high diversity. Many of the neuropeptides expressed in the *Platynereis* ANS and the vertebrate hypothalamus belong to ancient peptide families that evolved close to the origin of the nervous system (Jékely 2013; Mirabeau and Joly 2013). Neuropeptide genes have been identified in bilaterians, cnidarians, and even the early-branching metazoan *Trichoplax adhaerens*, that lacks a synaptic nervous system but has neurosecretory cells (Nikitin 2015; Smith et al. 2014). Chemical signalling by neuropeptides may have been important early during nervous system evolution in small metazoans where only peptide diffusion could coordinate physiological activities and behaviour. As metazoans grew larger, the coordination of their large complex bodies required control by a synaptic nervous system (Keijzer and Arnellos 2017). The separate origins of the chemical and the synaptic nervous system may still be reflected to varying degrees in contemporary brains. The *Platynereis* larval nervous system, and possibly the nervous system of other marine invertebrate larvae, shows a particularly clear segregation of non-synaptic and synaptic nervous systems.
The extent of non-synaptic signalling even in the relatively simple nervous system of the *Platynereis* larva highlights the importance of the combined study of connectomes and chemical signalling networks.

Methods

Electron microscopy reconstruction of *Platynereis* anterior neurosecretory plexus

We reconstructed the circuitry of cells in the anterior plexus from an existing 3-day-old *Platynereis* serial section transmission electron microscopy (ssTEM) dataset we generated previously (Randel et al. 2015). The dataset consists of 4845 layers of 40 nm thin sections. Preparation, imaging, montage, and alignment of the dataset is described (Randel et al. 2015). The cells were reconstructed, reviewed, 3D visualized, and the resulting synaptic network was analysed in Catmaid (Saalfeld et al. 2009; Schneider-Mizell et al. 2016).

Neuropeptide expression atlas in 2-day-old *Platynereis*

DIG-labelled antisense RNA probes were synthesized from clones sourced from a *Platynereis* directionally cloned cDNA library in pCMV-Sport6 vector (Conzelmann et al. 2013). Or PCR amplified and cloned into the vectors pCR-BluntII-TOPO or pCRII-TOPO. Larvae were fixed in 4% paraformaldehyde (PFA) in 1 X PBS with 0.1% Tween-20 for 1 h at room temperature. RNA *in situ* hybridization using nitroblue tetrazolium (NBT)/5-bromo-4-chloro-3-indolyl phosphate (BCIP) staining combined with mouse anti-acetylated-tubulin staining, followed by imaging with a Zeiss LSM 780 NLO confocal system and Zeiss ZEN2011 Grey software on an AxioObserver inverted microscope, was performed as previously described (Asadulina et al. 2012), with the following modification: fluorescence (instead of reflection) from the RNA *in situ* hybridization signal was detected using excitation at 633 nm in combination with a Long Pass 757 filter. Animals were imaged with a Plan-Apochromat 40x/1.3 Oil DIC objective.

We projected thresholded average gene expression patterns of >5 individuals per gene onto a common 2-day-old whole-body nuclear reference templates generated from DAPI (Asadulina et al. 2012). Thresholding was performed either manually or following (Vergara et al. 2017). Gene expression atlases were set up in the visualization software Blender (https://www.blender.org/) as described (Asadulina et al. 2015).

Deorphanization of receptor-peptide pairs

Platynereis GPCRs were identified in a reference transcriptome assembled from cDNA generated from 13 different life cycle stages (Conzelmann et al. 2013). GPCRs were cloned into pcDNA3.1(+) (Thermo Fisher Scientific, Waltham, USA) and deorphanization assays were carried out as previously described (Bauknecht and Jékely 2015).

Analysis of single cell transcriptome data

Fastq files containing raw paired-end RNA-Seq data for 107 single cells from the 48 hour old *Platynereis* larval episphere (Achim et al. 2015) were downloaded from ArrayExpress, accession number E-MTAB-2865 (https://www.ebi.ac.uk/arrayexpress/experiments/E-MTAB-2865/). Only those samples annotated as 'single cell' and with a corresponding spatial mapping prediction by Achim et al. 2015 (Achim et al. 2015) were used in our analysis.

Fastq files with raw paired end read data were loaded into CLC Genomics Workbench v6.0.4 (CLC Bio). Data was filtered to remove Illumina adapter primer sequences, low quality sequence (Quality Limit 0.05) and short fragments (less than 30 base pairs). Filtered data were mapped to the assembled *Platynereis* reference transcriptome (including only sequences with a BLASTX hit e-value <1e-5 to the SwissProt database, plus all previously described *Platynereis* genes, including 99 proneuropeptides, a total of 52,631 transcripts. Mapping was carried out in CLC Genomics Workbench v6.0.4 using the RNA-Seq Analysis function, with the following mapping parameters: paired distance 100 – 800 base pairs; minimum length fraction 0.8, minimum similarity fraction 0.9, maximum number of mismatches 2. The total number of reads mapped to each gene, normalized by gene length (reads per kilobase million (RPKM)) in each sample was assembled into one spreadsheet using the 'Experiment' function, and this spreadsheet was exported as an Excel file. RPKM data for each gene and sample were converted in Excel to counts per million (cpm) by dividing RPKM by with the total number of mapped reads in each sample and multiplying by 10^6 followed by conversion to a log base 10.

Single cell samples were sourced from populations consisting of dissociated cells of several individual larvae (Achim et al. 2015), therefore some of the RNA-Seq samples could represent sequencing of the same cell from different larvae. To determine a cut-off for transcriptome similarity to merge samples representing the same cell from different individuals, we calculated the all-against-all pairwise correlation coefficients. Plotting these correlation coefficients as a histogram showed a prominent peak of highly correlated samples. We interpret these as samples deriving from the re-isolation of the same cell from different larvae. We used a cut-off of 0.95 Pearson correlation as a cut-off, above which we merged samples as representing the same cell by using the mean normalized expression value for each gene.

Sample names were imported as nodes into software for graph visualization and manipulation, Gephi.0.8 beta (http://gephi.org). Nodes were manually placed in position in a Gephi map in an approximate 2D representation of the 3D spatial predictions of each cell generated by Achim et al. (Achim et al. 2015) based on a whole-mount *in situ* hybridization gene expression atlas of 72 genes (http://www.ebi.ac.uk/~jbpettit/map_ viewer/?dataset=examples/coord_full.

csv&cluster0=examples/resultsBio.csv). Samples with predicted bilateral symmetry were represented as two mirror image nodes in the map (left and right), while samples with predicted asymmetry were represented as single nodes. Node position coordinates for each sample were saved and exported as .gexf connectivity file for use in generating virtual gene expression patterns and peptide-receptor connectivity maps (Figure 3 – source data 3).

Virtual expression patterns for each gene were generated using a custom perl script that converted normalized log10 gene expression values into node colour intensity in the Gephi map. Connectivity files for each peptide-receptor pair were generated by preparation of connectivity data files as .csv files where the geometric mean of normalized log10 peptide expression from the 'sending cell' and corresponding GPCR expression from the 'receiving cell' was used as a proxy for connectivity strength. These connectivity data .csv files were imported into Gephi to generate .gexf connectivity maps, and random node positions were replaced with node position coordinates for each cell from the spatial position .gexf map described above. An 'all-by-all' connectivity map representing the potential cellular signalling generated by all known peptide-receptor pairs was generated by adding the connectivity data from each peptide-receptor pair into a single connectivity file.

Connectivity maps were analysed for degree of connectivity, graph density, modularity, number of connected components, and clustering coefficient in Gephi.0.8 beta. Nodes in connectivity maps were coloured by weighted in-degree (average number of incoming edges per node, adjusted for connectivity strength). Edge thickness was used to represent connectivity strength (geometric mean of peptide x receptor normalized gene expression). Authority was assigned to nodes using a Hyperlink-Induced Topic Search (HITS). Higher authority values indicate nodes that are linked to greater numbers of other nodes, or in the case of our peptidergic signalling maps, neurons with the capacity to receive signals from and send signals to the greatest number of other cells. Following export from gephi as .svg files, corresponding virtual neuropeptide expression for each connectivity map was used to colour signalling cells by overlaying in Adobe Illustrator CS6 V6.0.0 (Adobe Systems Inc.)

Immunohistochemistry

Whole-mount triple immunostaining of 2 and 3 day old *Platynereis* larvae fixed with 4% paraformaldehyde were carried out using primary antibodies raised against RGWamide neuropeptide in rat (CRGWamide) and achatin neuropeptide in rabbit (CGFGD), plus a commercial antibody raised against acetylated tubulin in mouse (Sigma T7451). Double immunostaining was carried out with primary antibodies raised against MIP, RYamide or DH31 neuropeptide raised in rabbit and commercial acetylated tubulin antibody raised in mouse. The synthetic neuropeptides contained an N-terminal Cys that was used for coupling during purification. Antibodies were affinity purified from sera as previously described (Conzelmann and Jékely 2012). Immunostainings were carried out as previously described (Conzelmann and Jékely 2012).

Calcium imaging experiments

Fertilized eggs were injected as previously described (Conzelmann et al. 2013) with capped and polA-tailed GCaMP6 RNA generated from a vector (pUC57-T7-RPP2-GCaMP6s) containing the GCaMP6 ORF fused to a 169 base pair 5′ UTR from the *Platynereis* 60S acidic ribosomal

protein P2. The injected individuals were kept at 18°C until 2-days-old in 6-well-plates (Nunc multidish no. 150239, Thermo Scientific). Calcium imaging was carried out on a Leica TCS SP8 upright confocal laser scanning microscope with a HC PL APO 40x/1.10 W Corr CS2 objective and LAS X software (Leica Microsystems) GCaMP6 signal was imaged using a 488-nm diode laser at 0.5 - 4% intensity with a HyD detector in counting mode. 2-day-old *Platynereis* larvae were immobilized for imaging by gently holding them between a glass microscope slide and a coverslip raised with 2 layers of tape as spacer. Larvae were mounted in 10 µl sterile seawater. For peptide treatment experiments, individual larvae were imaged for 2 minutes in the plane of the RGWamide interneurons and MC cell to assess the state of the larval nervous system prior to peptide treatment. For treatment, larvae were imaged for a further 5.5 min. 10 µl 50 µM synthetic D-achatin (G{dF}GD) (final concentration 25 µM) dissolved in seawater was added to the slide at the 1 minute mark by slowly dripping it into the slide-coverslip boundary, where it was sucked under the coverslip. As a negative control, larvae were treated with synthetic L-achatin (GFGD) at the same concentration. Receptor deorphanization experiments have shown that the D-form of achatin activates the achatin receptor GPCR, whereas the L-form of achatin does not (Bauknecht and Jékely 2015). D-achatin response was recorded from 12 larvae, and L-achatin response was recorded from 6 larvae. Calcium imaging movies were analysed with a custom Fiji macro and custom Python scripts. Correlation analyses were created using Fiji and a custom Python script (Verasztó et al. 2017).

References

Achim, K., Pettit, J.-B., Saraiva, L.R., Gavriouchkina, D., Larsson, T., Arendt, D. and Marioni, J.C. 2015. High-throughput spatial mapping of single-cell RNA-seq data to tissue of origin. *Nature Biotechnology* 33(5), pp. 503–509.

Arendt, D., Tessmar-Raible, K., Snyman, H., Dorresteijn, A.W. and Wittbrodt, J. 2004. Ciliary photoreceptors with a vertebrate-type opsin in an invertebrate brain. *Science* 306(5697), pp. 869–871.

Aros, B., Vigh, B. and Vigh-Teichmann, I. 1977. Intra- and extraganglionic nerve endings formed by neurosecretory cells of the cerebral ganglion of the earthworm (Lumbricus terrestris L.). *Cell Tissue Res* 180(4), pp. 537–553.

Asadulina, A., Conzelmann, M., Williams, E.A., Panzera, A. and Jékely, G. 2015. Object-based representation and analysis of light and electron microscopic volume data using Blender. *BMC Bioinformatics* 16, p. 229.

Asadulina, A., Panzera, A., Verasztó, C., Liebig, C. and Jékely, G. 2012. Whole-body gene expression pattern registration in Platynereis larvae. *EvoDevo* 3(1), p. 27.

Bargmann, C.I. 2012. Beyond the connectome: how neuromodulators shape neural circuits. *Bioessays: News and Reviews in Molecular, Cellular and Developmental Biology* 34(6), pp. 458–465.

Bauknecht, P. and Jékely, G. 2015. Large-Scale Combinatorial Deorphanization of Platynereis Neuropeptide GPCRs. *Cell Rep* 12(4), pp. 684–693.

Bentley, B., Branicky, R., Barnes, C.L., Chew, Y.L., Yemini, E., Bullmore, E.T., Vértes, P.E. and Schafer, W.R. 2016. The Multilayer Connectome of Caenorhabditis elegans. *PLoS Computational Biology* 12(12), p. e1005283.

Blitz, D.M., Christie, A.E., Coleman, M.J., Norris, B.J., Marder, E. and Nusbaum, M.P. 1999. Different proctolin neurons elicit distinct motor patterns from a multifunctional neuronal network. *The Journal of Neuroscience* 19(13), pp. 5449–5463.

Bluet-Pajot, M.T., Tolle, V., Zizzari, P., Robert, C., Hammond, C., Mitchell, V., Beauvillain, J.C., Viollet, C., Epelbaum, J. and Kordon, C. 2001. Growth hormone secretagogues and hypothalamic networks. *Endocrine* 14(1), pp. 1–8.

Campbell, J.N., Macosko, E.Z., Fenselau, H., Pers, T.H., Lyubetskaya, A., Tenen, D., Goldman, M., Verstegen, A.M.J., Resch, J.M., McCarroll, S.A., Rosen, E.D., Lowell, B.B. and Tsai, L.T. 2017. A molecular census of arcuate hypothalamus and median eminence cell types. *Nature Neuroscience*.

Chia, F.S. and Koss, R. 1984. Fine structure of the cephalic sensory organ in the larva of the nudibranch Rostanga pulchra (Mollusca, Opisthobranchia, Nudibranchia). *Zoomorphology* 104(3), pp. 131–139.
Conzelmann, M. and Jékely, G. 2012. Antibodies against conserved amidated neuropeptide epitopes enrich the comparative neurobiology toolbox. *Evodevo* 3(1), p. 23.
Conzelmann, M., Offenburger, S.-L., Asadulina, A., Keller, T., Münch, T.A. and Jékely, G. 2011. Neuropeptides regulate swimming depth of Platynereis larvae. *Proceedings of the National Academy of Sciences of the United States of America* 108(46), pp. E1174–83.
Conzelmann, M., Williams, E.A., Krug, K., Franz-Wachtel, M., Macek, B. and Jékely, G. 2013. The neuropeptide complement of the marine annelid Platynereis dumerilii. *BMC Genomics* 14, p. 906.
Conzelmann, M., Williams, E.A., Tunaru, S., Randel, N., Shahidi, R., Asadulina, A., Berger, J., Offermanns, S. and Jékely, G. 2013. Conserved MIP receptor-ligand pair regulates Platynereis larval settlement. *Proceedings of the National Academy of Sciences of the United States of America* 110(20), pp. 8224–8229.
Garcia, V.J., Daur, N., Temporal, S., Schulz, D.J. and Bucher, D. 2015. Neuropeptide receptor transcript expression levels and magnitude of ionic current responses show cell type-specific differences in a small motor circuit. *J Neurosci* 35(17), pp. 6786–6800.
Hadfield, M.G., Meleshkevitch, E.A. and Boudko, D.Y. 2000. The apical sensory organ of a gastropod veliger is a receptor for settlement cues. *The Biological Bulletin* 198(1), pp. 67–76.
Hartenstein, V. 2006. The neuroendocrine system of invertebrates: a developmental and evolutionary perspective. *J Endocrinol* 190(3), pp. 555–570.
Herget, U. and Ryu, S. 2015. Coexpression analysis of nine neuropeptides in the neurosecretory preoptic area of larval zebrafish. *Frontiers in Neuroanatomy* 9, p. 2.
Jékely, G. 2013. Global view of the evolution and diversity of metazoan neuropeptide signaling. *Proc Natl Acad Sci U S A* 110(21), pp. 8702–8707.
Jékely, G., Colombelli, J., Hausen, H., Guy, K., Stelzer, E., Nédélec, F. and Arendt, D. 2008. Mechanism of phototaxis in marine zooplankton. *Nature* 456(7220), pp. 395–399.
Keijzer, F. and Arnellos, A. 2017. The animal sensorimotor organization: a challenge for the environmental complexity thesis. *Biology & philosophy*.
Marder, E. 2012. Neuromodulation of neuronal circuits: back to the future. *Neuron* 76(1), pp. 1–11.
Marlow, H., Tosches, M.A., Tomer, R., Steinmetz, P.R., Lauri, A., Larsson, T. and Arendt, D. 2014. Larval body patterning and apical organs are conserved in animal evolution. *BMC Biology* 12, p. 7.
Mayorova, T.D., Tian, S., Cai, W., Semmens, D.C., Odekunle, E.A., Zandawala, M., Badi, Y., Rowe, M.L., Egertová, M. and Elphick, M.R. 2016. Localization of Neuropeptide Gene Expression in Larvae of an Echinoderm, the Starfish Asterias rubens. *Frontiers in Neuroscience* 10, p. 553.
Mirabeau, O. and Joly, J.S. 2013. Molecular evolution of peptidergic signaling systems in bilaterians. *Proc Natl Acad Sci U S A* 110(22), pp. E2028–37.
Moran, M.M., Xu, H. and Clapham, D.E. 2004. TRP ion channels in the nervous system. *Current Opinion in Neurobiology* 14(3), pp. 362–369.
Nikitin, M. 2015. Bioinformatic prediction of Trichoplax adhaerens regulatory peptides. *General and Comparative Endocrinology* 212, pp. 145–155.
Page, L.R. 2002. Apical sensory organ in larvae of the patellogastropod Tectura scutum. *The Biological Bulletin* 202(1), pp. 6–22.
Pettit, J.-B., Tomer, R., Achim, K., Richardson, S., Azizi, L. and Marioni, J. 2014. Identifying cell types from spatially referenced single-cell expression datasets. *PLoS Computational Biology* 10(9), p. e1003824.
Purschke, G. 1997. Ultrastructure of Nuchal Organs in Polychaetes (Annelida) - New Results and Review. *Acta Zoologica* 78(2), pp. 123–143.
Randel, N., Asadulina, A., Bezares-Calderón, L.A., Verasztó, C., Williams, E.A., Conzelmann, M., Shahidi, R. and Jékely, G. 2014. Neuronal connectome of a sensory-motor circuit for visual navigation. *elife* 3.
Randel, N., Shahidi, R., Verasztó, C., Bezares-Calderón, L.A., Schmidt, S. and Jékely, G. 2015. Inter-individual stereotypy of the Platynereis larval visual connectome. *elife* 4, p. e08069.
Root, C.M., Ko, K.I., Jafari, A. and Wang, J.W. 2011. Presynaptic facilitation by neuropeptide signaling mediates odor-driven food search. *Cell* 145(1), pp. 133–144.
Saalfeld, S., Cardona, A., Hartenstein, V. and Tomancak, P. 2009. CATMAID: collaborative annotation toolkit for massive amounts of image data. *Bioinformatics* 25(15), pp. 1984–1986.
Sakurai, T., Amemiya, A., Ishii, M., Matsuzaki, I., Chemelli, R.M., Tanaka, H., Williams, S.C., Richardson, J.A., Kozlowski, G.P., Wilson, S., Arch, J.R., Buckingham, R.E., Haynes, A.C., Carr, S.A., Annan, R.S., McNulty, D.E., Liu, W.S., Terrett, J.A., Elshourbagy, N.A., Bergsma, D.J. and Yanagisawa, M. 1998. Orexins and orexin receptors:

a family of hypothalamic neuropeptides and G protein-coupled receptors that regulate feeding behavior. *Cell* 92(4), pp. 573–585.
Schlegel, P., Texada, M.J., Miroschnikow, A., Schoofs, A., Hückesfeld, S., Peters, M., Schneider-Mizell, C.M., Lacin, H., Li, F., Fetter, R.D., Truman, J.W., Cardona, A. and Pankratz, M.J. 2016. Synaptic transmission parallels neuromodulation in a central food-intake circuit. *eLife* 5.
Schneider-Mizell, C.M., Gerhard, S., Longair, M., Kazimiers, T., Li, F., Zwart, M.F., Champion, A., Midgley, F.M., Fetter, R.D., Saalfeld, S. and Cardona, A. 2016. Quantitative neuroanatomy for connectomics in Drosophila. *elife* 5.
Shahidi, R., Williams, E.A., Conzelmann, M., Asadulina, A., Verasztó, C., Jasek, S., Bezares-Calderón, L.A. and Jékely, G. 2015. A serial multiplex immunogold labeling method for identifying peptidergic neurons in connectomes. *eLife* 4.
Siegmund, T. and Korge, G. 2001. Innervation of the ring gland of Drosophila melanogaster. *The Journal of Comparative Neurology* 431(4), pp. 481–491.
Smith, C.L., Varoqueaux, F., Kittelmann, M., Azzam, R.N., Cooper, B., Winters, C.A., Eitel, M., Fasshauer, D. and Reese, T.S. 2014. Novel cell types, neurosecretory cells, and body plan of the early-diverging metazoan Trichoplax adhaerens. *Current Biology* 24(14), pp. 1565–1572.
Steinmetz, P.R.H., Urbach, R., Posnien, N., Eriksson, J., Kostyuchenko, R.P., Brena, C., Guy, K., Akam, M., Bucher, G. and Arendt, D. 2010. Six3 demarcates the anterior-most developing brain region in bilaterian animals. *EvoDevo* 1(1), p. 14.
Stein, W., DeLong, N.D., Wood, D.E. and Nusbaum, M.P. 2007. Divergent co-transmitter actions underlie motor pattern activation by a modulatory projection neuron. *The European Journal of Neuroscience* 26(5), pp. 1148–1165.
Sternson, S.M., Nicholas Betley, J. and Cao, Z.F. 2013. Neural circuits and motivational processes for hunger. *Curr Opin Neurobiol* 23(3), pp. 353–360.
Terakita, A. 2005. The opsins. *Genome Biology* 6(3), p. 213.
Tessmar-Raible, K. 2007. The evolution of neurosecretory centers in bilaterian forebrains: insights from protostomes. *Seminars in Cell & Developmental Biology* 18(4), pp. 492–501.
Tessmar-Raible, K., Raible, F., Christodoulou, F., Guy, K., Rembold, M., Hausen, H. and Arendt, D. 2007. Conserved sensory-neurosecretory cell types in annelid and fish forebrain: insights into hypothalamus evolution. *Cell* 129(7), pp. 1389–1400.
Thirumalai, V. and Marder, E. 2002. Colocalized neuropeptides activate a central pattern generator by acting on different circuit targets. *The Journal of Neuroscience* 22(5), pp. 1874–1882.
Thorndyke, M.C., Crawford, B.D. and Burke, R.D. 1992. Localization of a SALMFamide Neuropeptide in the Larval Nervous System of the Sand Dollar *Dendraster excentricus*. *Acta Zoologica* 73(4), pp. 207–212.
Tosches, M.A. and Arendt, D. 2013. The bilaterian forebrain: an evolutionary chimaera. *Curr Opin Neurobiol* 23(6), pp. 1080–1089.
Verasztó, C., Ueda, N., Bezares-Calderón, L.A., Panzera, A., Williams, E.A., Shahidi, R. and Jékely, G. 2017. Ciliomotor circuitry underlying whole-body coordination of ciliary activity in the Platynereis larva. *bioRxiv*. Available at: https://doi.org/10.1101/108035.
Vergara, H., Bertucci, P., Hantz, P., Tosches, M.A., Achim, K., Vopalensky, P. and Arendt, D. 2017. A whole-organism cellular gene expression atlas reveals conserved cell types in the ventral nerve cord of *Platynereis dumerilii*. *Proceedings of the National Academy of Sciences of the United States of America* in press.
Watts, D.J. and Strogatz, S.H. 1998. Collective dynamics of "small-world" networks. *Nature* 393(6684), pp. 440–442.
Williams, E.A. and Jékely, G. 2016. Towards a systems-level understanding of development in the marine annelid Platynereis dumerilii. *Current Opinion in Genetics & Development* 39, pp. 175–181.
Wirmer, A., Bradler, S. and Heinrich, R. 2012. Homology of insect corpora allata and vertebrate adenohypophysis? *Arthropod Struct Dev* 41(5), pp. 409–417.

Acknowledgments

We thank Luis Bezares, Martin Gühmann and Nobuo Ueda for comments on the manuscript. The research leading to these results received funding from the European Research Council under the European Union's Seventh Framework Programme (FP7/2007-2013)/ European Research

Council Grant Agreement 260821. The research was supported by a grant from the DFG - Deutsche Forschungsgemeinschaft (Reference no. JE 777/1).

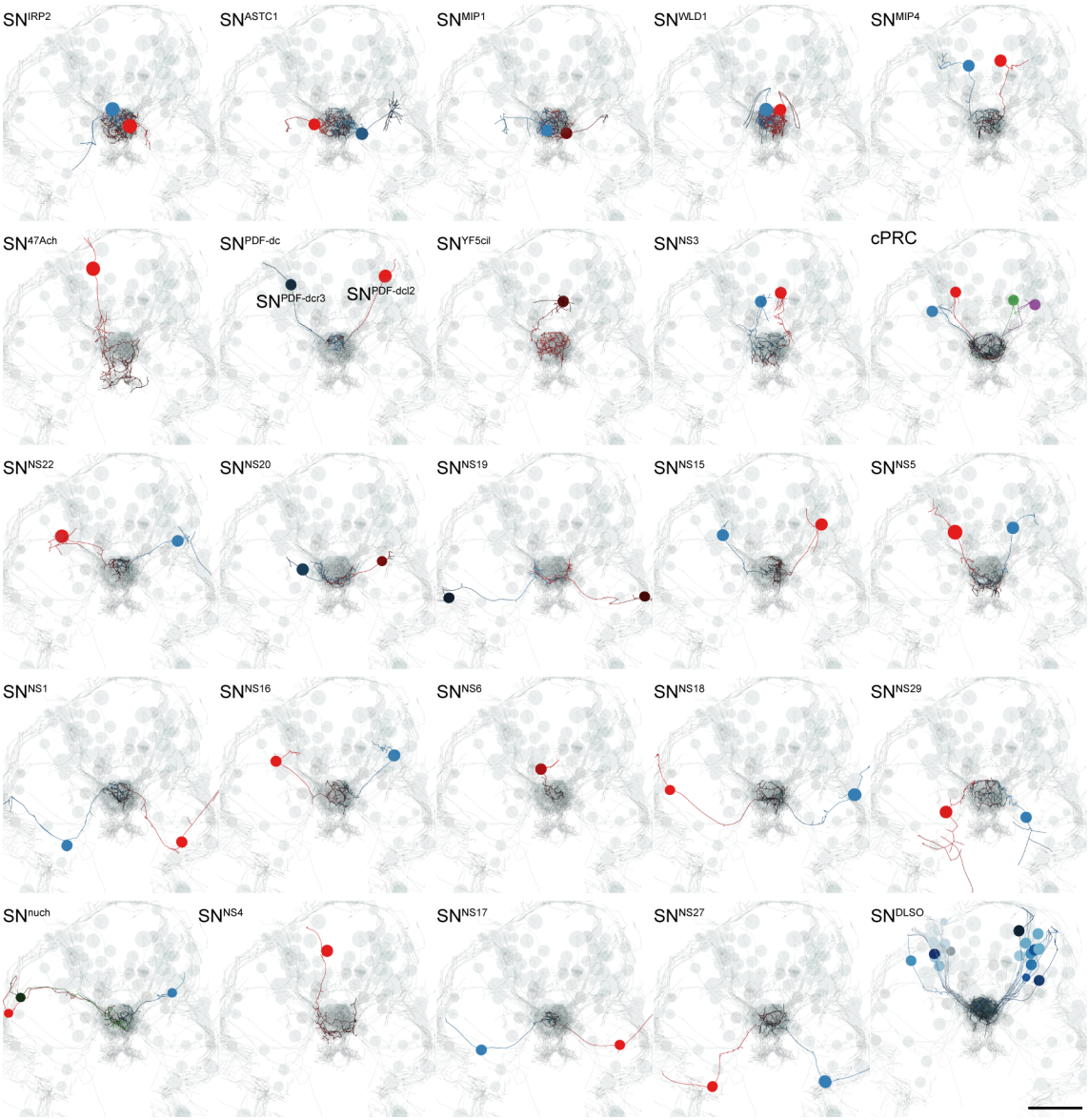

Supplement 1 to Figure 1.
TEM reconstruction of ANS neurons. Bilaterally symmetric pairs and single asymmetric sensory neurons are shown in anterior view. Axons and dendrites appear as lines and cell body positions are represented by spheres. The reconstructed ciliary band cells and all ANS cells (grey) are included to show the perimeter of the head. Scale bar: 30 µm.

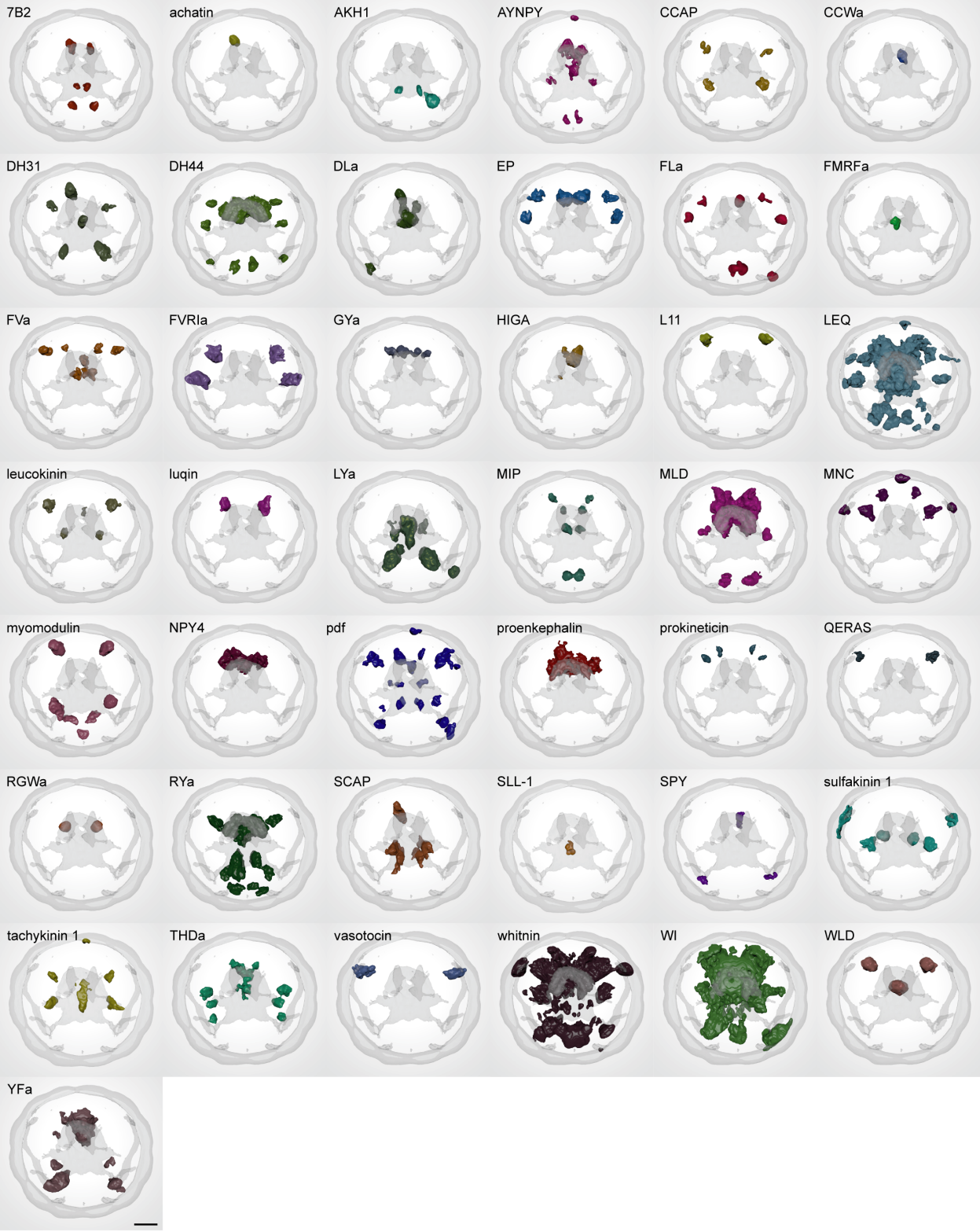

Supplement 2 to Figure 1.

Average gene expression patterns of individual proneuropeptide from a whole-body gene expression atlas from 2-day-old larvae, anterior view. Scale bar: 30 µm.

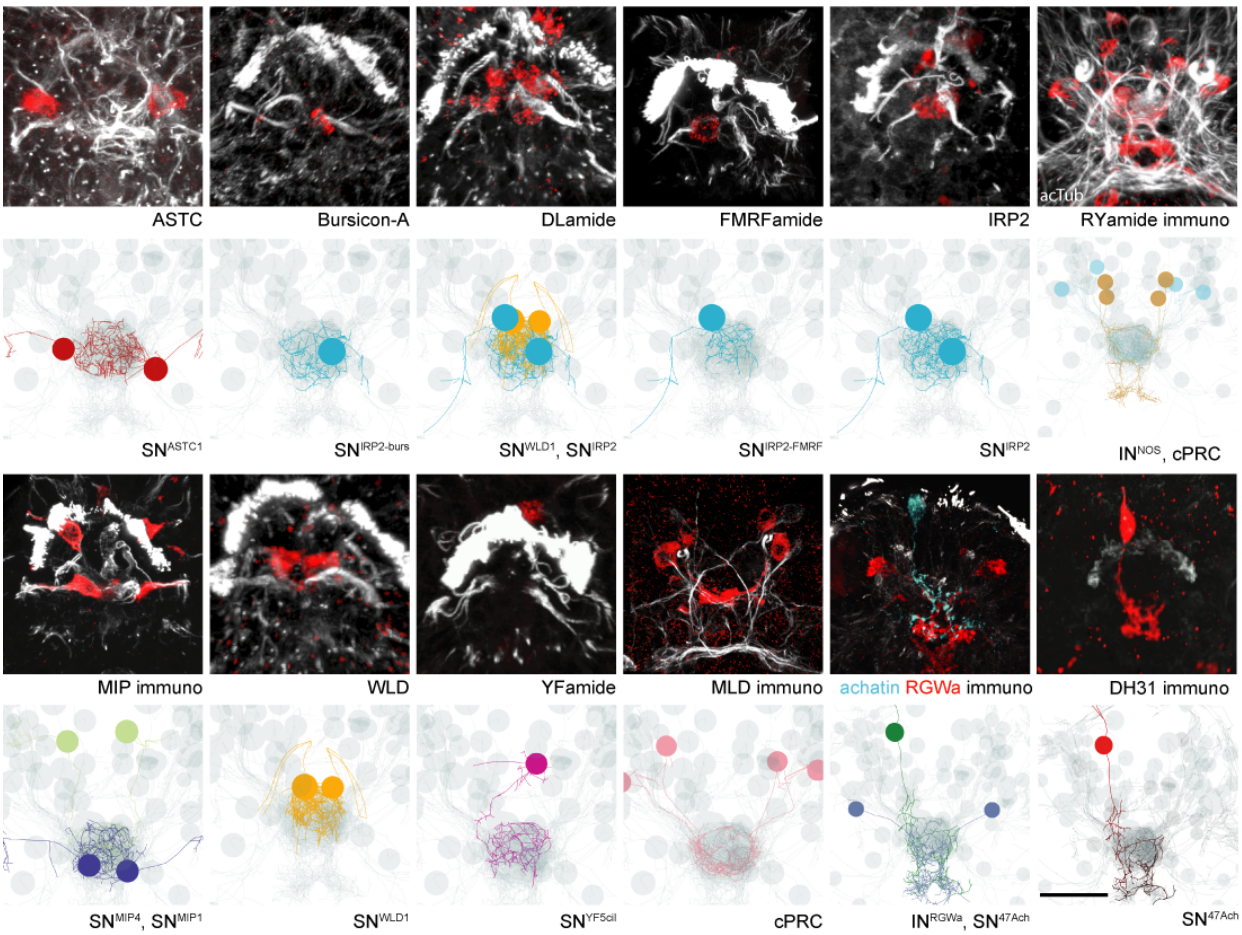

Supplement 3 to Figure 1.
Expression of proneuropeptides in ciliated *Platynereis* larval sensory cells. Confocal microscope scans of whole-mount *in situ* hybridization of proneuropeptides (red) counterstained with anti-acetylated tubulin antibody (white). Close-up images show the apical sensory cilia of ANS neurons in 2-day-old larvae. The confocal stacks facilitated the assignation of neuropeptidergic identities to reconstructed neurons in the TEM connectome dataset. Scale bar: 25 µm.

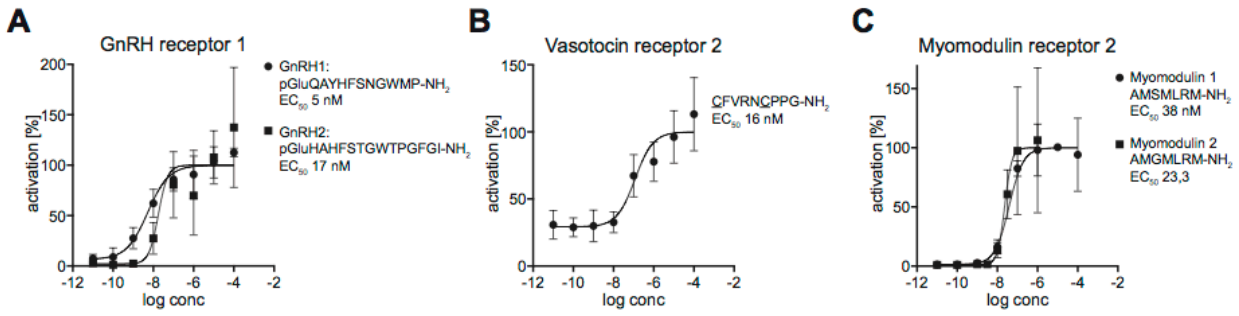

Supplement 1 to Figure 3.
Dose-responsive curves of *Platynereis* deorphanized GPCRs treated with varying concentrations of peptides. Data, representing luminescence units relative to the maximum of the fitted dose-response curves, are shown as mean +/- SEM (n = 3). EC_{50} values and peptide sequences are shown beside each graph.

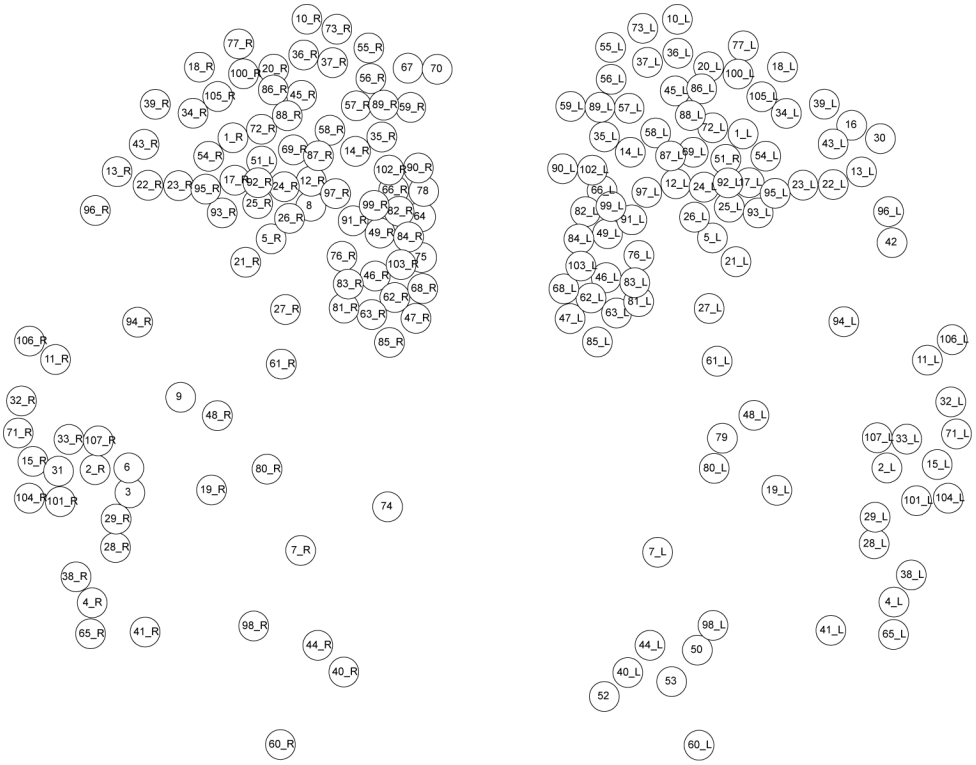

Supplement 2 to Figure 3.
Spatial map of single cell RNA-Seq data from Achim et al. (Achim et al. 2015). The position of each node on the map is an approximation based on the spatial predictions of each RNA-seq sample generated by Achim et al. from comparisons of transcriptome expression with a whole mount *in situ* hybridization gene expression atlas of 72 genes. The correspondence of node IDs to original sample IDs from Achim *et al.* 2015 is listed in Supplementary table1.

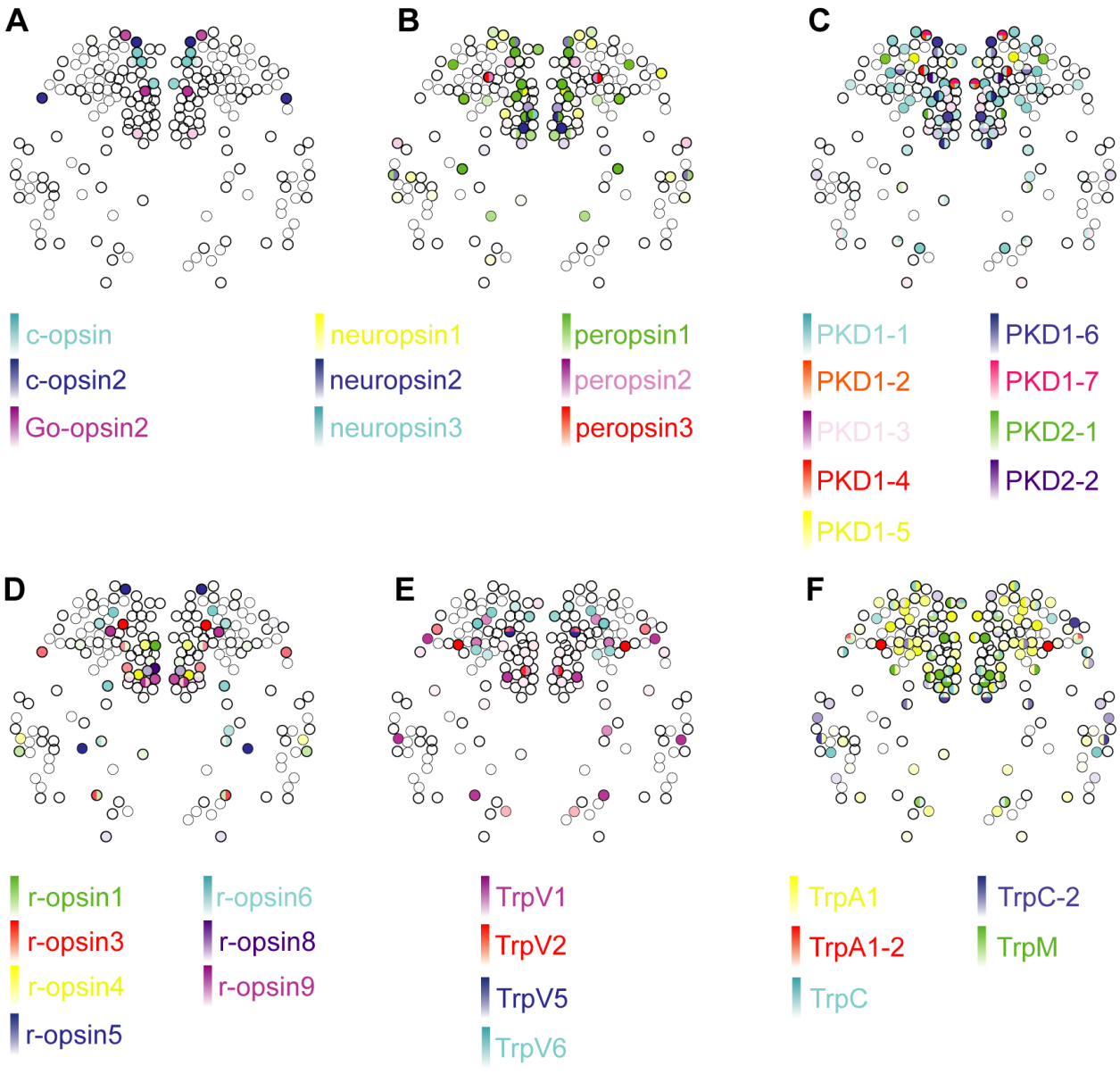

Supplement 3 to Figure 3. Expression of opsins and Trp channels in the *Platynereis* larval head. Colour intensity reflects relative normalized gene expression levels. Cells of the apical nervous system (i.e., cells expressing any combination of *Phc2*, *dimmed*, *Otp* and *nk2.1*) are indicated by a bold border.

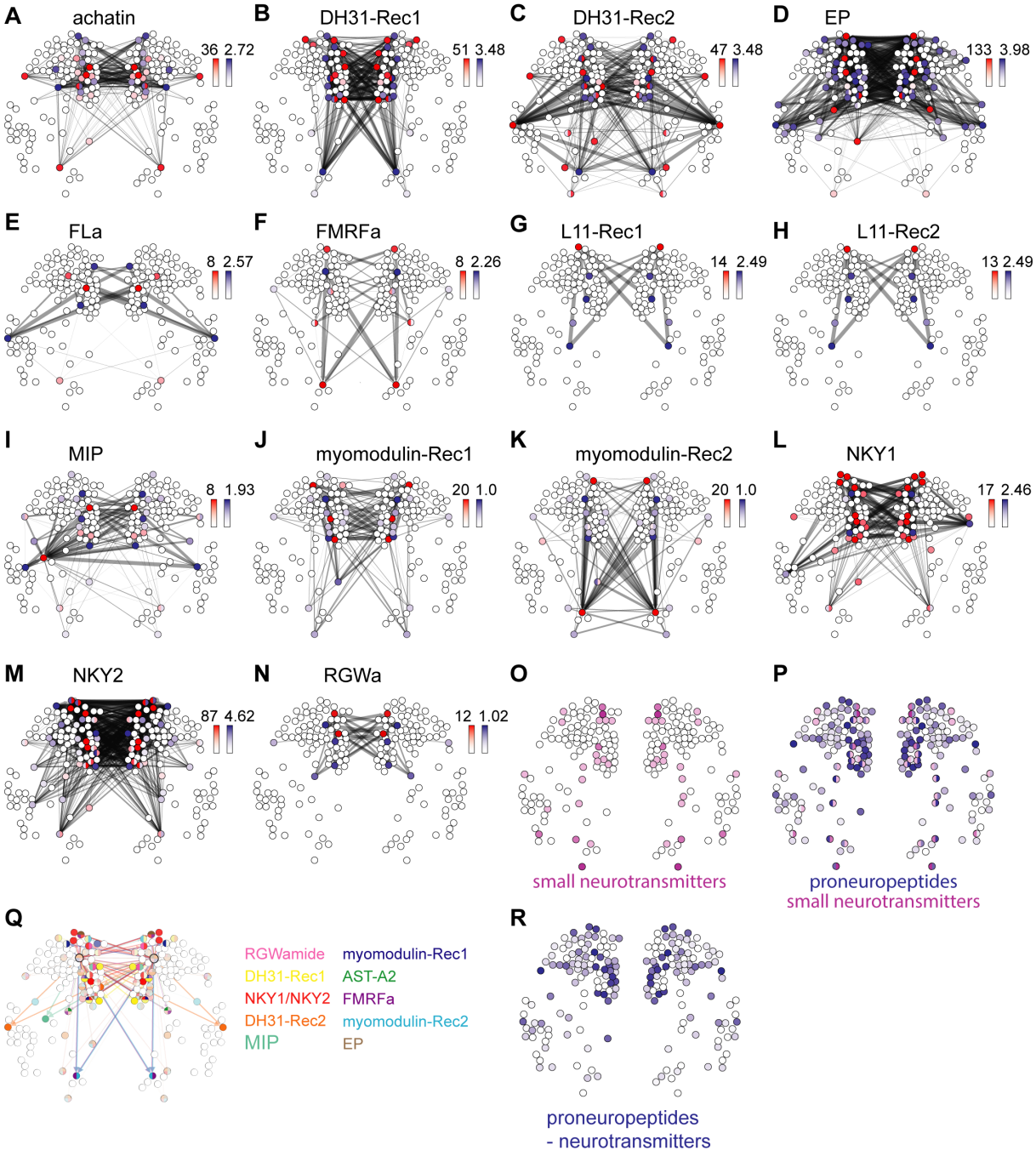

Supplement 4 to Figure 3. Neuropeptide-GPCR chemical connections in the *Platynereis* larval head. (**A-N**) Connectivity maps of individual neuropeptide-GPCR pairs, coloured by weighted in-degree (red) and proneuropeptide $\log_{10}$ normalized expression (blue). Arrows indicate direction of signalling. Arrow thickness determined by geometric mean of $\log_{10}$ normalized proneuropeptide expression of signalling cell and $\log_{10}$ normalized GPCR expression of corresponding receiving cell. (**O**) Expression map of small neurotransmitter synthesis markers. (**P**) Expression map of proneuropeptides and small neurotransmitter markers. (**Q**) Multichannel signalling from a highly peptidergic cell. (**R**) Expression map of proneuropeptides shown for those cells that do not express small neurotransmitter markers.

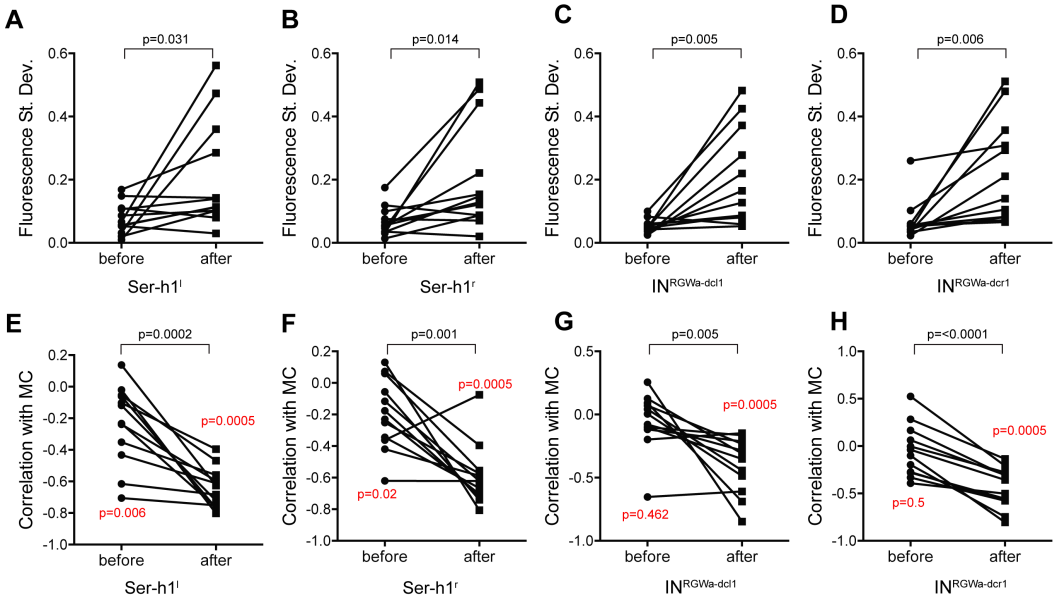

Supplement 1 to Figure 4.
(**A**-**D**) Standard deviation in fluorescent calcium signal of the (**A**) Ser-h1^{l}, (**B**) Ser-h1^{r}, (**C**) IN$^{RGWa\text{-}dcl1}$ and (**D**) IN$^{RGWa\text{-}dcr1}$ neurons in 2-day-old larvae before and after treatment with 25 µM D-achatin. (**E**-**H**) Correlation of neuronal calcium signals of (**E**) Ser-h1^{l}, (**F**) Ser-h1^{r}, (**G**) IN$^{RGWa\text{-}dcl1}$ and (**H**) IN$^{RGWa\text{-}dcr1}$ with calcium signals measured from the MC cell in 2-day-old larvae before and after treatment with 25 µM D-achatin. Individual data points represent different larvae before and after treatment. P-values of pairwise t-tests are shown above the square brackets. In (**E**-**H**) a Wilcoxon Signed Rank Test was also used to test if medians area significantly different from 0. The p-values are shown next to the data points.

Supplementary Table 1
.xls file containing ANS synaptic connectivity spreadsheet, node ID to cell ID key, chemical network parameters, and log10 normalized expression values from mapping of single cell data for neuropeptides, GPCRs, sensory genes and neurotransmitter synthesis enzymes in separate worksheets.

Video 1.
EM reconstruction of the anterior nervous system in a 72-hr post fertilization *Platynereis* larva. The head ciliary band (grey) and the adult eye photoreceptor cells (transparent blue) are shown for reference.

Author contributions
E.A.W and G.J. designed the study. E.A.W did single cell mapping, calcium imaging experiments, immunostaining and *in situ* hybridizations. C.V. and G.J. reconstructed neurons. S.J. did *in situ* hybridizations and generated the neuropeptide atlas. R.S. generated the EM dataset. P.B. deorphanized neuropeptide GPCRs. E.A.W. and G.J. wrote the paper.